



University of Thessaly

School of Engineering

Department of Mechanical Engineering

Diploma Thesis

**Automated Modal Identification of Structures using the DD-SSI
Algorithm and Clustering Techniques**

by

Chanopoulou Ioanna

Thesis Supervisor: **Dr. Costas Papadimitriou**

Submitted in partial fulfillment of the requirements for the Mechanical Engineering Diploma
from the University of Thessaly.

Volos, 2019

© 2019 Chanopoulou Ioanna

The approval of this thesis by the Mechanical Engineering Department of the School of Engineering of University of Thessaly does not imply the acceptance of the personal views of the author (L. 5343/32 ar. 202 par. 2)

Certified by the members of the Thesis Committee:

First Examiner
(Supervisor)

Costas Papadimitriou

Professor of Structural Dynamics, Department of Mechanical Engineering, University of Thessaly

Second Examiner

Spyros Karamanos

Professor of Numerical Methods - Finite Elements - Structural Mechanics, Department of Mechanical Engineering, University of Thessaly

Third Examiner

Georgios Charalampous

Assistant Professor of Thermofluid Processes with Energy Applications, Department of Mechanical Engineering, University of Thessaly

*This thesis is dedicated to
my father*

Acknowledgements

First of all, I would like to express my gratitude to my professor and advisor, prof. Costas Papadimitriou for his help, patience and guidance through our collaboration for this thesis.

Also, I would like to thank my family and friends, who have been by my side through good and rough times during the studying years.

Abstract

This thesis focuses on the estimation and identification of the real modal properties (modal frequencies, damping ratios and mode shapes) of a structure, which is submitted to unknown excitations, in a completely automated way. For this purpose a software has been developed, engaging an output-only technique called Data Driven Stochastic Subspace Identification (DD-SSI), followed by a clustering-based methodology for the automation of the production of the stabilization diagram.

The application of this theory has been conducted using the time histories obtained from experimental measurements with sensors attached on three bridges in Greece. The results of this automated process for each bridge are also presented in the current thesis. In addition, a comparison is made between the results of this software and the results obtained by two other software, which have been developed in the System Dynamics Laboratory of UTH, based on different theories. Finally, some conclusions concerning the quality of the data and the mechanical behavior of analyzed of structures are deduced.

1. Introduction	8
2. Stochastic Subspace Identification algorithms	10
2.1. State-Space Representation of Linear Dynamic Systems.	11
2.2. Data - Driven Stochastic Subspace Identification (DD-SSI)	12
2.2.1. The algorithm.	12
2.2.2. Modal parameters	15
2.2.3. User-defined parameters	15
3. Automated interpretation of DD-SSI output	20
3.1. Pre - filtering criteria	21
3.2. Clustering	23
4. Software for modal analysis	29
5. Applications	31
5.1. Bridge 1: Metsovo	33
5.1.1. Results from the developed software	34
5.1.2. Results from Software 1	61
5.1.3. Conclusions	67
5.2. Bridge 2	68
5.2.1. Results from the developed software	69
5.2.2. Results from Software 2	81
5.2.3. Conclusions	84
5.3. Bridge 3.	85
5.3.1. Results from the developed software	87
5.3.2. Results from Software 2	111
5.3.3. Conclusions	113
6. Conclusions	114
7. Literature	121

APPENDIX

APPENDIX A: Developed software for the automated modal identification	116
APPENDIX B: Output of Software 2	119

1. Introduction

The examination of civil infrastructure systems through the conduction of vibration tests is vital for monitoring their health. Monitoring can track the health condition and report the abnormal status of structures at an earlier stage to prevent their failure. In civil engineering, for example, such systems are buildings, bridges etc., which play an important role in a human's everyday life. There have been developed various methodologies concerning the acquisition of the modal properties of a structure using experimental measurements.

Traditional methods of modal analysis rely on the measurements of both the applied input and the corresponding response output and, for this reason they are referred to as input-output (I/O) methods. Unfortunately, it is very difficult to specify the input excitations for a number of engineering applications, such as bridges in civil engineering, so output-only (O/O) methods, referred to as operational modal analysis (OMA) methods, are perfectly suited for these cases [3]. Output-only methods use only the measured structural response and they do not require measurements of the input. Especially for the bridges, which need to be operational during monitoring, the most commonly used measurements are those of the structural response induced by traffic or by the wind. As mentioned above, this kind of excitations are very difficult (close to impossible) to be defined. Therefore, the O/O methods offer the possibility of performing a structural identification without the need to compute the applied input excitation. However, the lack of the input data introduces several limitations in the analysis that can be performed.

In the last decades, several automated procedures have been developed based on OMA techniques including the time domain parametric identification methods such as Stochastic Subspace Identification (SSI) [1], Eigensystem Realization Algorithm (ERA)[13], and the frequency domain non-parametric method, i.e. Frequency Domain Decomposition (FDD)[12]. Among these methods, SSI has attracted a significant amount of attention owing to its clear mathematical background and steady performance with a number of successful applications to real civil engineering structures. This algorithm uses directly the output measurements without the need of computing the covariance between outputs. Such Data-Driven SSI depend on the use of linear algebra tools such as orthogonal projection, singular value decomposition, QR factorization etc. and on a certain number of user-defined parameters. Such algorithms are more suited in the analysis of systems whose measurements represent the surrounding vibration response. The effectiveness of the algorithm is strongly affected by some user-defined parameters. These parameters are linked to the dimensions of the Hankel matrix. In linear algebra, a Hankel matrix (or catalecticant matrix), is a square matrix in which each ascending skew-diagonal from left to right is constant. In the DD-SSI algorithm the Hankel matrix is formed by the measurements of the output response and its subpartitions (the past output and the future output subpartition).

Having to deal with the monitoring of a structure one has to use an O/O technique such as the DD-SSI algorithm in order to achieve the modal identification. Modal identification by using the conventional modal analysis methods, involving the manual intervention, is time-consuming due to the substantial amount of engineer judgement and experiences. Therefore, developing robust and efficient automated modal analysis approaches is of great interest for applications to real engineering structures. However, in the produced modes real as well as spurious modes are manifested. So, the need of cleaning the acquired results and identifying the real modes is vital. For this reason, a clustering methodology is followed along with some pre-filtering conditions, so that the real physical modes are distinguished from the spurious ones. There are several methods of clustering introduced in literature and each one proposes different alterations of the main methodology, trying to make the results more robust[6,8]. The most revolutionary about the methodologies is the fact that the process of determining the real modes is automated and doesn't require interference from the user. Usually, the stabilization diagrams[10] are produced with the help of the user but in this case the procedure of the stabilization diagrams is fully automated.

This thesis is organized as follows: in chapter 2 the Data - Driven Stochastic Subspace Identification (DD-SSI) algorithm is presented, while in chapter 3 the clustering techniques are described. In chapter 4, there is a brief reference to the used software and especially the developed one in the context of this thesis. In chapter 5 the results of three applications are presented and finally, in chapter 6 the conclusions of this work are reported.

2. Stochastic Subspace Identification algorithms

Stochastic Subspace Identification (SSI) modal estimation algorithms have been around the latest years. They are a really efficient tool for natural input (ambient loading) modal analysis of systems. Any structure can make up a system. In order for engineers to deal with a problem, such as the monitoring of a structure, they try to capture it by using a dynamic model like the one, which can be seen in fig.2.1.

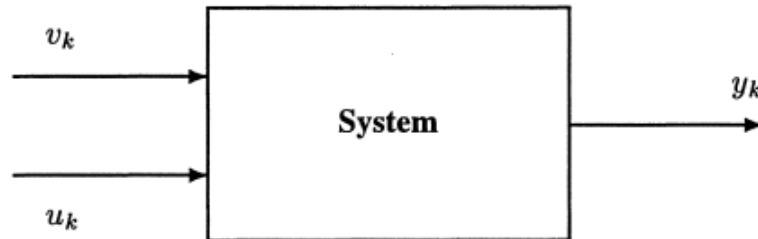


Figure 2.1. The arrows represent vector signals and k is the discrete time index. The input vectors are the input u_k and the noise v_k . The output vector is y_k . In the output only techniques only the output signals y_k are used and the input information is missing.

First of all, subspace identification algorithms are based on concepts from system theory, linear algebra and statistics. The way they work is summarized and illustrated in the following table[1]. When only the output is measured and the external input u_k is unknown, we talk about the subspace identification of stochastic systems. Stochastic Subspace Identification (SSI) algorithms compute state-space models from given output data .

System	Geometry	Algorithm
High order state sequence	Orthogonal projection	QR-decomposition
Low order state sequence	Determine finite dimensional subspace	Singular value decomposition
System matrices	Linear relations	Least squares

Table 2.1.The summarized way of working of Subspace Identification algorithms

2.1. State-Space Representation of Linear Dynamic Systems

The equation that characterizes a linear structural dynamics problem is formulated by the following continuous time, second order differential equation of motion:

$$\mathbf{M}\ddot{\mathbf{u}}(t) + \mathbf{C}\dot{\mathbf{u}}(t) + \mathbf{K}\mathbf{u}(t) = \mathbf{B}\mathbf{f}(t) \quad (2.1)$$

and the measurement equation can be defined as :

$$\mathbf{y}(t) = \mathbf{D}[u(t)^T \dot{u}(t)^T \ddot{u}(t)^T] \quad (2.2)$$

,where $\mathbf{u}(t) \in \mathbb{R}^{n \times 1}$ is a vector which stands for the displacement response as a function of time t and $\mathbf{K}, \mathbf{M}, \mathbf{C} \in \mathbb{R}^{n \times n}$ are symmetric matrices that represent stiffness, mass and damping respectively. The notation of n represents the degrees of freedom (DOF) of the system. The input matrix \mathbf{B} represents the spatial distribution (among the DOFs) of the vector $\mathbf{f}(t) \in \mathbb{R}^n$ which is the external excitation force. The output vector $\mathbf{y}(t) \in \mathbb{R}^{m \times 1}$ represents the measured system response and the output matrix \mathbf{D} captures each possible linear combination of the velocity, the acceleration and the displacement vectors.

The DD-SSI algorithm uses the transformed problem into a discrete-time, state-space form, more suitable for system identification purposes. The formulation to the state – space condition is accomplished by introducing the state vector, $\mathbf{x}(t) \in \mathbb{R}^{2n \times 1}$, which is an arbitrary, linear combination of the displacement, $u(t)$ and the velocity, $\dot{u}(t)$. So the equation in the state-space form is:

$$\begin{aligned} \dot{\mathbf{x}}(t) &= \mathbf{F}\mathbf{x}(t) + \mathbf{G}\mathbf{f}(t) \\ \mathbf{y}(t) &= \mathbf{H}\mathbf{x}(t) + \mathbf{E}\mathbf{f}(t) \end{aligned} \quad (2.3)$$

, where $\mathbf{F} \in \mathbb{R}^{2n \times 2n}$ is the *state matrix*, $\mathbf{G} \in \mathbb{R}^{2n \times r}$ is the *input matrix*, $\mathbf{H} \in \mathbb{R}^{m \times 2n}$ is the *output matrix* and $\mathbf{E} \in \mathbb{R}^{m \times r}$ is the *feed-through matrix*. All of them define, completely, a linear dynamic system with an r - dimensional forcing function, $\mathbf{f}(t)$ and an m - dimensional output measurement, $\mathbf{y}(t)$.

Considering as an example of measuring output, the acceleration of a monitored structure, the matrices would have the following form. To begin with, state vector $\mathbf{x}(t)$ would be equal to : $\mathbf{x}(t) = [u(t) \quad \dot{u}(t)]^T$ and $\mathbf{y}(t) = \ddot{u}(t)$ with $\mathbf{D} = [0(n \times n) \quad 0(n \times n) \quad \mathbf{I}(n \times n)]$ in equation (2.2). So the matrices in the state-space form in equations (2.3) can be written as :

$$\mathbf{F} = \begin{pmatrix} \mathbf{0} & \mathbf{I} \\ -\mathbf{M}^{-1}\mathbf{K} & -\mathbf{M}^{-1}\mathbf{C} \end{pmatrix}, \mathbf{G} = \begin{pmatrix} \mathbf{0} \\ -\mathbf{M}^{-1}\mathbf{B} \end{pmatrix}, \mathbf{H} = [-\mathbf{M}^{-1}\mathbf{K} \quad -\mathbf{M}^{-1}\mathbf{C}], \mathbf{E} = [-\mathbf{M}^{-1}\mathbf{B}]$$

The above matrices are completely defined by the mass, damping and stiffness of equation (2.1).

A final step towards the state-space representation for modal identification purposes, would be the discretization of time . Typically, measurements of the output $y(t)$ are acquired at discrete times $t=k\Delta t$, $k=0,1,2,3,\dots$ with a constant sampling time Δt . Assuming a generic stochastic process as input and a sampling time interval equal to Δt , the discrete time state-space representation of a linear ,time-invariant system of order \mathbf{n} would be:

$$\begin{aligned} \mathbf{x}((k+1)\Delta t) &= \mathbf{A}_d \mathbf{x}(k\Delta t) + \mathbf{w}(k\Delta t) \\ \mathbf{y}(k\Delta t) &= \mathbf{C} \mathbf{x}(k\Delta t) + \mathbf{v}(k\Delta t) \end{aligned} \quad (2.4)$$

, where \mathbf{k} is the time step ($k=0, 2, \dots, s$, s being the total number of samples), $\mathbf{x}(\mathbf{k}) \in R^{n \times 1}$ is the discrete time state vector and $\mathbf{y}(\mathbf{k}) \in R^{m \times 1}$ contains the output measurements, with \mathbf{m} representing the number of output histories. The two unknown vectors, $\mathbf{w}(k) \in R^{n \times 1}$, $\mathbf{v}(k) \in R^{m \times 1}$ represent, respectively, the process and the measurement noises at the k -th time step. [2, 3]

2.2. Data – Driven Stochastic Subspace Identification (DD-SSI)

2.2.1. The algorithm

The DD-SSI algorithm belongs to the subspace methods. It uses directly output response data without requiring any correlation between them. As already mentioned the DD-SSI algorithm is based on linear algebra tools , such as orthogonal projection, Singular value decomposition ,QR factorization and some user defined parameters . The steps of which the algorithm consists are the following :

- Step 1 : The output data is arranged in a block of **Hankel matrix** $\mathbf{H} \in R^{mixj}$. The number of block rows of the Hankel matrix is noted as \mathbf{i} and the number of its columns as \mathbf{j} . This matrix is then split in two partitions. The first is the past output partition Y_p and the second is the future output partition Y_f . The number of block rows of the past output subpartition Y_p are noted with \mathbf{g} and the number of block rows of the future output subpartition Y_f with \mathbf{h} . The correlation between \mathbf{g} and \mathbf{h} is : $\mathbf{g} + \mathbf{h} = \mathbf{i}$. The Hankel matrix can be interpreted as follows:

$$H = \begin{pmatrix} y_p \\ y_f \end{pmatrix} = \begin{pmatrix} y(0) & \cdots & y(j-1) \\ y(1) & \cdots & y(j) \\ \vdots & \ddots & \vdots \\ y(g-1) & \cdots & y(g+j-2) \\ y(i-h) & \cdots & y(i-h+j-1) \\ y(i-h+1) & \cdots & y(i-h+j) \\ \vdots & \ddots & \vdots \\ y(i-1) & \cdots & y(i+j-2) \end{pmatrix} \quad (2.5)$$

More thoroughly explained, each element of the Hankel matrix $\mathbf{y}(k)$, is a **vector**, which contains the output measurements, for the whole number of the output - histories, at the time step k . If we assume that we have a system, with a number of output histories, m , and a number of measured samples, s , at the k -th time step, as it is shown in fig2.2 below:

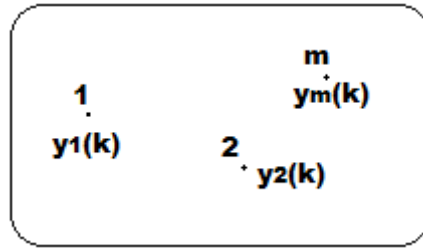


Figure2.2. The box represents a system and the points are the measurements made on it, where m represents the number of measurements and $y_n(k)$, $n=1, \dots, m$, $k=1, \dots, s$ the output measurements that can be accelerations, velocities or displacements.

The vector $\mathbf{y}(k) \in R^{m \times 1}$, which is used in the Hankel matrix, can be expressed as :

$$\mathbf{y}(k) = \begin{Bmatrix} y_1(k) \\ \vdots \\ y_m(k) \end{Bmatrix}$$

- Step 2: The next step is the computation of the **orthogonal projection** $\Pi \in R^{mh \times j}$ of the row space of the future outputs onto the row space of the past outputs. This is expressed as :

$$\Pi = Y_f / Y_p = Y_f Y_p^T (Y_p Y_p^T)^+ Y_p \quad (2.6)$$

, where $+$ denotes the pseudoinverse.

It is beneficial for the noise reduction to multiply matrix Π with two weighting matrices, W_1 and W_2 :

$$P = W_1 \Pi W_2 \quad (2.7)$$

where $P \in R^{mh \times mg}$, $W_1 \in R^{mh \times mh}$, $W_2 \in R^{j \times mg}$. By using these weighting matrices different methods such as Partial Least Square, Multiple Linear

Regression, etc. are derived and also various quantities are optimized in the identification process. The algorithm which is presented in the current thesis does not use the weighting matrices.

- Step 3: Since matrix P is computed the extraction of the observability range space follows. For this reason it is conducted the **SVD** of the matrix P :

$$P = USV^T = (U_1 \ U_2) \begin{pmatrix} S_1 & 0 \\ 0 & S_2 \end{pmatrix} \begin{pmatrix} V_1^T \\ V_2^T \end{pmatrix} \quad (2.8)$$

where $U \in R^{mh \times mh}$ and $V \in R^{mg \times mg}$ are the orthogonal matrices of the left and right singular vectors . $S \in R^{mh \times mg}$ is the diagonal matrix of the singular values . The dimensions of S_1 indicate the order of the system (n) and can be determined ,theoretically, by considering the non-zero singular values of P . On the other hand S_2 contains the zero singular values of P . The maximum model order of the system is determined by the user the good choice of which is discussed further on this thesis.

The extended observability matrix, O can be extracted by the equation [4]:

$$O = U_1 S_1^{1/2} T \quad (2.9)$$

where T is a non-singular , similarity transformation matrix which can be set equal to identity matrix, $T=I$.

- Step 4: The last step includes the extraction of matrices A_d and C (eqs.2.4) by taking advantage of the observability matrix, using its shift invariance property. So, finally, the matrices that characterize the linear, time-invariant system are obtained from :

$$\begin{aligned} A_d &= \underline{O}^+ O(m+1: mh, :) \\ C &= O(1: m, :) \end{aligned} \quad (2.10)$$

where \underline{O}^+ is the pseudoinverse of the matrix O without the last block m rows.

Once the above matrices of the system are computed, the extraction of the modal parameters is able to be done directly.

2.2.2. Modal Parameters

After the discrete time state-space model (2.4) has been identified, a modal model can be obtained by the correlation between the identified matrix A_d :

$$A_d = e^{A\Delta t} \quad (2.11)$$

and the continuous-time state matrix A :

$$A = \frac{1}{\Delta t} \ln A_d \quad (2.12)$$

By acquiring the *eigenvalues* l of A (the continuous state-space matrix), which are in the form of complex conjugate pairs if the system is properly constrained, it is possible to obtain the **eigenfrequencies** ω_n and the **damping ratios** ζ_n of the structure:

$$\omega_n = |l| \quad \text{and} \quad \zeta_n = -\text{Re}(l)/\omega_n \quad (2.13)$$

Finally, the **modeshapes**, which are in correspondence to the sensor locations are the columns of a matrix named $\Phi \in \mathbb{C}^{m \times n}$ and are extracted from the complex *eigenvectors* of A , $\Psi \in \mathbb{C}^{n \times n}$, by the usage of the output matrix C in eqs. (2.4), defined in (2.10):

$$\Phi = C\Psi \quad (2.14)$$

2.2.3. User - defined parameters

The DD-SSI algorithm is highly affected by the choice of some user defined parameters and this fact makes them very important for the efficiency of the algorithm. The main parameters are these, which form the size of the Hankel matrix: i, j, g, h . Some other parameters can be the choice of the minimum and the maximum model order, between which the modes are computed. The number of modes to be identified is determined by the model order n , which is the size of the state-space matrices, so the appropriate definition of the model's order range plays an important role to the acquired results.

As far as the parameters of the Hankel matrix are concerned, there are several constraints [3], that have to be taken into account for the best operation of the algorithm. The conditions that must be considered for the Hankel matrix parameters are:

$$1. \quad i+j-1 \leq s \Rightarrow j \leq s-i+1 \quad (2.15)$$

where s : the number of samples in the time history

$$2. \quad \frac{i}{f_s} f_1 > n_c \Rightarrow i > n_c \frac{f_s}{f_1} \quad (2.16)$$

where n_c : cycles of the lowest frequency f_1 and f_s : the sampling frequency

$$3. \quad g+h=i \quad (2.17)$$

Furthermore, this Hankel matrix parameters have their own *minimum values* that are acceptable. If we assume that there must be only one cycle of the lowest structural frequency, so $n_c=1$, then the lowest value of parameter i should be:

$$i_{min} = \frac{f_s}{f_1} \quad (2.18)$$

having a value lower than that, would mean that there is not even a full cycle of the lowest structural frequency in the segment of time histories and this would have a negative effect on finding an accurate estimation of the lower frequencies. However, it should be noted that although large values of i offer a better handling of the information at the same time more spurious modes are produced and also the computational effort becomes substantially bigger (fig.2.3). Moreover, the value of the parameter i defines the amount of time that is taken into account from the measurements. For instance, if the sampling time of a measurement is equal to $dt=0.01 \text{ sec}$ and the chosen value of the parameter i is $i=100$, then the size of the time segment used for the modal analysis by the DD-SSI, is $i*dt=100*0.01=10\text{sec}$. Despite that, a selection of a high value for the parameter i does not promise the acquirement of better results, although more samples are entered, as we will discuss further.

As far as the lowest value of h is concerned, the restriction is :

$$h_{min} = \max\left(\frac{f_1}{f_s} n_c, 0.5i\right) \quad (2.19)$$

The parameters h, g define whether the Hankel matrix is symmetric or not . Different cases according to this are distinguished:

1. $h=0.5i$: symmetric . The number of block rows of Y_f and Y_p are equal and the problem presents only one solution as it is determined.
2. $h<0.5i$: the past output subpartition Y_p has more rows than the future one Y_f and this makes the problem undetermined and there is not enough information to obtain a unique solution.
3. $h>0.5i$: the future output subpartition Y_f has more rows than the past one, Y_p and this makes the problem overdetermined .

In the current thesis, the algorithm DDSSI has been used only for the case that the Hankel matrix is symmetric, so $h=0.5i= g$ (since $g = i - h$). So the minimum value of g is decided by the minimum value of h .

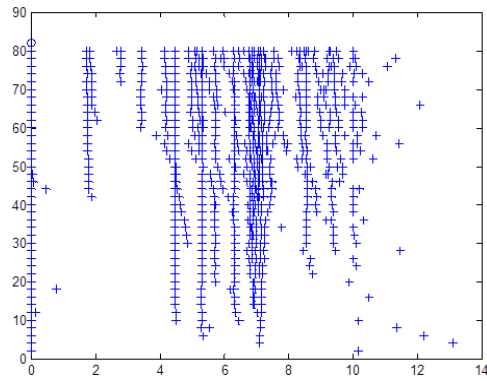
Finally, the minimum value of j could be defined as :

$$j \geq i \frac{h}{g} \quad (2.20)$$

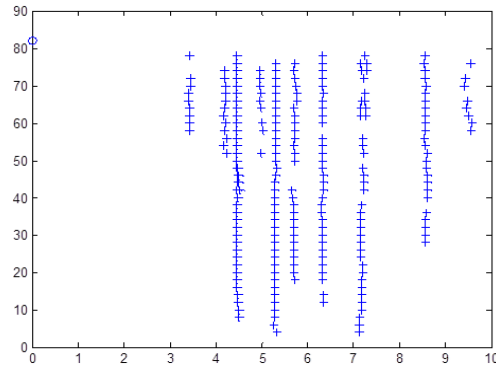
The best solution for the selection of j is to choose the maximum available value for it, because it helps in the reduction of the measurement noise. The disadvantage of a

large value for j is the increase in the computational effort. Therefore, a good choice of the parameter j should be a good trade-off between these two aspects. Also, it should be noted that in the block Hankel matrices, the number of block rows and columns are chosen in such a way by the user so that $j \gg 2i$ [5]. The effect on the results of the DDSSI algorithm of different values of i is presented in the following figures.

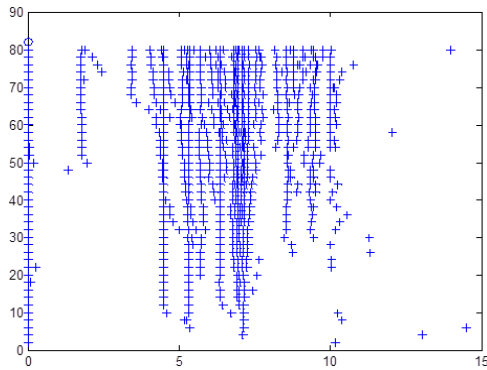
The following examples concern a standard value of j equal to the whole number of the available measurements minus the parameter i ($j = \text{measurements} - i$) with a varying value of i each time. We start from a low value of i until we reach a big enough value of it and notice the different changes.



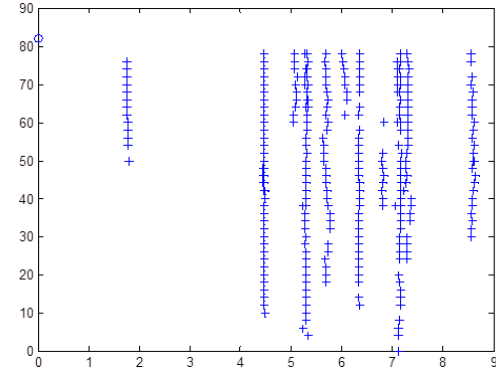
(a)



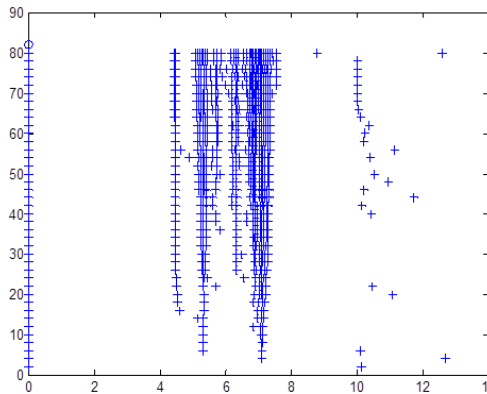
(b)



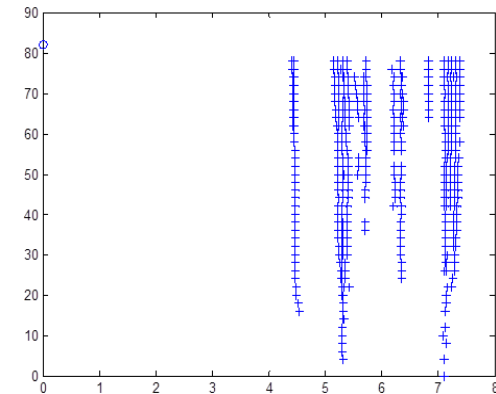
(c)



(d)



(e)



(f)

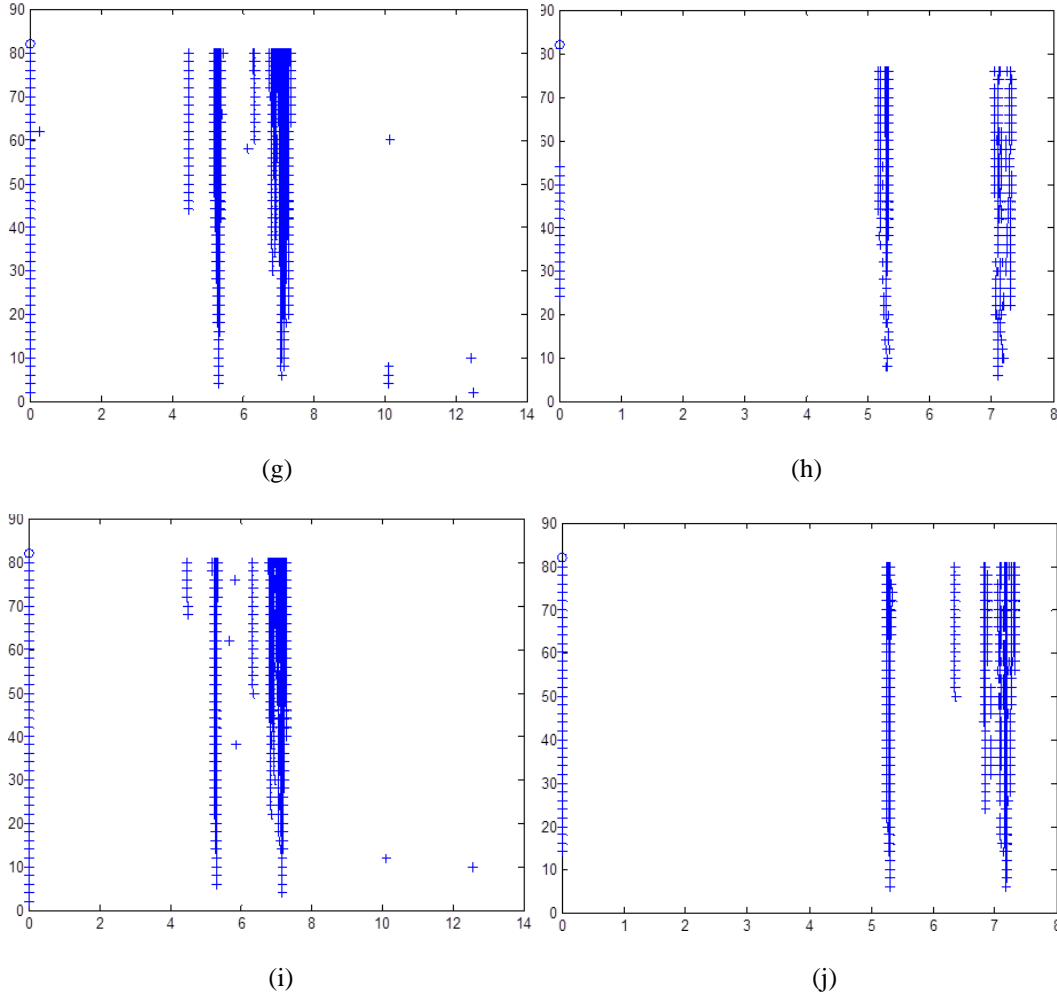


Figure 2.3. The figures above show the unfiltered DDSSI output (left figure) and the filtered and clustered modes output(right figure) for different values of parameter i . The vertical axes represent the model order and horizontal ones the modal frequencies. Figures (a),(b) are for $i=80$, (c),(d) are for $i=100$, (e),(f) are for $i=500$, (g),(h) are for $i=2000$ and (i),(j) are for $i=5000$.

By observing the figures in fig.2.3 we can easily assume that as the value of i gets higher more spurious modes tend to be produced by the DD-SSI algorithm and in the clustered results the modes, which survive, don't offer a clear picture of the identified frequencies, because there are too many modes around a specific value of frequency. On the contrary, for lower values of i ($i=80$ or $i=100$) the modes produced by the DD-SSI algorithm are less and the ones that remain from the clustering method, which is still not presented, show clearly which frequencies are the modal frequencies. In addition, the computational effort rises as the value of i increases. Another observation that can be made is that for $i=5000$, $2i=10000$, and $j=24000-5000=19000$, so j is not $\gg 2i$, the mode around 4.5 Hz does not "survive" although it is clearly produced for the previous runs with lower values of i . So we can conclude that for a higher value of i the results don't get better.

As already mentioned, the other user-defined parameters that the DD-SSI algorithm requires, is the system's model order, maximum and minimum, between which the modes are computed. Knowledge of a good model order is requested for modal analysis. The number of block rows i , determines the maximum number of orders that

can be calculated [4]. By practical experience it is known that it is more useful to over-specify the model order and then eliminate the spurious modes that are produced. However, it is almost impossible to predict which model order range will produce the desired DD-SSI output. Since the model order is linked to the number of the identified modes, it's easily understood that the lower bound of the system model order (n_{\min}) should be at least the number of the expected modes to be identified. The upper bound (n_{\max}) should be high enough, so that the weakly excited modes can be successfully identified.

User- defined parameters	Definition
i	Hankel matrix rows
j	Hankel matrix columns
g	rows of the past output subpartition Y_p
h	rows of the future output subpartition Y_f
nmin,nmax	minimum and maximum model orders

Table 2.2. User-defined parameters for the DD-SSI algorithm

3. Automated interpretation of DD-SSI output

The total number of modes generated by the DD-SSI algorithm does not represent the reality. Unfiltered DD-SSI results are shown in fig.3.1. It is essential to develop a method, so that the real modes are distinguished from the mathematical-spurious ones. This method is the creation of a stabilization diagram [10], using clustering techniques, which consists of modes plotted for various model orders. Due to the large amount of collected data from online structural monitoring, a manual interpretation of real modes is impossible. Therefore, the solution is the automation of such a process. In this thesis, an automated clustering technique is used so that the production of the stabilization diagrams is accomplished without needing the user to interfere.

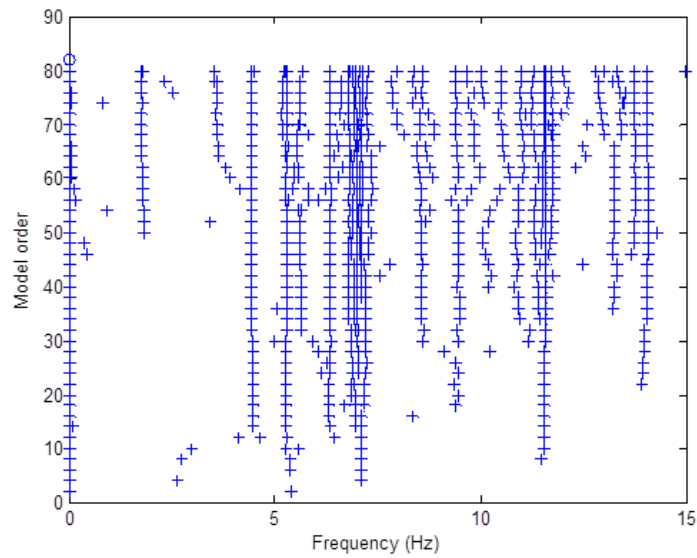


Figure 3.1. The output of the DD-SSI algorithm without being filtered.

The clustering procedure consists of three stages [6]. The first one is a pre-filtering of the modes using some *criteria*, the second stage is a *clustering* procedure and the third one is a *cluster merging* procedure. After the first stage, the modes are cleaned according to these criteria and as a result fewer modes remain. Afterwards, the modes pass through a clustering technique, which uses some self-adapting criteria that automatically group the physical modes into larger clusters and diffuse the spurious modes to smaller ones. The cluster containing elements less than a number, which is the threshold, will be identified as spurious and the modes it contains will be eliminated from the DD-SSI output. The cluster merging procedure, which is also developed and arranged after the clustering methodology, makes sure that the acquired results are more robust and offers a further elimination of the clusters, which include a fewer number of modes and this indicates that they are spurious.

3.1. Pre-filtering criteria

Since the output of the DD-SSI algorithm is acquired, as mentioned above, there must take place a pre-filtering of the produced modes because certain spurious modes can be effectively removed at an earlier stage and alleviate the computational burden. This filtering of the modes is achieved by using three conditions, which determine whether the modes are physical or mathematical based on frequencies, damping ratios and modeshapes. These conditions are the criteria, which are presented below:

1. The damping ratio ζ_n

If the damping ratio [8] of a mode is not within the range of 0–10% it is considered to be spurious. Negative damping ratios and high damping ratios suggest that the mode is certainly non-physical. So we keep all the modes that satisfy the following condition:

$$0 < \zeta_n < 0.10 \quad (3.1)$$

2. Modal Phase Collinearity (MPC)

The complexity of a single mode is investigated by the modal phase collinearity (MPC) [7]. For classical normal (real) modes, all locations on the structure vibrate exactly in-phase or out-of-phase with one another. MPC quantifies the degree of monophase behaviour by comparing the relative size of the eigenvalues of the variance- covariance matrix.

Let's assume that we have mode k and Φ_k is the identified complex modeshape corresponding to the mode k . Calculating the variance and covariance of the real and imaginary parts :

$$\begin{aligned} S_{xx} &= \text{Re}(\Phi_k)^T \text{Re}(\Phi_k) \\ S_{yy} &= \text{Im}(\Phi_k)^T \text{Im}(\Phi_k) \\ S_{xy} &= \text{Re}(\Phi_k)^T \text{Im}(\Phi_k) \end{aligned} \quad (3.2)$$

Letting

$$\eta = \frac{S_{xx} + S_{yy}}{2S_{xy}} \quad (3.3)$$

the eigenvalues of the variance-covariance matrix are :

$$\lambda_1 = \frac{S_{xx} + S_{yy}}{2} + S_{xy} \sqrt{\eta^2 + 1} \quad (3.4)$$

$$\lambda_2 = \frac{S_{xx} + S_{yy}}{2} - S_{xy}\sqrt{\eta^2 + 1}$$

MPC for mode k is then defined as follows:

$$MPC_k = \left(\frac{\lambda_1 - \lambda_2}{\lambda_1 + \lambda_2}\right)^2 \quad (3.5)$$

The MPC value can be between 0 and 1, with the first indicating a completely spurious mode and the latter a physical mode. In the current thesis, a threshold for MPC is proposed, $\text{thres} = 0.8$. Modes with higher values than that will be considered as possibly physical. In any case, this threshold should be adjusted by the user, according to the desired results. It might be looser or stricter than desired.

3. Modal frequencies

Higher frequencies, usually, do not include eigenfrequencies, so the frequencies [8] of the mode that are not between zero and half of the sampling frequency, f_s , should be immediately eliminated. Therefore, the modes that are qualified to the next level of processing satisfy the following condition:

$$0 < f_{mode} < \frac{f_s}{2} \quad (3.6)$$

Once more, the threshold for the higher frequency level can be adjusted by the user if it is considered that less than half of the sampling frequency is needed.

To sum up, the pre – filtering criteria are the ones depicted in the next table:

Pre - filtering Criteria	
1.	$0 < \zeta_{mode} < 0.10$
2.	$MPC_{mode} > \text{thres}$
3.	$0 < f_{mode} < \frac{f_s}{2}$

Table 3.1.The pre- filtering criteria

There are no standard threshold values under ambient vibration testing. Deciding a value for the thresholds relies on the noise conditions, the linear or non-linear behavior of the structure and the quality of the conducted measurements. Also, the expected dynamic characteristics of the structure play a major role in the selection and adaptation of the pre-filtering criteria. Generally, when dealing with clear data input it is acceptable to use strict thresholds whereas not so well acquired data require looser values for the thresholds.

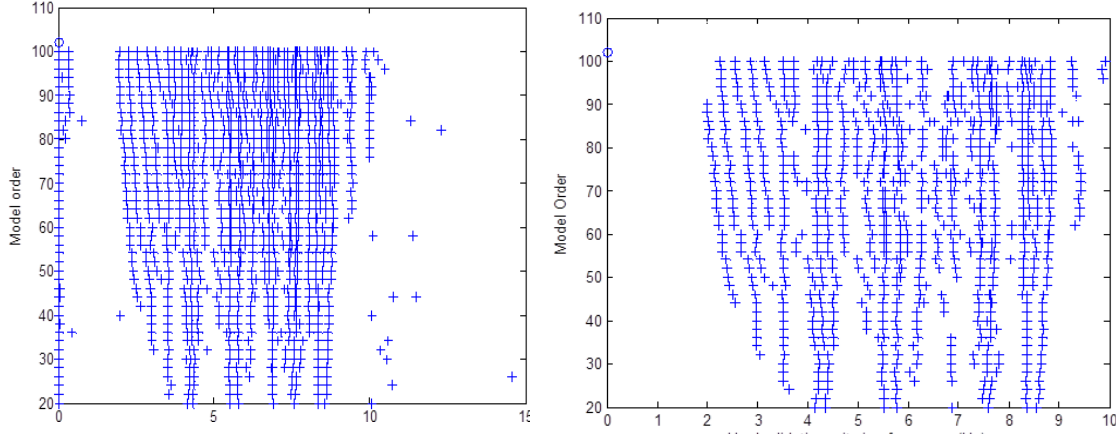


Figure 3.2. The modes after the application of the pre-filtering criteria (right figure) in comparison with the non-filtered modes of the DD-SSI output (left figure).

The figures above show the unfiltered results of the DD-SSI algorithm and the results after the application of the pre-filtering criteria, presented in Table 3.1. It is obvious that the modes, which didn't satisfy these criteria have been excluded. A clearer view of the modes is provided after the application of pre-filtering but still the clustering procedure will reveal the real ones.

3.2. Clustering

The previously presented pre – filtering criteria are used for the elimination of some spurious modes before the clustering procedure begins, so that the computational effort is reduced. However, in order to further remove the spurious modes, a clustering procedure is adopted. This clustering methodology takes a mode from a certain model order, which remains from the pre-filtering section and compares it with all the modes of the next model order, until all orders are covered, and arranges the modes that satisfy certain conditions, concerning the modal frequencies, damping ratios and the modeshapes, into different clusters. The thresholds that concern the modal parameters automatically change according to a proposed range, based on statistics [11]. As a result, clusters with real modes and spurious ones are produced and are distinguished by their size. The clusters with the real modes consist of a bigger number of modes whereas the spurious modes are scattered in small clusters.

The input for the clustering procedure is actually the filtered results of the DD-SSI output. First of all, the definition of the Modal Assurance Criterion (MAC) should be given. The modal assurance criterion (MAC) compares the similarity between the unscaled modeshapes Φ_j and Φ_k of modes j and k , respectively, as [8]:

$$MAC(\Phi_j, \Phi_k) = \frac{|\{\Phi_j\}^H \{\Phi_k\}|^2}{(\{\Phi_j\}^H \{\Phi_j\})(\{\Phi_k\}^H \{\Phi_k\})} \quad (3.7)$$

where $\{\Phi_j\}^H$ denotes the Hermitian of $\{\Phi_j\}$. In mathematics, a **Hermitian matrix** (or **self-adjoint matrix**) is a complex square matrix that is equal to its own conjugate transpose. The value of MAC lies between 0 and 1, where 1 indicates the maximum similarity between two modes.

As mentioned above, during the clustering procedure several thresholds are used that consider the frequencies, T_f , the damping ratios, T_z , the MAC, T_{MAC} and the MPC, T_{MPC} . These thresholds are applied to four validation criteria[8], which are presented below:

1. The dimensionless distance between the frequencies of two compared modes, k, m :

$$df = \frac{|f_k - f_m|}{\max(f_k, f_m)} \quad (3.8)$$

2. The dimensionless distance between the frequencies of two random modes, k, m :

$$dz = \frac{|\zeta_k - \zeta_m|}{\max(\zeta_k, \zeta_m)} \quad (3.9)$$

3. The MAC between two modeshape vectors of two modes, defined in eq.(3.7).
4. The Modal Phase Collinearity, which is defined in eq. (3.5).

The ideal values of the validation criteria that indicate a physical mode according to literature[8] can be defined as:

Modal parameters	Ideal value for a real mode
df	0
dz	0
MAC	1
MPC	1

Table 3.2. The ideal clustering validation criteria of frequency, damping ratio, MAC and MPC

The above criteria are updated each time the number of elements in the current cluster exceeds a satisfying number in correlation with the number of the model orders. The interpretation of the DD-SSI output stabilization diagram is automated and no

intervention by the user is needed. The steps of the hierarchical clustering methodology [6] are described in the following paragraph.

The modes that remained from the pre-filtering conditions are collected into clusters, and the mutual distance between two random modes, i and k , is computed by:

$$d_f = d(f_i, f_k) + 1 - MAC(\Phi_i, \Phi_k) \quad (3.10)$$

Once the mode with the minimum distance has been identified then it is collected into the cluster. Each cluster is combined with the closest mode into a single cluster and the average distance between the elements are computed as the new modal properties that characterize the cluster and are to be compared with the modal properties of the other modes, so that the next closest mode is located. This procedure keeps going on until all modes are collected into clusters. During the clustering, the validation criteria that concern the mode acceptance into a cluster change whenever a threshold for the mode number inside a cluster is exceeded.

The clustering strategy is illustrated with an example, shown in fig.3.3. A random mode i , which is in a red circle, is characterized by three modal properties: the modal frequency, the modal damping ratio and the modeshape. The modal frequency is depicted on the diagram in accordance with the model orders. So, what actually happens during clustering is that a mode's modal properties are compared to the modal properties of every other mode in the successive model orders, which are depicted in yellow circles in fig.3.3., and if certain criteria, described step by step above, are met, then the mode becomes a member of a cluster. This process is repeated for every ungrouped mode until all of them are compared to each other and allocated to a group. Consequently, the procedure ends when we reach the maximum model order, which can also be seen in fig.3.3.

Furthermore, another example of the results of the clustering procedure is presented in fig.3.4, so that the effect of clustering in the modal identification process is made clear. In fig.3.4, the output, after the statistics - based clustering procedure is applied, is shown next to the graph of the hard validation criteria output, which can also be seen in fig.3.2, for an easier comparison. As we can see, the results after the clustering give a sufficient view of which, actually, the real modes are, compared to the vague picture we get from the hard validation criteria alone. For example, after the clustering procedure is conducted, it can be easily concluded that there is a mode at around 3.5Hz, since the modes, at this frequency, have similar modal properties and are persistent(fig3.4).

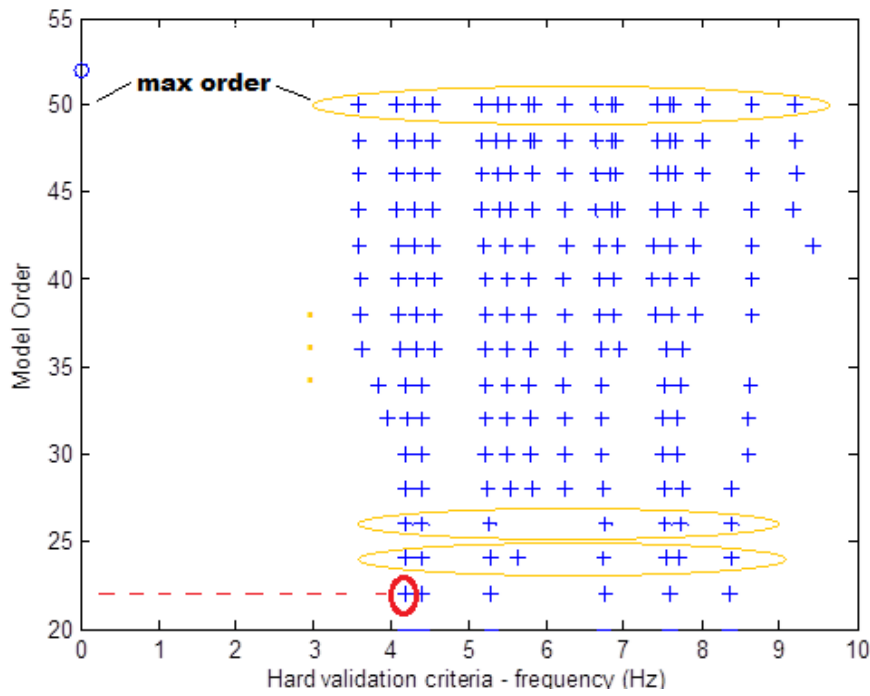


Figure 3.3. A random mode i (in the red circle) and the modes in the successive model orders, to which it is compared during the clustering procedure, circled with yellow colour.

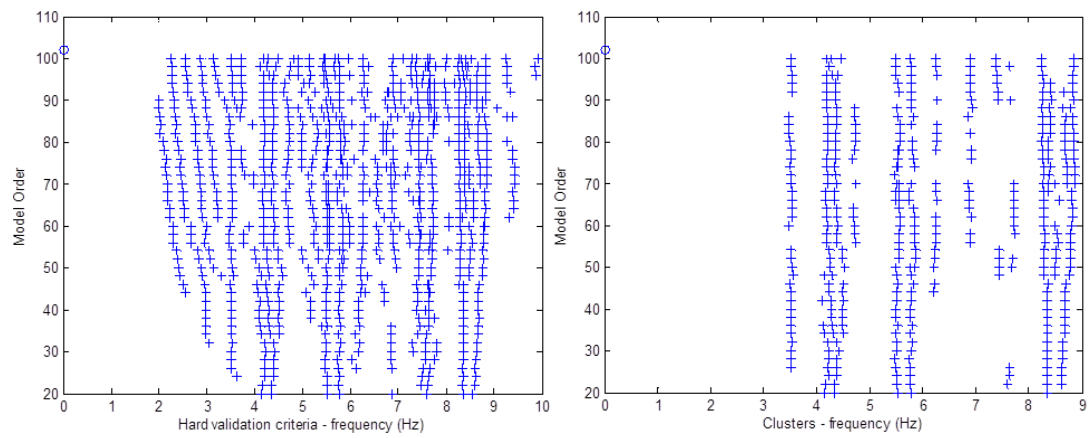


Figure 3.4. On the left figure we see the modes after the hard validation criteria are applied and on the right figure we see the clustered modes, after the statistics - based clustering procedure is applied.

After the above clustering procedure all of the modes are merged into bigger clusters based on their similar properties. Although the number of mathematical (spurious) modes is significantly reduced after the elimination of the clusters containing few modes, a few clusters consisting of spurious modes may possibly pass through the threshold. The cluster merging process will further merge the physical clusters into larger ones and eliminate the smaller spurious clusters.

The merging routine is based on the confidence interval of the estimations of frequencies. Every cluster is characterized by two limits of the confidence intervals of their mean frequency, damping ratio and MPC values. Certain criteria around these measurements are applied in order to determine whether or not the clusters will become merged.

At the end of the clustering merging procedure another step takes place. Since the clusters are merged into new, bigger ones, the smaller clusters represent the spurious modes. Consequently, a new threshold is adopted and the clusters, which contain less modes than half of the total model order become eliminated. In that way we get the final stable modes result, without any intervention from the user. A picture of the automated stabilization diagram, after the cluster merging, is illustrated in the following figures(fig3.5).

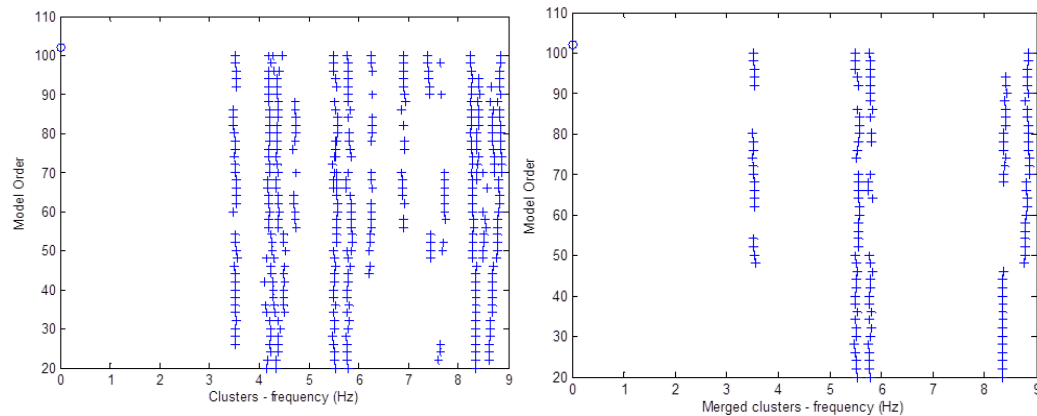


Figure 3.5. The clustered modes are on the left figure and the merged clusters on the right figure, with the elimination of the ones that have less modes than 50% of the total model order.

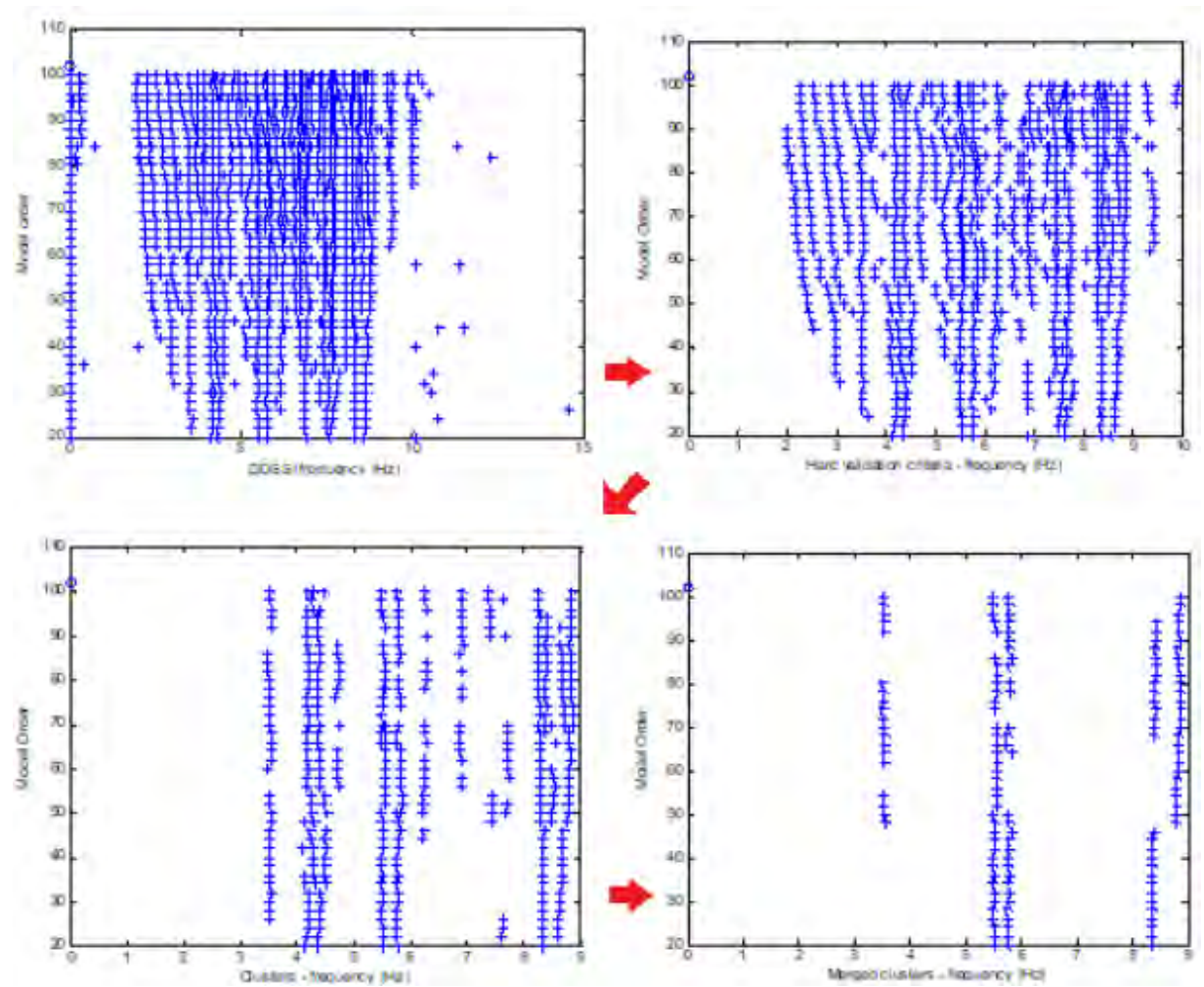


Figure 3.6. A summary of the results of the procedures that the modes go through. Pre- filtering criteria (up right)-Statistics-based clustering (down left) - Cluster merging (down right).

To sum up, the above figures illustrate the step by step elimination of the spurious modes. At first, we notice a mild clearance of the modes after the pre - filtering criteria are applied and as the clustering takes place, we get a better view of the possible physical modes. Finally, after the cluster merging and the elimination of the clusters with less than half of the total model order, we get the stabilized values for the eigenfrequencies. So, through the above procedures we manage to automate the physical modes identification and get the stabilization diagram without user intervention.

4. Software for modal analysis

The developed software

Within this thesis, software was developed for experimental output-only (ambient) modal analysis. The followed methodology can be depicted in the following simplified flow diagram (fig.4.1). The code requires only some input variables from the user and gives automatically the modal identification results. More information about the developed MATLAB code is presented in Appendix A.

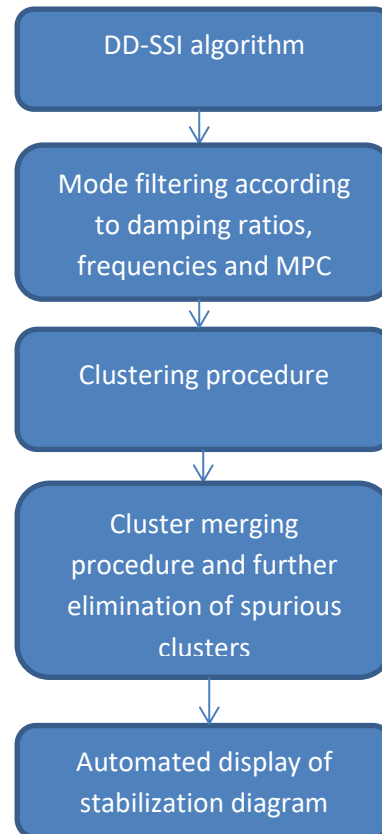


Figure 4.1. Simplified flowchart of the strategy used in the developed software

However, the results of two more software have been reported in this thesis, in order to compare and check the robustness of the results provided by the developed software, which is based on the DD-SSI algorithm and the clustering techniques and produces automated stabilization diagrams. The theory on which the other two softwares are based on is presented below.

Software 1

The first software [9] for Ambient (Output-only) Modal Identification uses a recently proposed Bayesian methodology in order to estimate the modal frequencies, mode shapes, damping ratios, and their uncertainties for each sensor configuration. The method is based on the Fast Fourier Transform (FFT) of the acceleration signals in specific frequency bands of interest. The software also includes other modules for data insertion, pre-processing of the signals (for quality-checking of the

measurements and for the specification of the frequency bands of interest), and post-processing of the results (mainly for performing mode shape assembly). The software also supports the insertion of the geometry of the measured structure, for visual representation of the mode shapes in the post-processing module. The modeshape assembly methodology is similar to the one presented in [14].

Software 2

The second software used, Software 2 [15], includes a strong core for the analysis of the signal that comes from the structure, which is furtherly processed with various methods for modal identification, in order to compute the desired modal properties. The user of software 2 chooses the measured signals (accelerations), which come from a net of sensors on the structure, transfers them to the field of frequency (FFT, PSD), depending on the kind of the loading and assigns the range of the frequencies ,in which the identification will be done. Furthermore, the user chooses the number of modes, which he wants to determine and gives estimations for the value of them. This is done either with the help of the stabilization diagrams, which are computed, or with the observation of the PSD diagram. Finally, after the user chooses the methodology that will be used during the identification, he starts the algorithm, which computes the eigenfrequencies, the damping ratios and the modeshapes.

5. Applications

In the previous chapters 2 and 3, a presentation of the steps and methodology for the computation of the modes and the distinction of the real from the spurious ones is made. In this chapter, applications of the developed software, in real structures, will be presented. Although the software developed can be used in any civil, mechanical and aerospace structure, here the applications have to do with measurements acquired from bridges that exist and operate in Greece.

Since the formulation of the developed software has already been presented (chapter 4), let's move on to introduce the applications. The available input data has been extracted from vibration measurements on 3 bridges. One of them is the bridge of Metsovo in Egnatia Motorway. First of all, there should be made a quick reference to the method of monitoring and the equipment used for the vibration measurements. The measuring instruments used are some triaxial and uniaxial accelerometers, pictures of which can be seen in Figure 5.1. The sensors are synchronized with each other through a GPS module. The system is wireless (everything is powered by a battery) and can be easily moved from one location in the structure to another. These accelerometers are put throughout the deck of a bridge in different sensor set ups (configurations), so that all of it is covered. In every set up some of the sensors remain in the same position (reference sensors), in order to provide common measurement points amongst different configurations and enable the assembling of the total mode shape from partial mode shape components measured from the different configurations. An example of sensor configurations concerning the bridge of Metsovo is provided in Figures 5.2 and 5.3, where green points correspond to reference sensors and blue points correspond to the moving sensors of the specific sensor configuration [9]. Also in these figures we can see the assigned degrees of freedom (DOF) to each node of the bridge.



(a)



(b)

Figure 5.1.(a) A triaxial accelerometer (b) Uniaxial accelerometer, junction box, and unit including recorder, battery pack and GPS module (taken from [9])

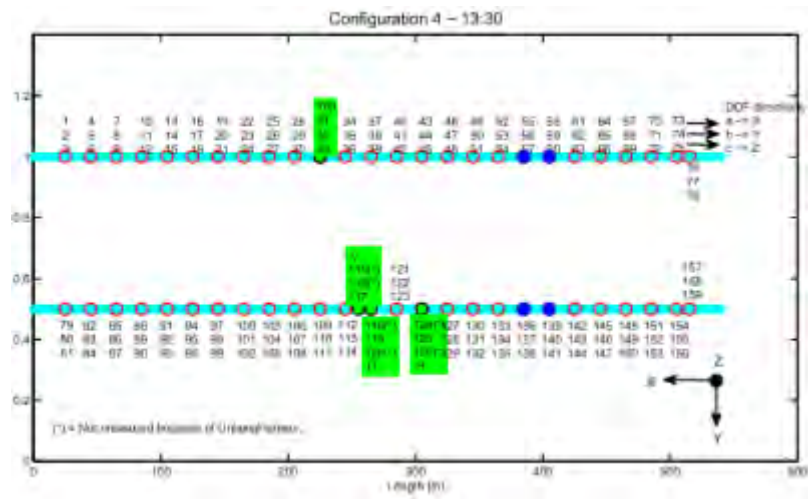


Figure 5.2. Sensor configuration 4 of the bridge of Metsovo (taken from [9])

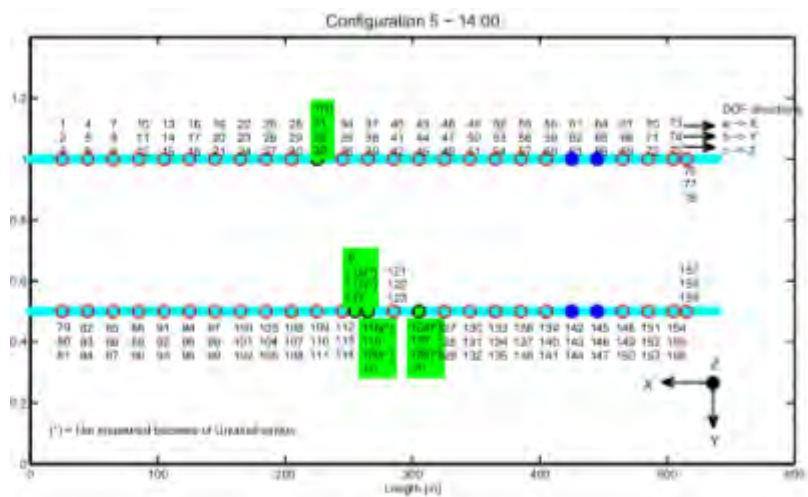


Figure 5.3. Sensor configuration 5 of the bridge of Metsovo (taken from [9])

The above figures demonstrate a good example of the way the measurements are made, so that the whole deck of the bridge is covered. To start with, in sensor configuration 4 (fig .5.2) there are three reference sensors in green and four moving sensors in blue. In configuration 5 (fig.5.3), the position of the blue points has changed to the neighboring unmeasured nodes. However, the reference sensors are kept in the same position. This happens throughout the whole experimental measurements. The reference sensors are kept still and the moving ones cover the area of the bridge by being put in different node positions each time. By the end of this procedure, information about the modal properties in all the locations of the bridge has been acquired and it can be utilized, in order to produce the assembled modeshape of the structure, using the methods proposed in [9] ,[14].

5.1. Bridge 1: Metsovo

The recorded responses of the bridge of Metsovo (fig 5.1.1) are mainly due to road traffic, which ranged from light vehicles to heavy trucks, and environmental excitation such as wind loading, which classifies this case as ambient (operational) modal identification. Multiple sets of repeated measurements had to be performed for accurate mode shape identification, given the limited number of sensors and the large length of the deck. Specifically, the entire length of the deck was covered in 13 sensor configurations, shown in Figure 5.1.2 with each configuration recording for 20 minutes at a sampling rate of 100 Hz [9].



Figure 5.1.1 The ravine bridge of Metsovo(taken from [9])

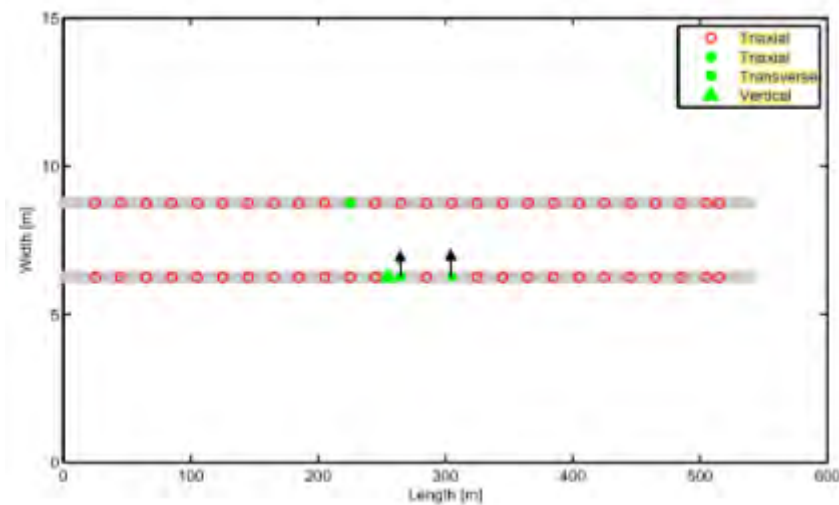


Figure 5.1.2 Measured locations on the bridge (reference sensors in green) (taken from [9])

The 13 available sensor configurations for the bridge of Metsovo, have been used as an input for the software developed using the DD-SSI and clustering techniques as well as for the already existing software1 .The acquired results are presented below.

5.1.1. Results from the developed software

Using the *developed software*, based on DD-SSI and clustering, the modal frequencies, damping ratios and the modeshapes are extracted. The modeshapes have not been plotted on the bridge's geometry, so there are no such results presented. The results for each sensor configuration, which are presented below, consist of the identified modal frequencies according to the model order of the system, depicted on the same graph as the PSD (Power Spectral Density). For the first configuration there are also the complex modeshapes given, acquired from the mean modeshapes of all the model orders, as an example of the output. Finally, the mean and standard deviation of all the identified modes, in every configuration are calculated and presented in Table 5.1.14, so that a comparison to the results acquired from *software 1*, can be made.

Configuration 1 (time 12:00)

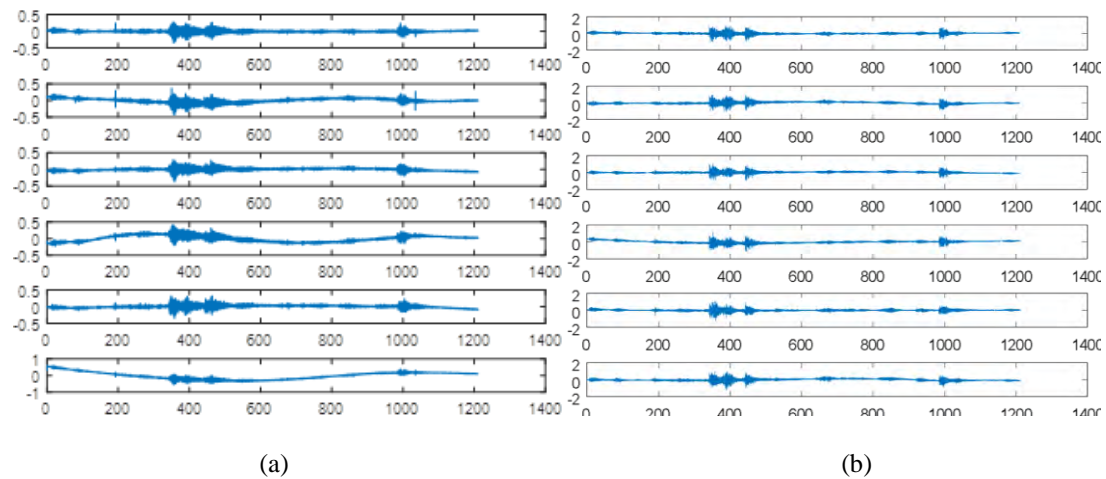


Figure 5.1.1. Representative active response time histories. The vertical axis is accelerations (m/s^2) and the horizontal is time (sec). (a) transverse (b) vertical sensors

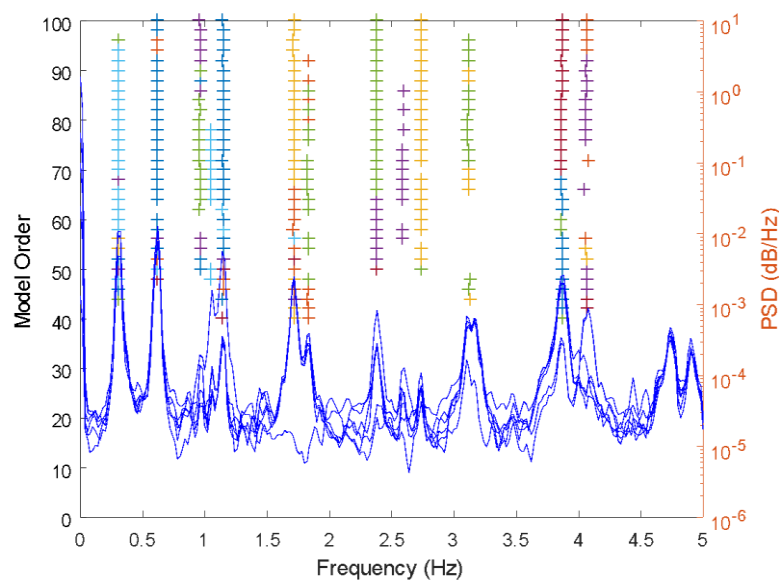


Figure 5.1.2. Modes after cluster merging depicted on the PSD- log scale (**transverse** sensors)

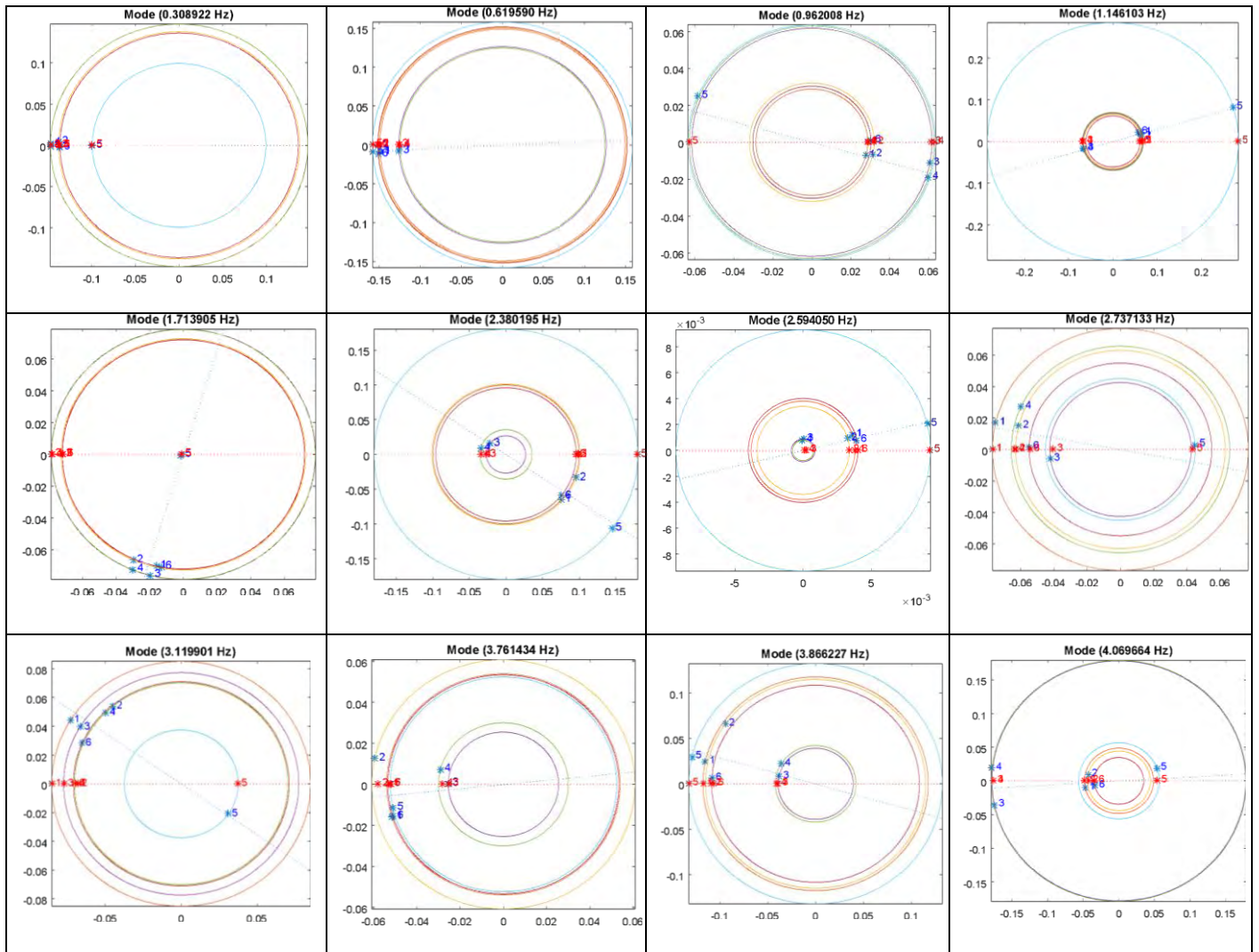


Figure 5.1.3. Complex modeshapes for the identified modes in the **transverse** direction

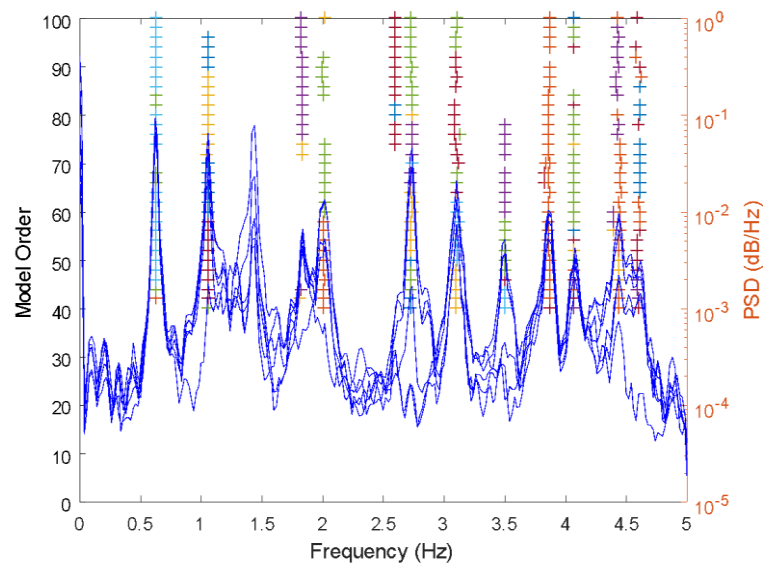


Figure 5.1.4. Modes after cluster merging depicted on the PSD-log scale (**vertical** sensors)

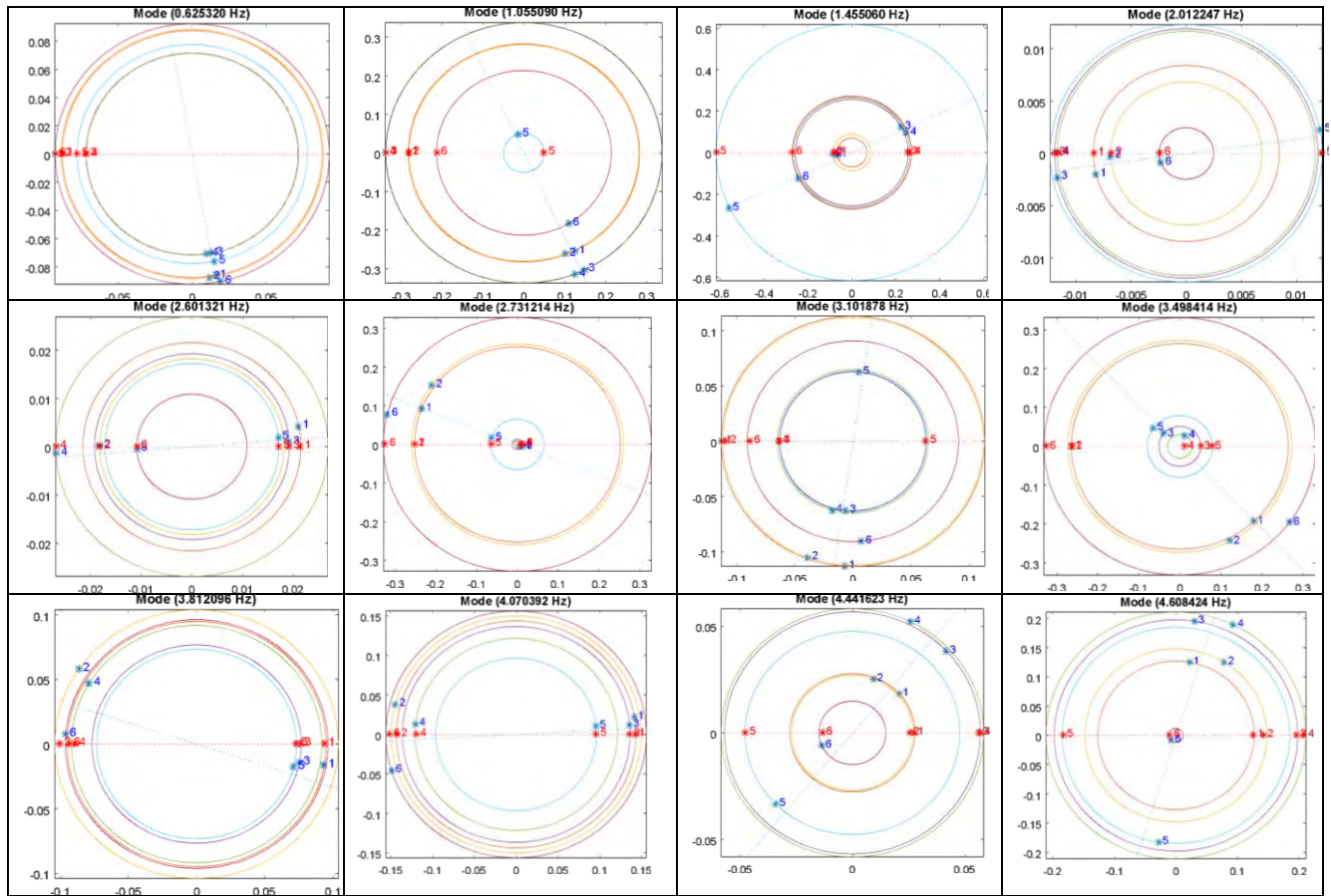


Figure 5.1.5. Complex modal shapes for the identified modes in the **vertical** direction.

Configuration 1 (12:00)			
Mode	Type	Frequency (Hz)	Damping ratio
1	Transverse	0.3089	0.0123
2	>>	0.6196	0.0086
3	>>	0.9620	0.0185
4	>>	1.1461	0.0070
5	>>	1.7139	0.0067
6	>>	2.3802	0.0091
7	>>	2.5940	0.0105
8	>>	2.7371	0.0039
9	>>	3.1199	0.0058
10	>>	3.7614	0.0118
11	>>	3.8662	0.0046
12	>>	4.0697	0.0051
13	Vertical	0.6253	0.0065
14	>>	1.0549	0.0098
15	>>	2.013	0.0080
16	>>	2.6013	0.0166
17	>>	2.73	0.00957
18	>>	3.10	0.00455
19	>>	3.49	0.00319
20	>>	3.86	0.00577
21	>>	4.07	0.00582
22	>>	4.44	0.00713

Table 5.1.1. Identified modes and damping ratios of configuration 1.

The results are presented in two groups, the group of the identified modes in the *transverse* direction and the group of the ones in the *vertical* direction. This is done

because some of the modes have very close value to each other ,so when all of the sensors are used as an input in the developed software, some of them do not survive. So, it is a better strategy to run the software independently for the transverse and the vertical direction, respectively. In the following result presentation no complex modeshapes are depicted but only the identified modes.

Configuration 2 (time 12:30)

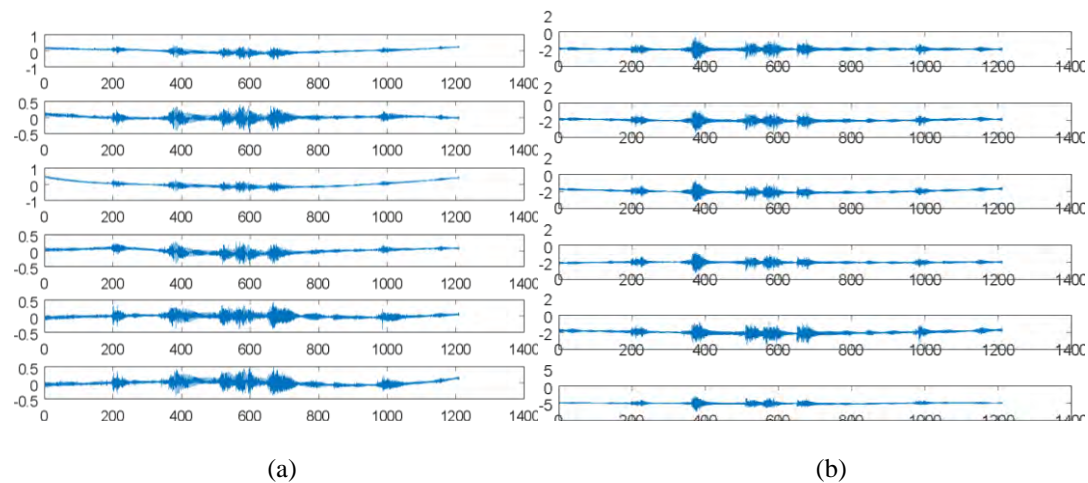


Figure 5.1.6. Active response time histories. The vertical axis is accelerations (m/s^2) and the horizontal is time (sec). (a) transverse (b) vertical sensors.

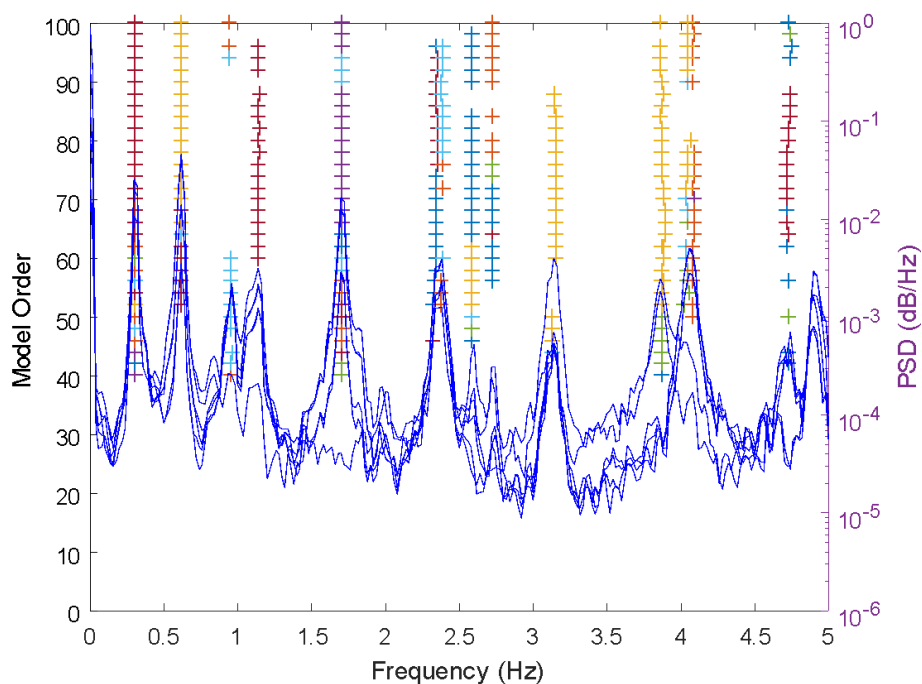


Figure 5.1.7. Modes after cluster merging depicted on the PSD-log scale (**transverse**)

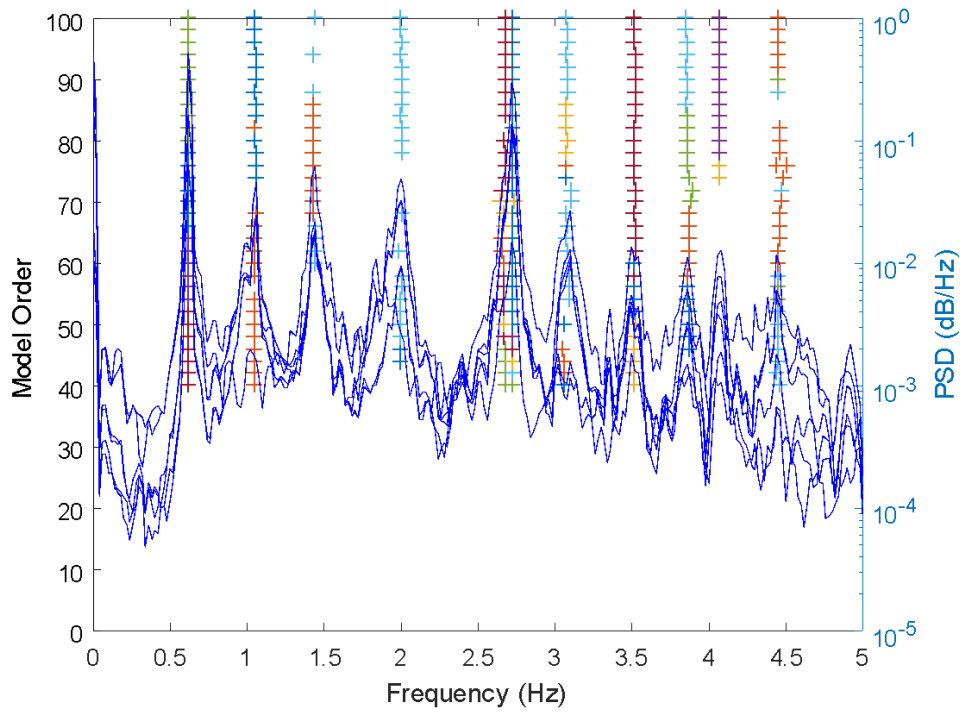


Figure5.1.8. Modes after cluster merging depicted on the PSD-log scale (**vertical**)

Configuration 2 (12:30)			
Mode	Type	Frequency (Hz)	Damping ratio
1	Transverse	0.3075	0.0114
2	>>	0.6189	0.0126
3	>>	0.9510	0.0146
4	>>	1.1437	0.0210
5	>>	1.7042	0.0066
6	>>	2.3486	0.0102
7	>>	2.59	0.0068
8	>>	2.7282	0.0051
9	>>	3.1476	0.0063
10	>>	3.8693	0.0074
11	>>	4.0415	0.0078
12	Vertical	0.6225	0.0053
13	>>	1.0508	0.0132
14	>>	1.4332	0.0165
15	>>	.2.0019	0.0150
16	>>	2.7253	0.0030
17	>>	3.0781	0.0090
18	>>	3.5143	0.0078
19	>>	3.8669	0.0083
20	>>	4.0695	0.0049
21	>>	4.45	0.0062

Table5.1.2.Identified modes and damping ratios of sensor configuration 2.

Configuration 3 (time 13:00)

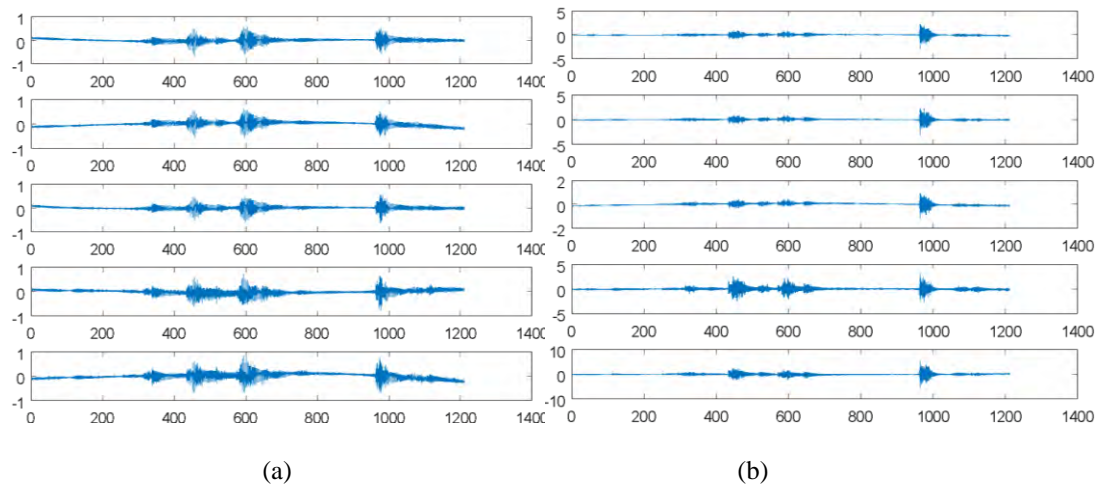


Figure 5.1.9. Active response time histories. The vertical axis is accelerations (m/s^2) and the horizontal is time (sec). (a) transverse (b) vertical sensors.

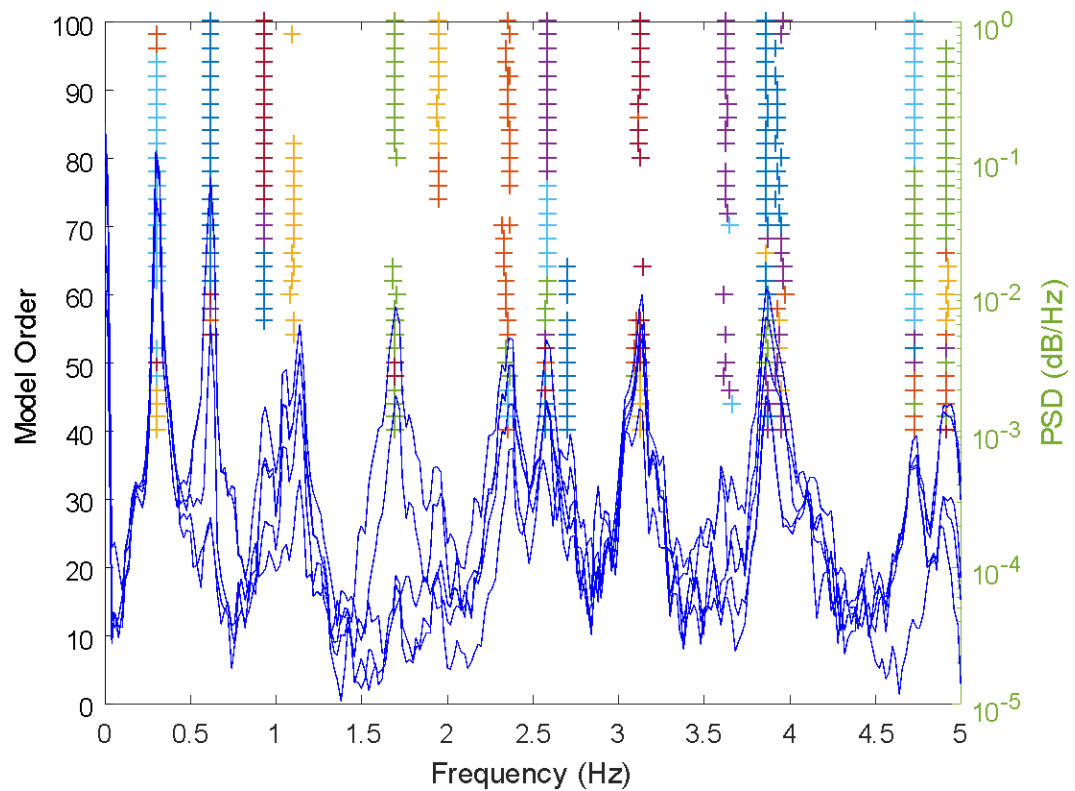


Figure 5.1.10. Modes after cluster merging depicted on the PSD-log scale (transverse)

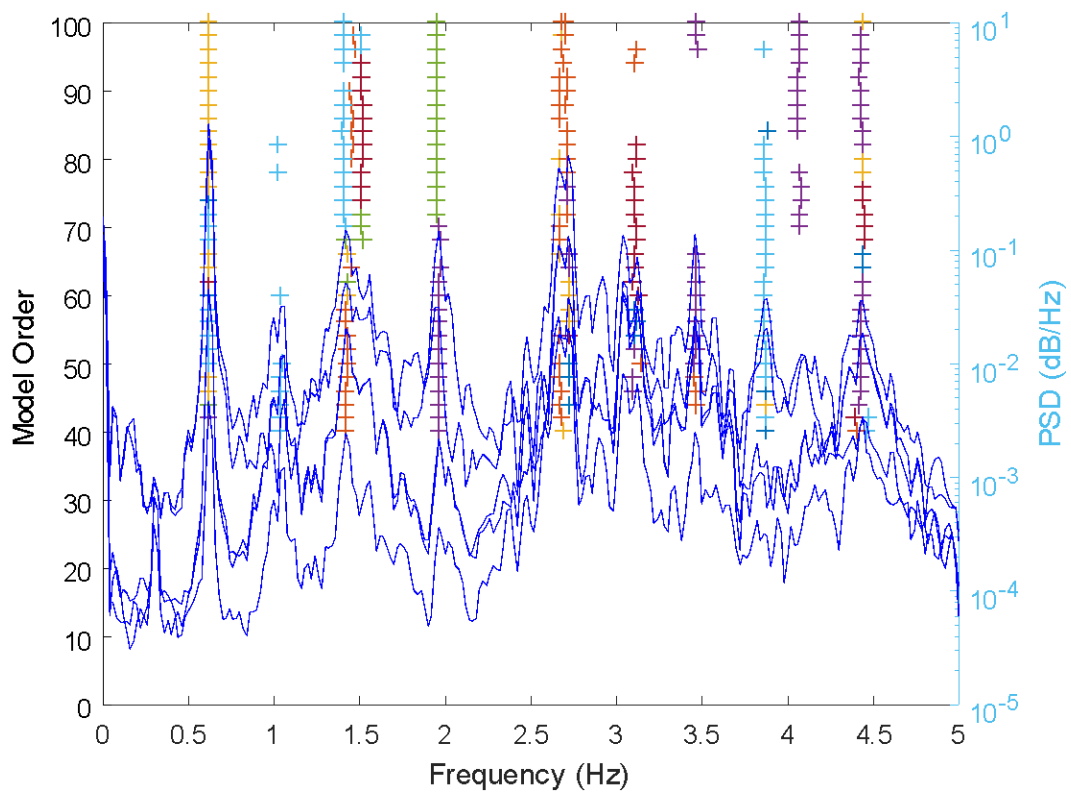


Figure5.1.11. Modes after cluster merging depicted on the PSD-log scale (vertical)

Configuration 3 (13:00)			
Mode	Type	Frequency (Hz)	Damping ratio
1	Transverse	0.3059	0.0096
2	>>	0.6185	0.0079
3	>>	0.9297	0.0252
4	>>	1.1053	0.025
5	>>	1.6966	0.011
6	>>	2.357	0.0160
7	>>	2.5787	0.0049
8	>>	2.6997	0.0068
9	>>	3.1314	0.0034
10	>>	3.6349	0.0079
11	>>	3.8657	0.0051
12	Vertical	0.6232	0.0040
13	>>	1.0347	0.0247
14	>>	1.4217	0.0191
15	>>	1.9606	0.0085
16	>>	2.6724	0.0049
17	>>	3.1107	0.0175
18	>>	3.4657	0.0032
19	>>	3.8679	0.0057
20	>>	4.0672	0.0056
21	>>	4.4352	0.0115

Table5.1.3. Identified modes and damping ratios of sensor configuration 3.

Configuration 4 (time 13:30)

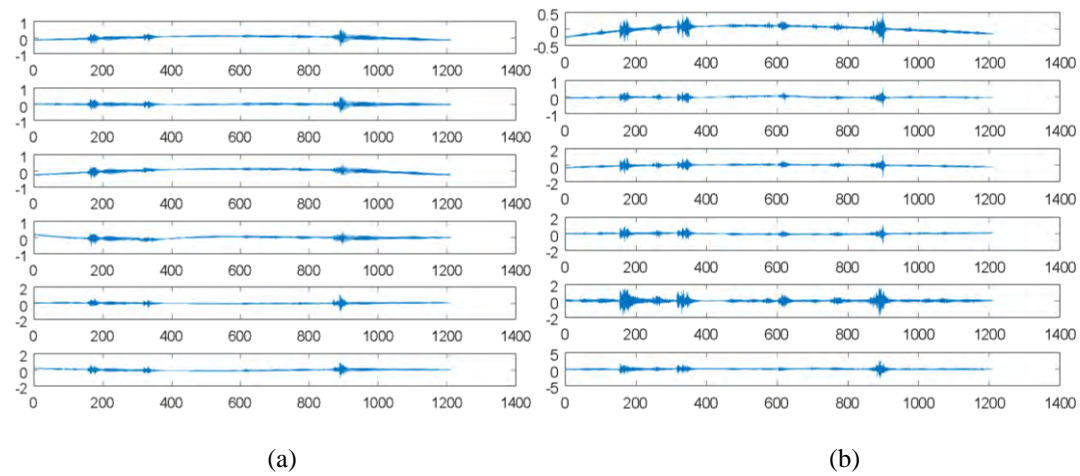


Figure 5.1.12. Active response time histories. The vertical axis is accelerations (m/s^2) and the horizontal is time (sec). (a) transverse (b) vertical sensors.

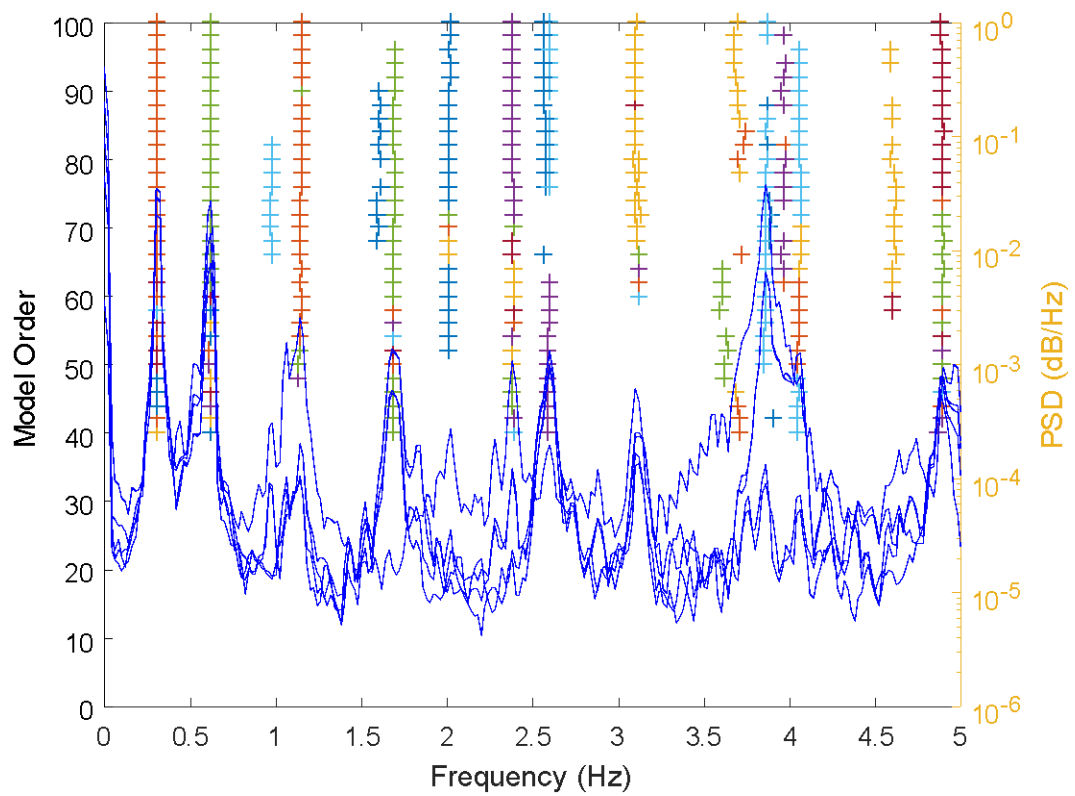


Figure 5.1.13. Modes after cluster merging depicted on the PSD-log scale (**transverse**)

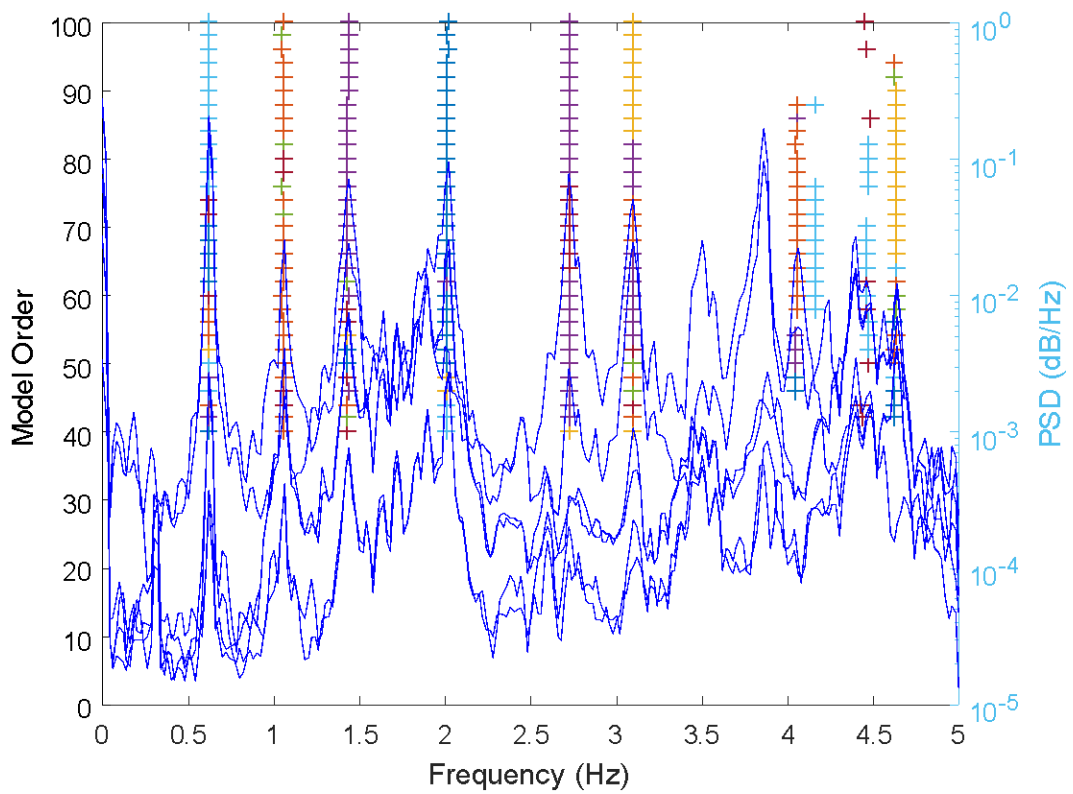


Figure5.1.14. Modes after cluster merging depicted on the PSD-log scale (**vertical**)

Configuration 4 (13:30)			
Mode	Type	Frequency (Hz)	Damping ratio
1	Transverse	0.3088	0.0079
2	>>	0.6138	0.0068
3	>>	0.9732	0.0287
4	>>	1.1348	0.0159
5	>>	1.6869	0.0080
6	>>	2.3808	0.0079
7	>>	2.5910	0.0058
8	>>	2.7353	0.0109
9	>>	3.12	0.0055
10	>>	3.6108	0.0067
11	>>	3.8570	0.0029
12	>>	4.0527	0.0027
13	Vertical	0.6234	0.005
14	>>	1.054	0.0132
15	>>	1.4341	0.0162
16	>>	2.0127	0.0069
17	>>	2.729	0.0063
18	>>	3.0937	0.0056
19	>>	4.0509	0.005
20	>>	4.1628	0.0042
21	>>	4.4547	0.0087
22	>>	4.6327	0.0047

Table5.1.4. Identified modes and damping ratios of sensor configuration 4.

Configuration 5 (time 14:00)

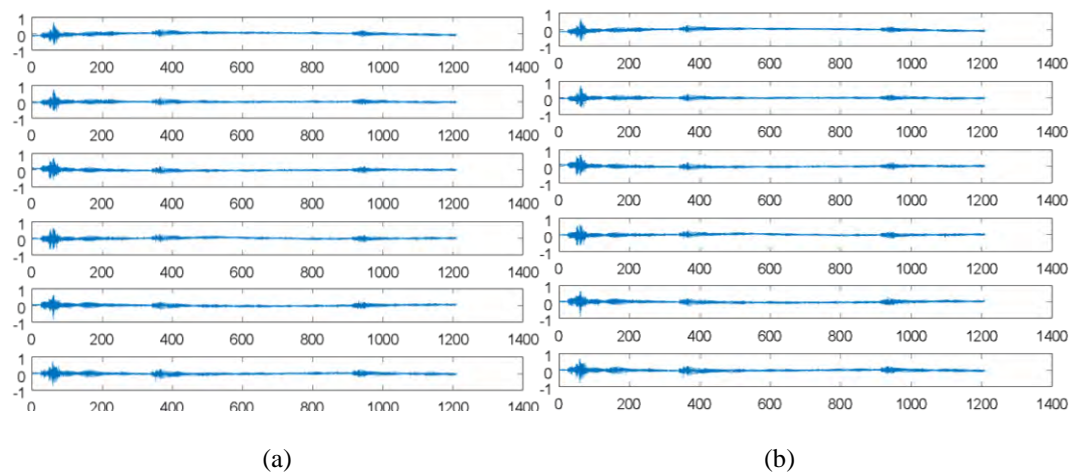


Figure5.1.15. Active response time histories. The vertical axis is accelerations (m/s^2) and the horizontal is time (sec). (a) transverse (b) vertical sensors.

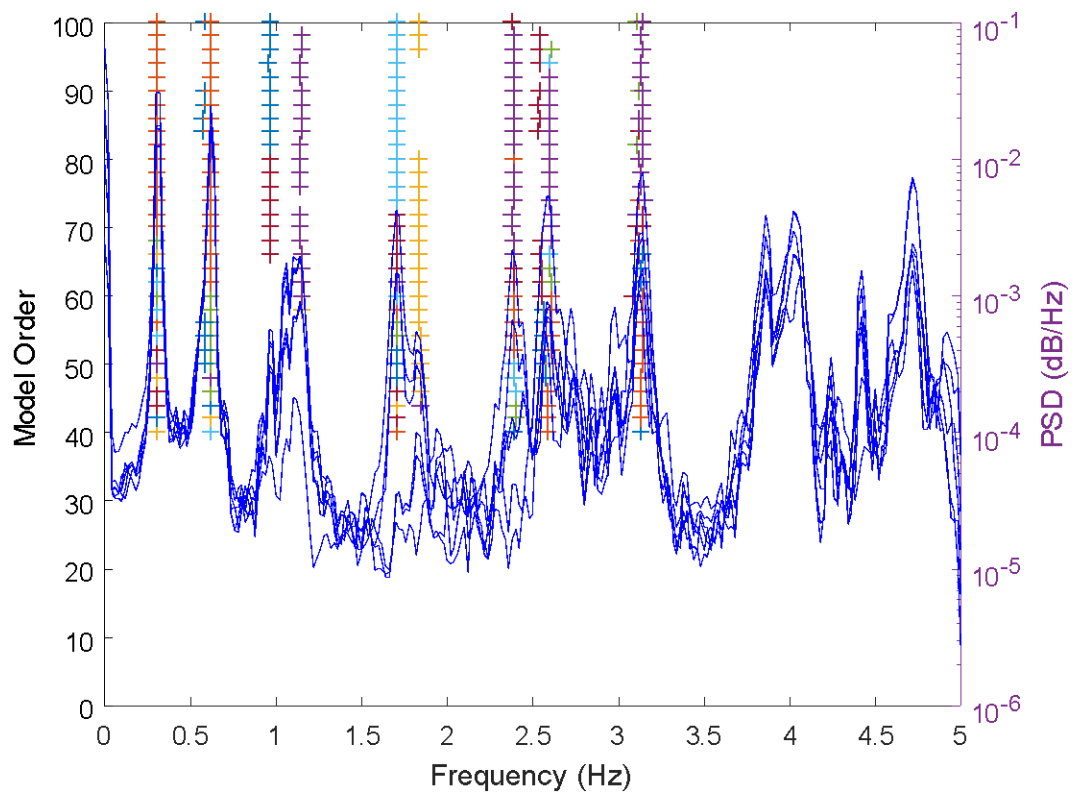


Figure5.1.16. Modes after cluster merging depicted on the PSD-log scale (**transverse**)

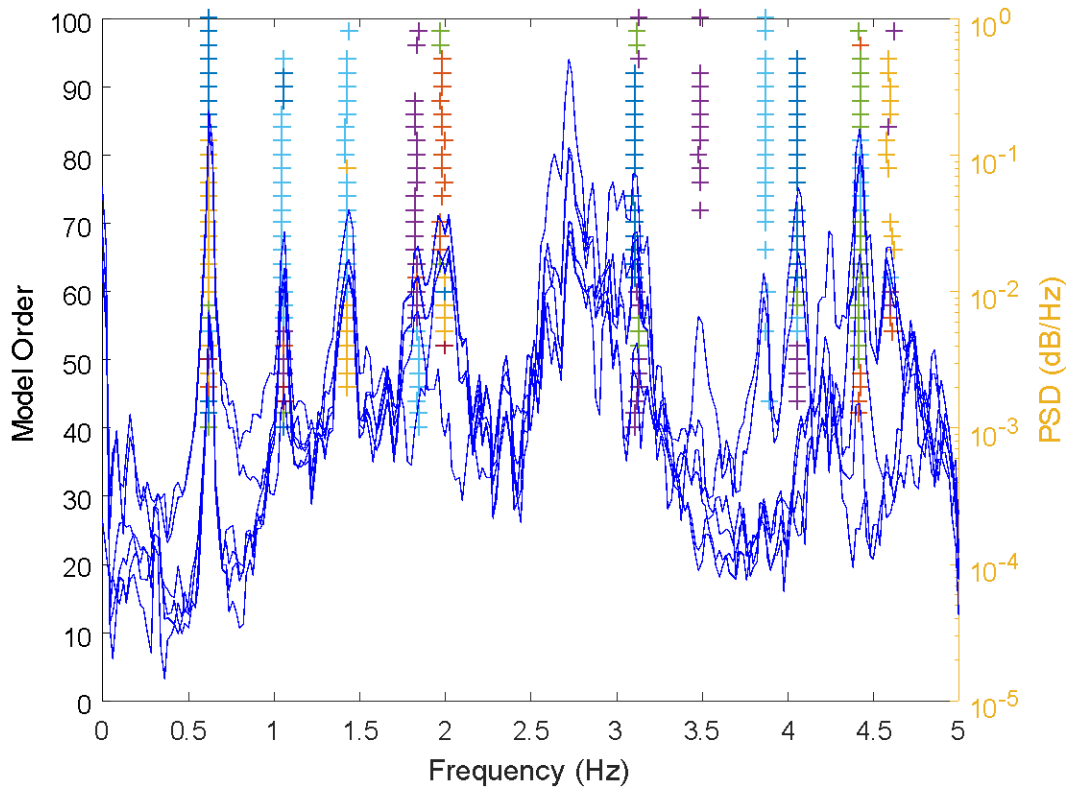


Figure5.1.17. Modes after cluster merging depicted on the PSD-log scale (**vertical**)

Configuration 5 (14:00)			
Mode	Type	Frequency (Hz)	Damping ratio
1	Transverse	0.3098	0.006
2	>>	0.6215	0.0044
3	>>	0.9678	0.0133
4	>>	1.1462	0.0132
5	>>	1.7061	0.0102
6	>>	2.3882	0.0076
7	>>	2.57	0.0047
8	>>	3.1368	0.0040
9	Vertical	0.6241	0.0059
10	>>	1.0534	0.0106
11	>>	1.4267	0.0168
12	>>	1.8409	0.0193
13	>>	1.9903	0.0167
14	>>	2.5163	0.0049
15	>>	3.1160	0.0061
16	>>	3.4887	0.0079
17	>>	3.8738	0.0032
18	>>	4.0578	0.0039
19	>>	4.4237	0.0018
20	>>	4.6052	0.0049

Table5.1.5. Identified modes and damping ratios of sensor configuration 4.

Configuration 6 (time 14:30)

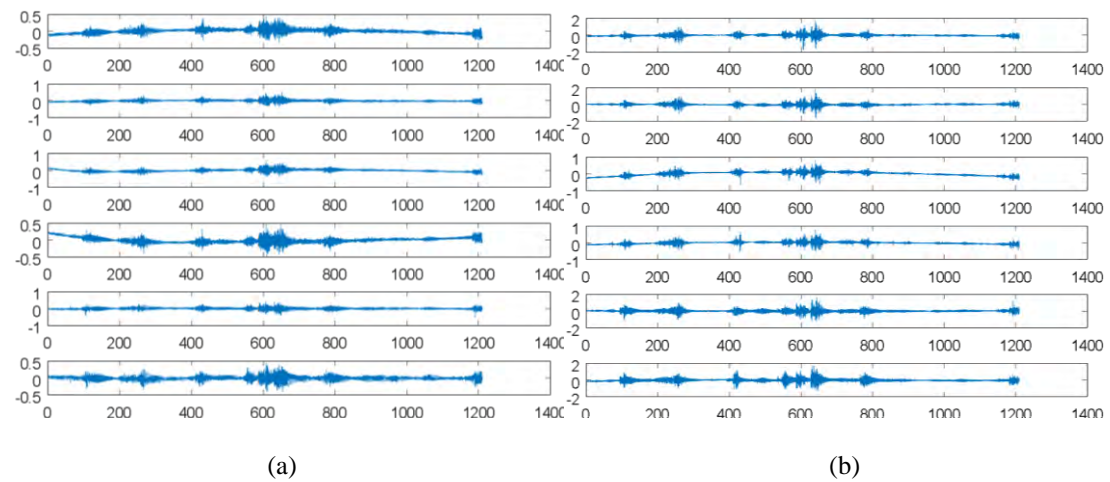


Figure 5.1.18. Active response time histories. The vertical axis is accelerations (m/s^2) and the horizontal is time (sec). (a) transverse (b) vertical sensors.

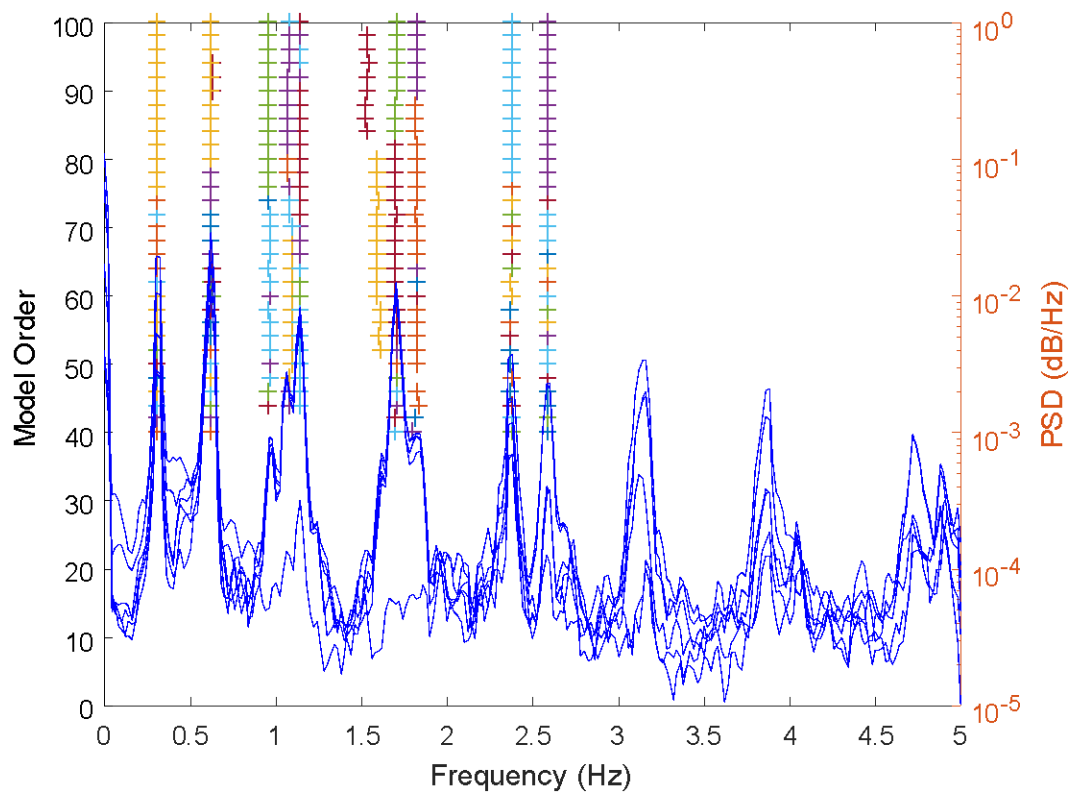


Figure 5.1.19. Modes after cluster merging depicted on the PSD-log scale (**transverse**)

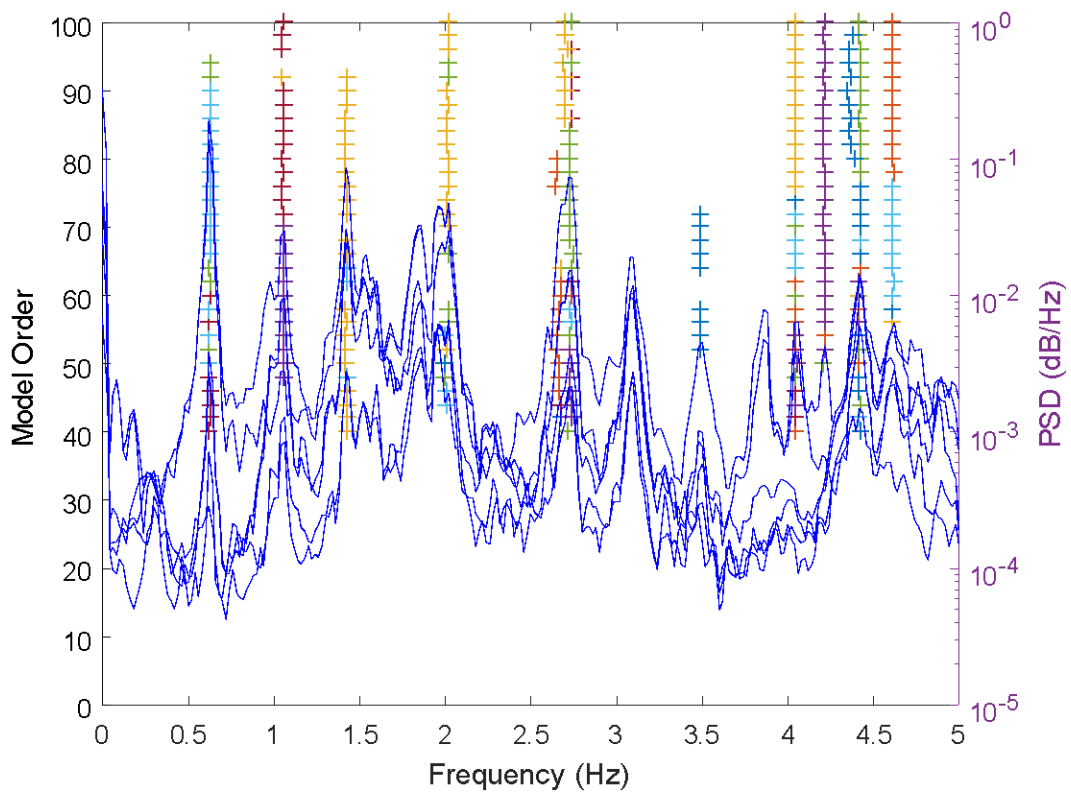


Figure5.1.20. Modes after cluster merging depicted on the PSD-log scale (**vertical**)

Configuration 6 (14:30)			
Mode	Type	Frequency (Hz)	Damping ratio
1	Transverse	0.3093	0.0116
2	>>	0.6215	0.0127
3	>>	0.9606	0.0216
4	>>	1.1396	0.0046
5	>>	1.5980	0.0174
6	>>	1.7015	0.0075
7	>>	2.3732	0.0058
8	>>	2.5840	0.0051
9	Vertical	0.6249	0.0110
10	>>	1.0547	0.0115
11	>>	1.4242	0.008
12	>>	2.0053	0.0083
13	>>	2.7288	0.0078
14	>>	3.4867	0.0066
15	>>	4.0496	0.0052
16	>>	4.2132	0.0045
17	>>	4.4210	0.0058
18	>>	4.6121	0.0097

Table5.1.6. Identified modes and damping ratios of sensor configuration 6.

Configuration 7 (time 15:00)

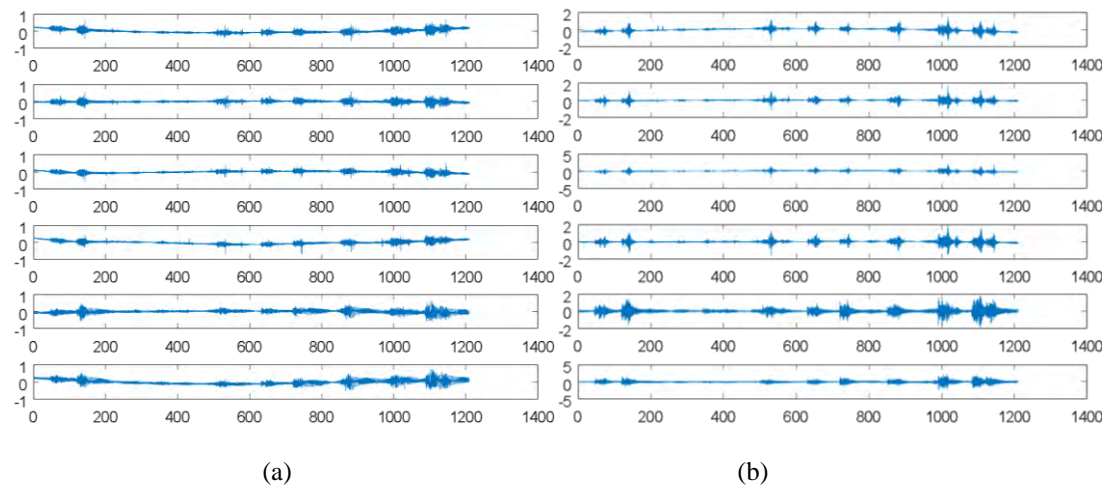


Figure 5.1.21. Active response time histories. The vertical axis is accelerations (m/s^2) and the horizontal is time (sec). (a) transverse (b) vertical sensors.

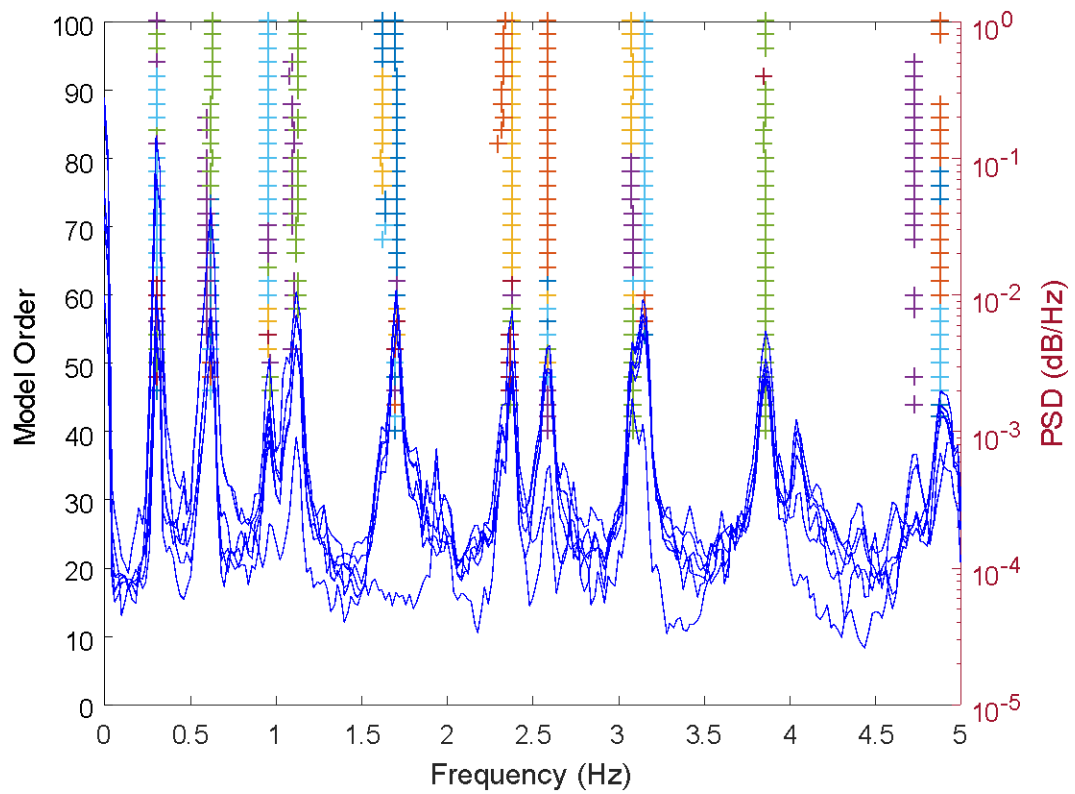


Figure 5.1.22. Modes after cluster merging depicted on the PSD-log scale (**transverse**)

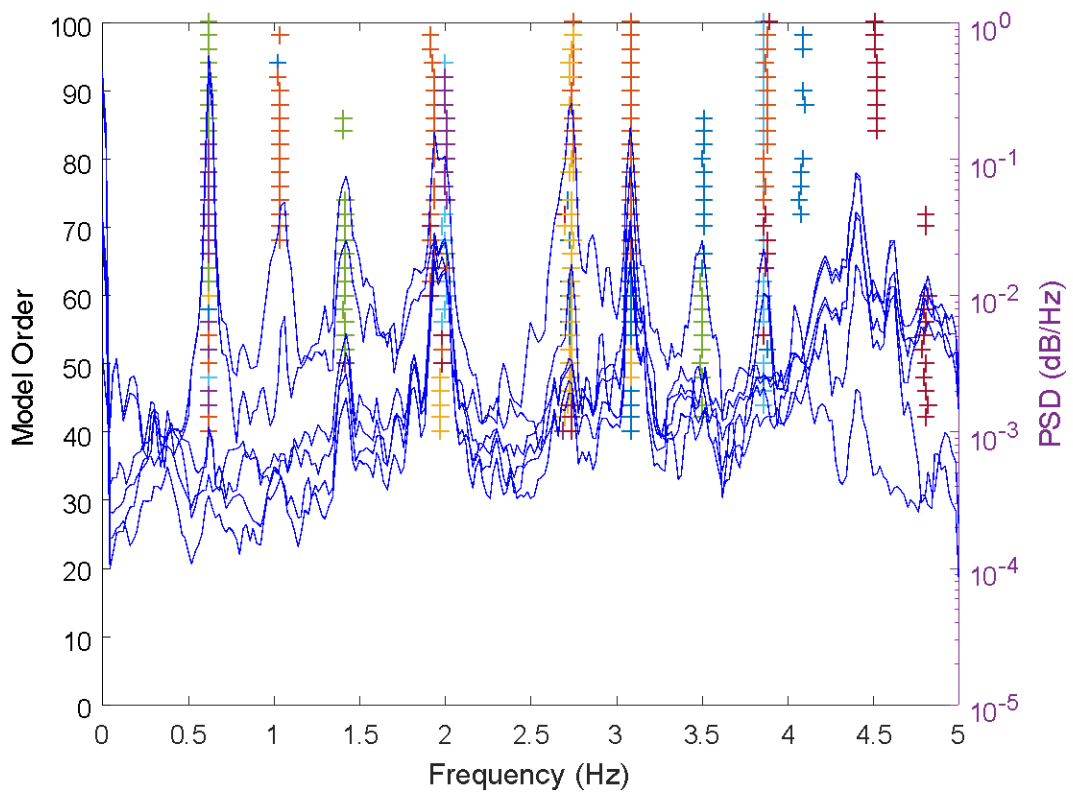


Figure5.1.23. Modes after cluster merging depicted on the PSD-log scale (vertical)

Configuration 7 (15:00)			
Mode	Type	Frequency (Hz)	Damping ratio
1	Transverse	0.3070	0.0095
2	>>	0.6242	0.0068
3	>>	0.9533	0.0180
4	>>	1.0943	0.0245
5	>>	1.7021	0.0076
6	>>	2.3731	0.0052
7	>>	2.5847	0.0072
8	>>	3.0876	0.0046
9	>>	3.8589	0.0055
10	Vertical	0.6229	0.0061
11	>>	1.0334	0.0209
12	>>	1.4130	0.0164
13	>>	1.9768	0.0107
14	>>	2.7197	0.0214
15	>>	3.0819	0.0028
16	>>	3.5011	0.0049
17	>>	3.8618	0.0064
18	>>	4.0869	0.024
19	>>	4.5172	0.0049

Table5.1.7. Identified modes and damping ratios of sensor configuration 7.

Configuration 8 (time 16:00)

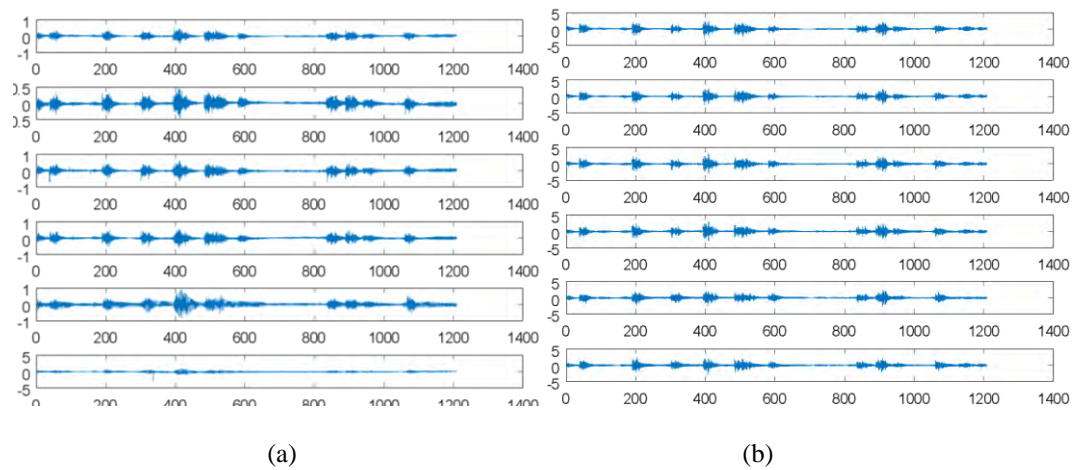


Figure 5.1.24. Active response time histories. The vertical axis is accelerations (m/s^2) and the horizontal is time (sec). (a) transverse (b) vertical sensors.

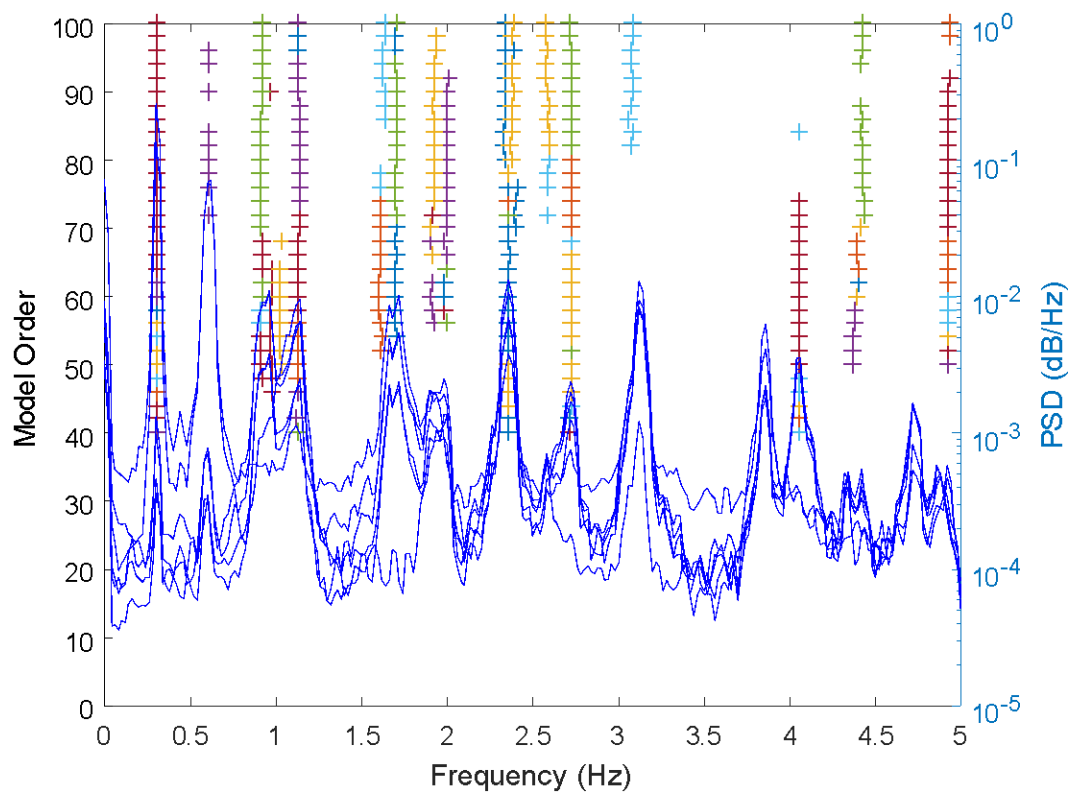


Figure 5.1.25. Modes after cluster merging depicted on the PSD-log scale (**transverse**)

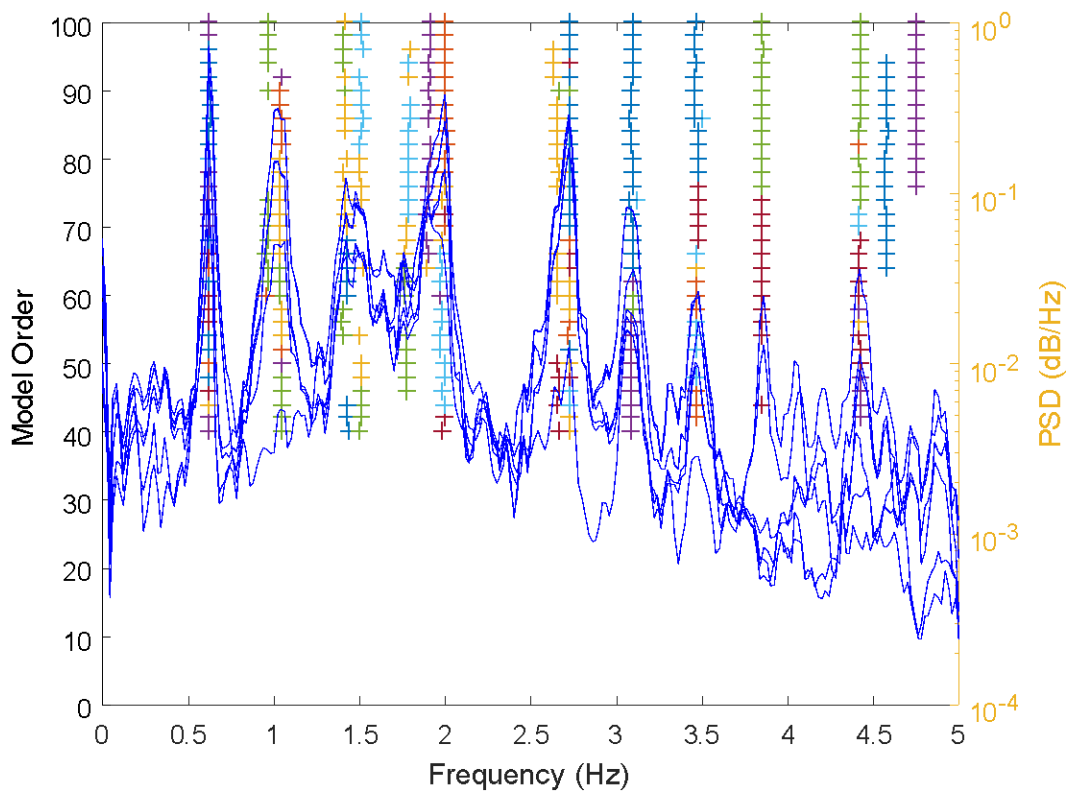


Figure5.1.26. Modes after cluster merging depicted on the PSD-log scale (**vertical**)

Configuration 8 (16:00)			
Mode	Type	Frequency (Hz)	Damping ratio
1	Transverse	0.3046	0.0052
2	>>	0.6110	0.0058
3	>>	0.9706	0.0176
4	>>	1.1331	0.0180
5	>>	1.6116	0.0084
6	>>	1.9139	0.0240
7	>>	2.3559	0.0088
8	>>	2.5910	0.0062
9	>>	2.7222	0.0095
10	>>	3.0752	0.0197
11	>>	4.0565	0.0067
12	>>	4.3867	0.0078
13	Vertical	0.6228	0.0124
14	>>	1.048	0.0275
15	>>	1.4300	0.0277
16	>>	1.7735	0.0156
17	>>	1.9893	0.0092
18	>>	2.7226	0.0056
19	>>	3.0898	0.0107
20	>>	3.4683	0.0089
21	>>	3.8535	0.0049
22	>>	4.4229	0.0068

Table5.1.8. Identified modes and damping ratios of sensor configuration 8.

Configuration 9 (time 16:30)

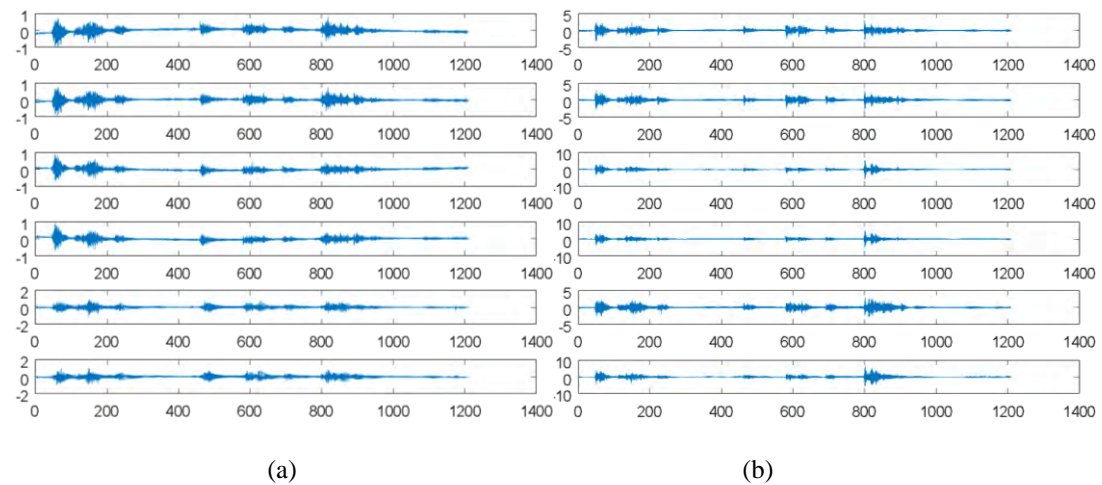


Figure 5.1.27. Active response time histories. The vertical axis is accelerations (m/s^2) and the horizontal is time (sec). (a) transverse (b) vertical sensors.

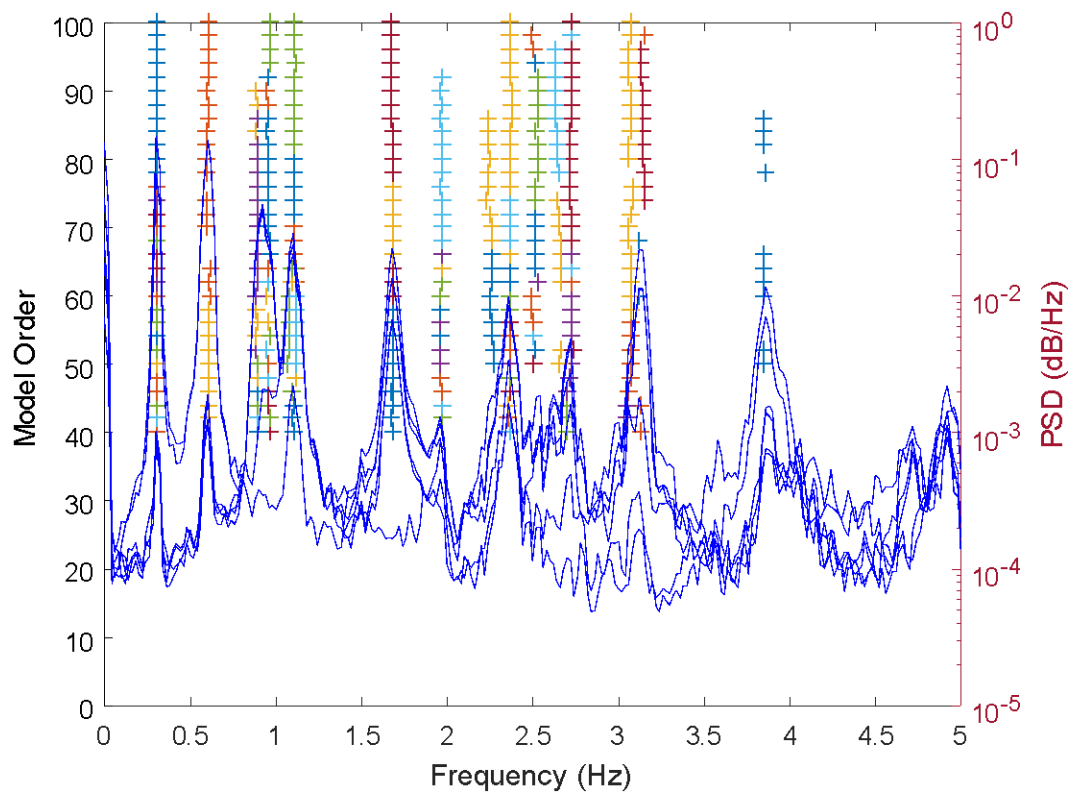


Figure 5.1.28. Modes after cluster merging depicted on the PSD-log scale (**transverse**)

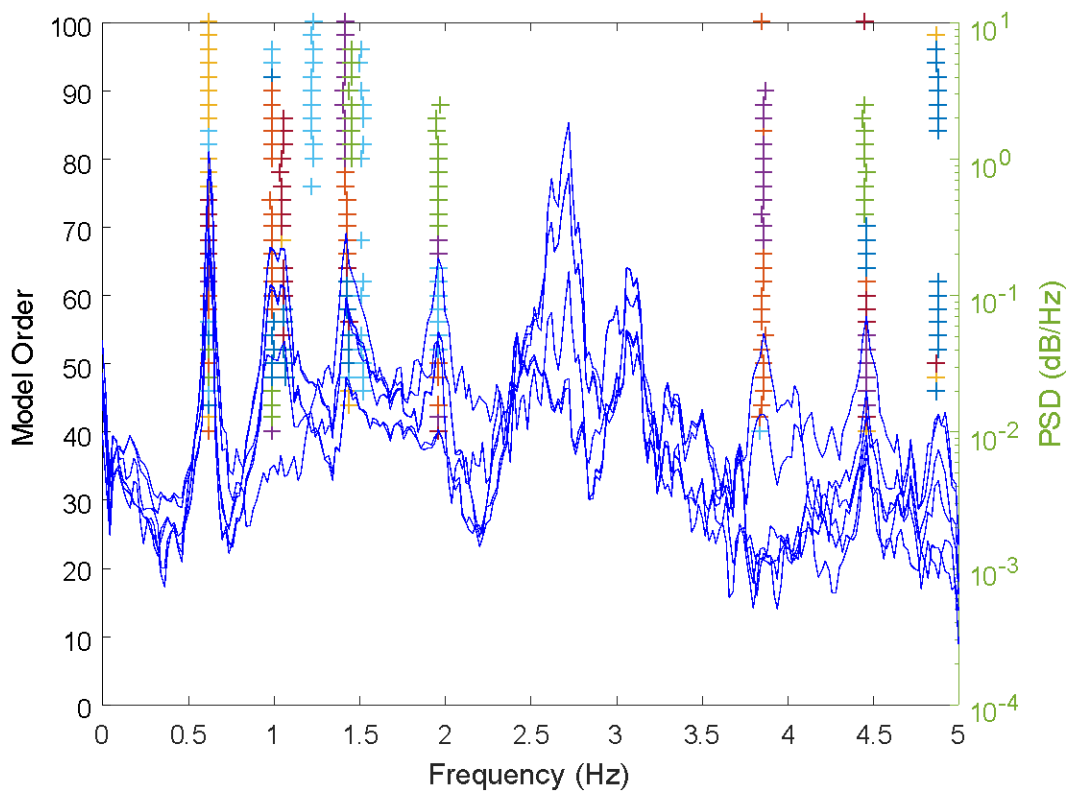


Figure5.1.29. Modes after cluster merging depicted on the PSD-log scale (**vertical**)

Configuration 9 (16:30)			
Mode	Type	Frequency (Hz)	Damping ratio
1	Transverse	0.3051	0.0083
2	>>	0.6102	3.0044
3	>>	0.9570	0.0202
4	>>	1.1030	0.0206
5	>>	1.682	0.0146
6	>>	2.2623	0.0170
7	>>	2.3668	0.0118
8	>>	2.5053	0.0229
9	>>	2.7138	0.0081
10	>>	3.1362	0.0055
11	>>	3.8475	0.0068
12	Vertical	0.6221	0.0072
13	>>	0.9933	0.0298
14	>>	1.2259	0.0150
15	>>	1.4432	0.0211
16	>>	1.9624	0.0156
17	>>	3.8246	0.0091
18	>>	4.4594	0.0088

Table5.1.9. Identified modes and damping ratios of sensor configuration 9.

Configuration 10 (time 17:00)

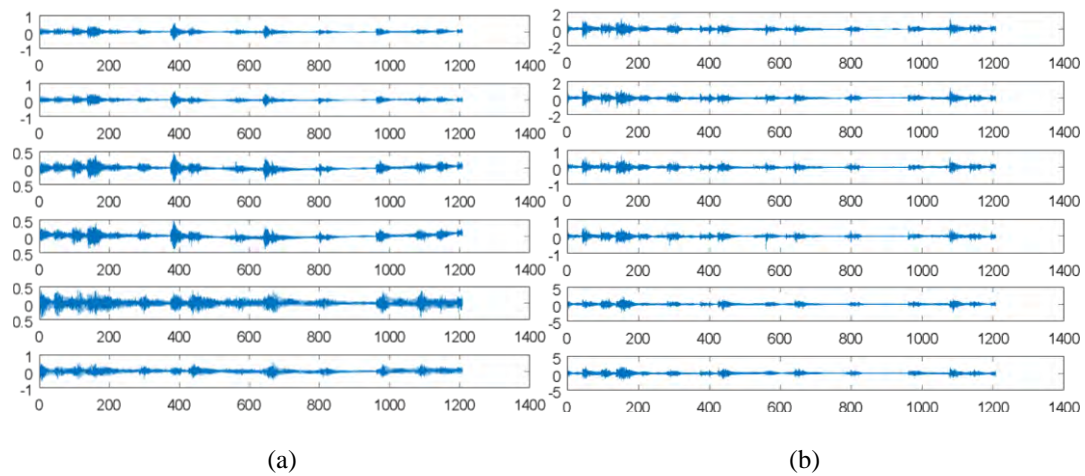


Figure 5.1.30. Active response time histories. The vertical axis is accelerations (m/s^2) and the horizontal is time (sec). (a) transverse (b) vertical sensors.

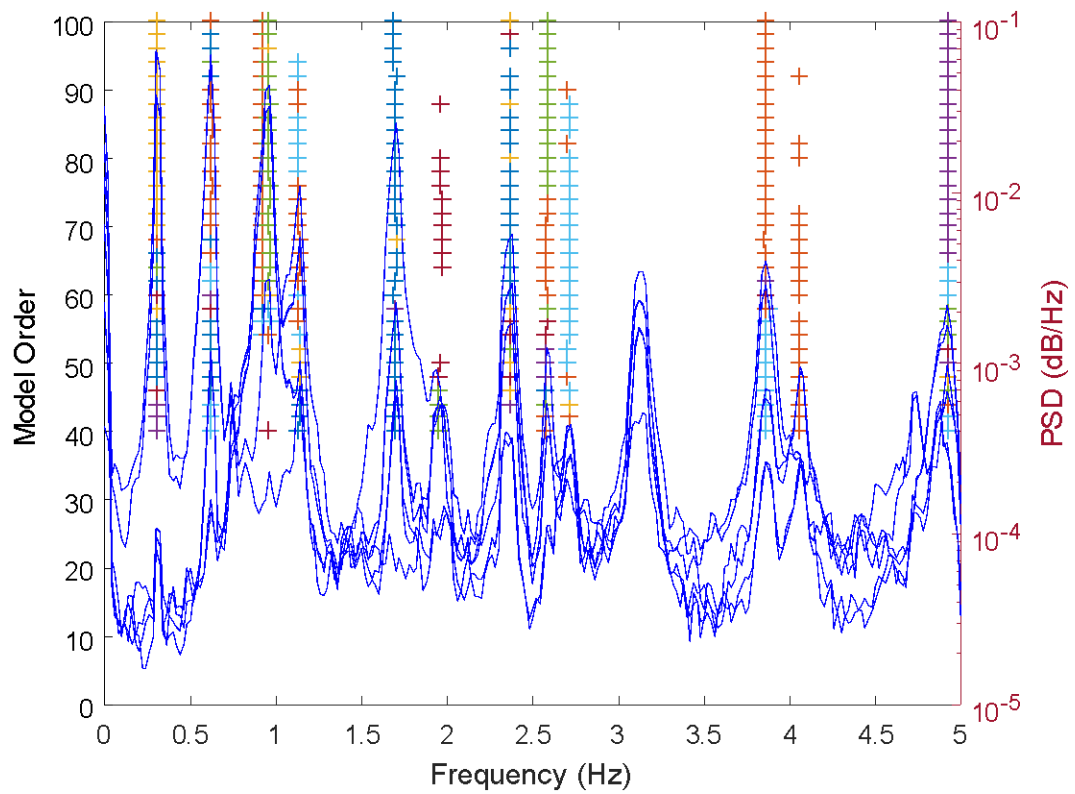


Figure 5.1.31. Modes after cluster merging depicted on the PSD-log scale (**transverse**)

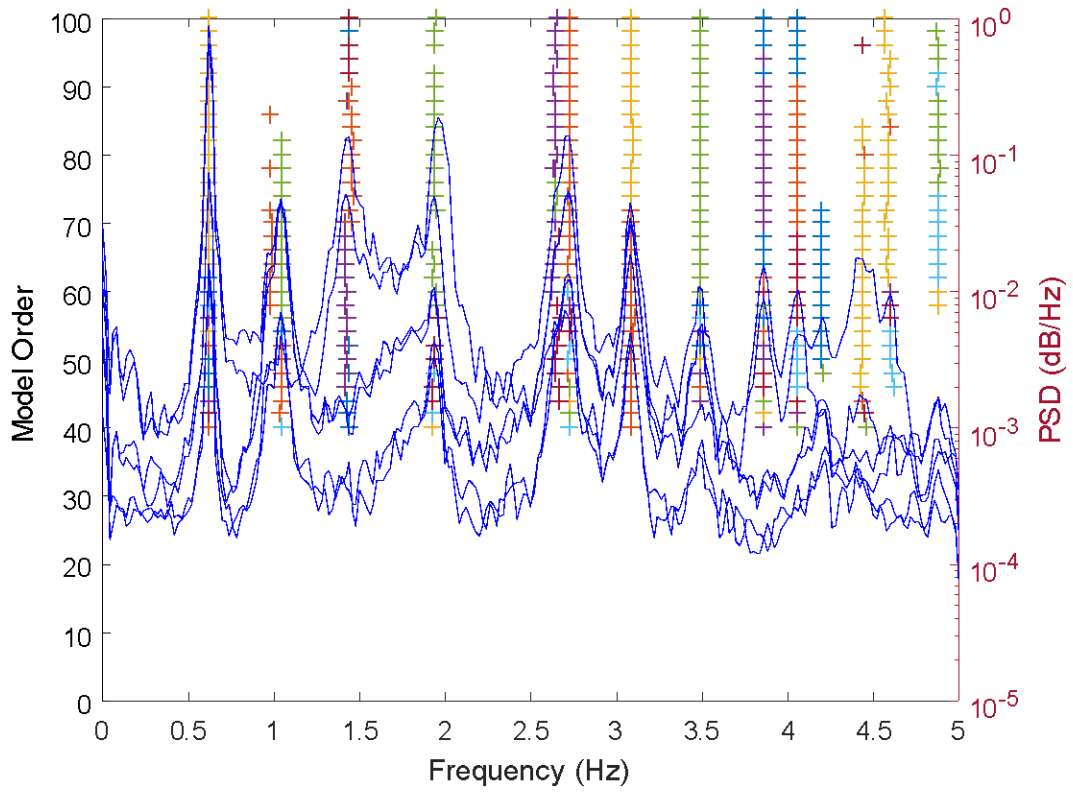


Figure5.1.32. Modes after cluster merging depicted on the PSD-log scale (vertical)

Configuration 10 (17:00)			
Mode	Type	Frequency (Hz)	Damping ratio
1	Transverse	0.3077	0.0104
2	>>	0.6201	0.0095
3	>>	0.9599	0.0095
4	>>	1.1366	0.0114
5	>>	1.6948	0.0101
6	>>	2.3651	0.0073
7	>>	2.5731	0.0047
8	>>	2.7127	0.0109
9	>>	3.8579	0.0061
10	>>	4.0602	0.0086
11	Vertical	0.6224	0.0075
12	>>	1.0437	0.0179
13	>>	1.4377	0.0272
14	>>	1.9383	0.0085
15	>>	2.7220	0.0076
16	>>	3.0878	0.0073
17	>>	3.4904	0.0088
18	>>	3.8589	0.0071
19	>>	4.0560	0.0080
20	>>	4.4412	0.0101

Table5.1.10. Identified modes and damping ratios of sensor configuration 10.

Configuration 11 (time 17:30)

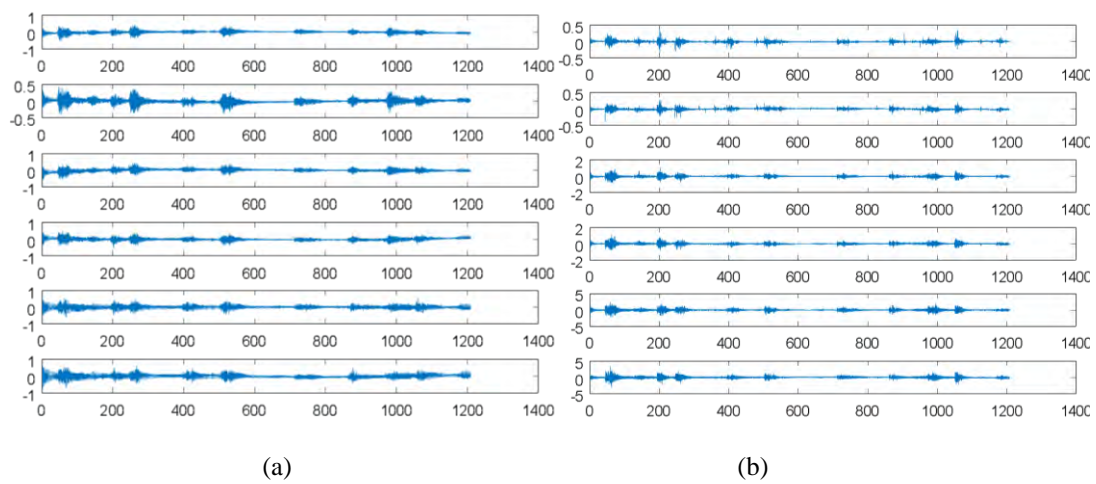


Figure 5.1.33. Active response time histories. The vertical axis is accelerations (m/s^2) and the horizontal is time (sec). (a) transverse (b) vertical sensors.

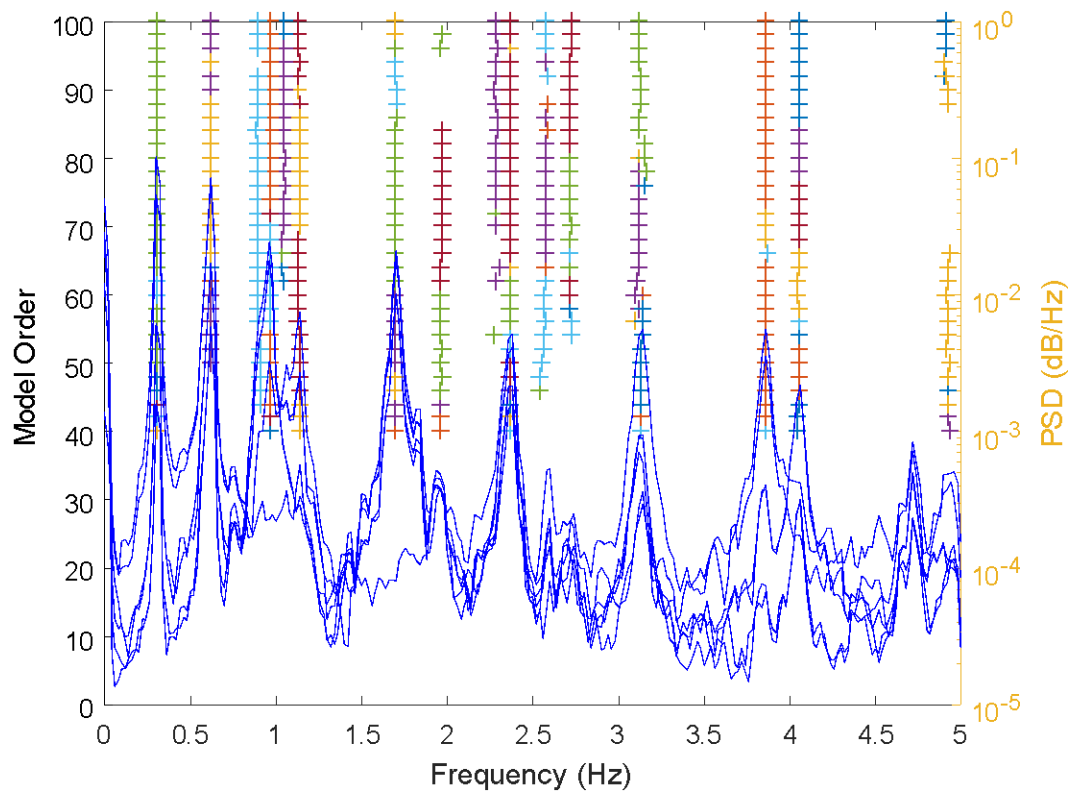


Figure 5.1.34. Modes after cluster merging depicted on the PSD-log scale (**transverse**)

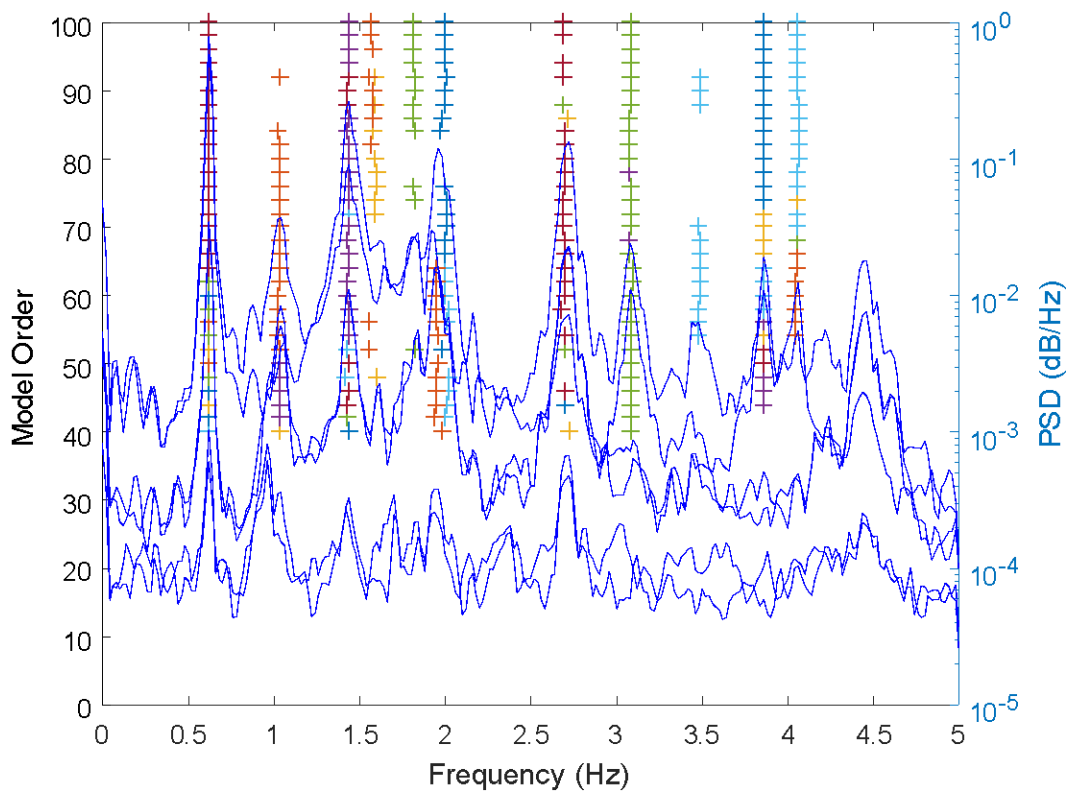


Figure5.1.35. Modes after cluster merging depicted on the PSD-log scale (**vertical**)

Configuration 11 (17:30)			
Mode	Type	Frequency (Hz)	Damping ratio
1	Transverse	0.3065	0.0103
2	>>	0.3135	0.0130
3	>>	3.9646	0.0102
4	>>	1.1361	0.0172
5	>>	1.6983	0.0079
6	>>	2.3662	0.0080
7	>>	2.5713	0.0100
8	>>	2.7186	0.0064
9	>>	3.1305	0.0065
10	>>	3.8596	0.0052
11	>>	4.0517	0.0083
12	Vertical	0.6212	0.0068
13	>>	1.0325	0.0256
14	>>	1.4362	0.0143
15	>>	1.5947	0.0142
16	>>	1.8173	0.0096
17	>>	1.9977	0.0729
18	>>	2.7005	0.0083
19	>>	3.0848	0.0094
20	>>	3.4864	0.0123
21	>>	3.8609	0.0039
22	>>	4.0580	0.0080

Table5.1.11. Identified modes and damping ratios of sensor configuration 11.

Configuration 12 (time 18:00)

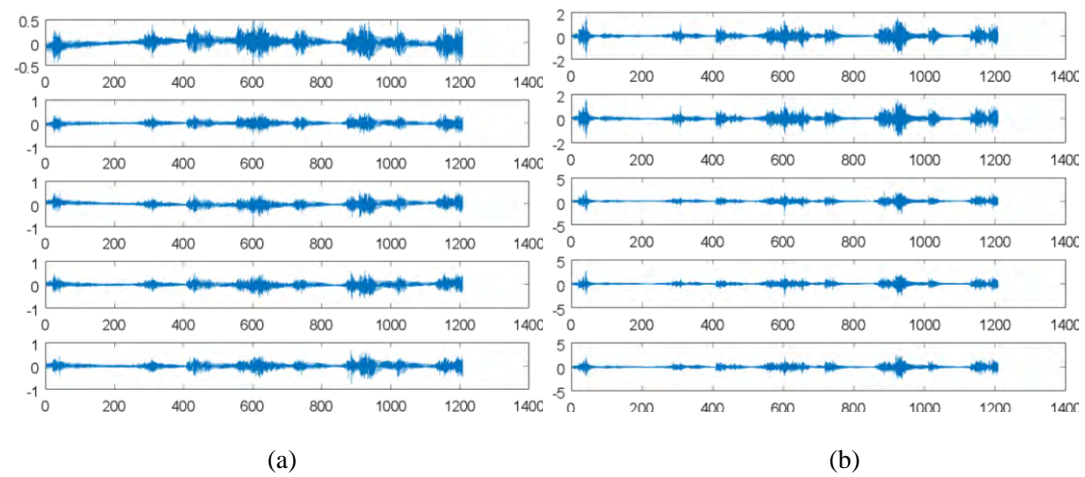


Figure 5.1.36. Active response time histories. The vertical axis is accelerations (m/s^2) and the horizontal is time (sec). (a) transverse (b) vertical sensors.

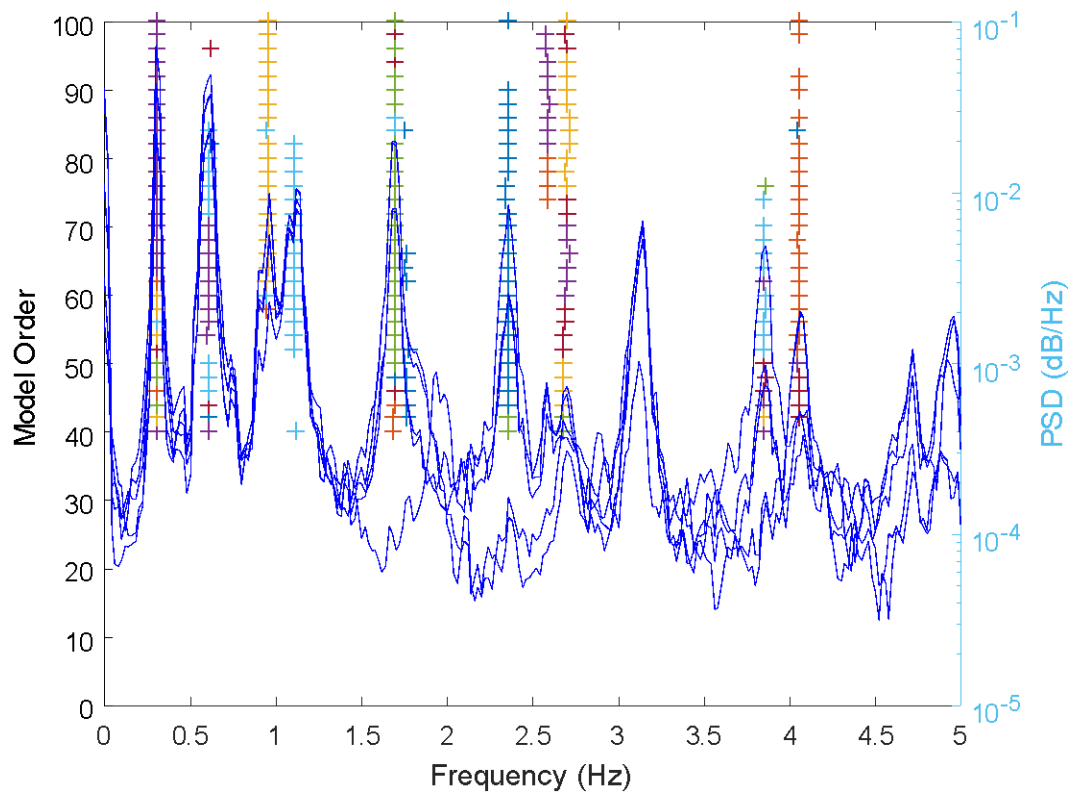


Figure 5.1.37. Modes after cluster merging depicted on the PSD-log scale (**transverse**)

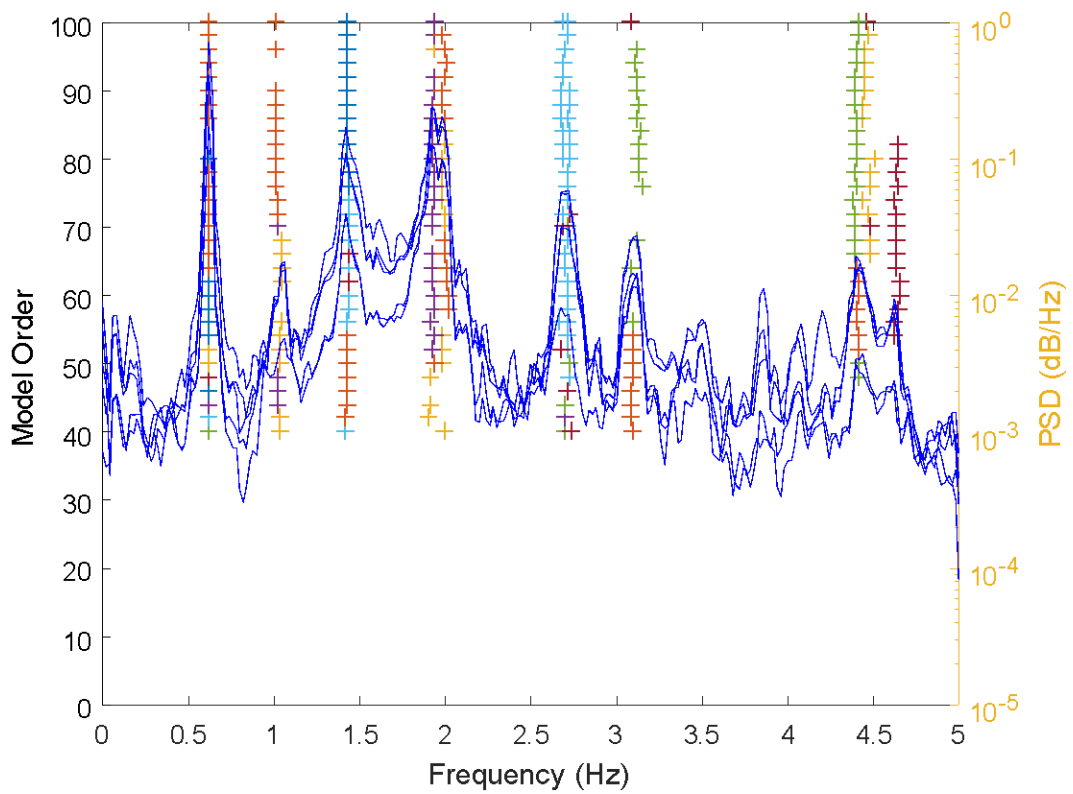


Figure 5.1.38. Modes after cluster merging depicted on the PSD-log scale (**vertical**)

Configuration 12 (18:00)			
Mode	Type	Frequency (Hz)	Damping ratio
1	Transverse	0.3054	0.0105
2	>>	0.6112	0.0268
3	>>	0.9467	0.0219
4	>>	1.1030	0.0281
5	>>	1.6916	0.0091
6	>>	2.3516	0.0098
7	>>	3.8517	0.0079
8	>>	4.0562	0.0064
9	Vertical	0.6211	0.0084
10	>>	1.0442	0.0251
11	>>	1.4306	0.0124
12	>>	1.9930	0.0049
13	>>	2.7163	0.0118
14	>>	3.0907	0.0110
15	>>	4.4059	0.0084
16	>>	4.6373	0.0046

Table 5.1.12. Identified modes and damping ratios of sensor configuration 12.

Configuration 13 (time 18:30)

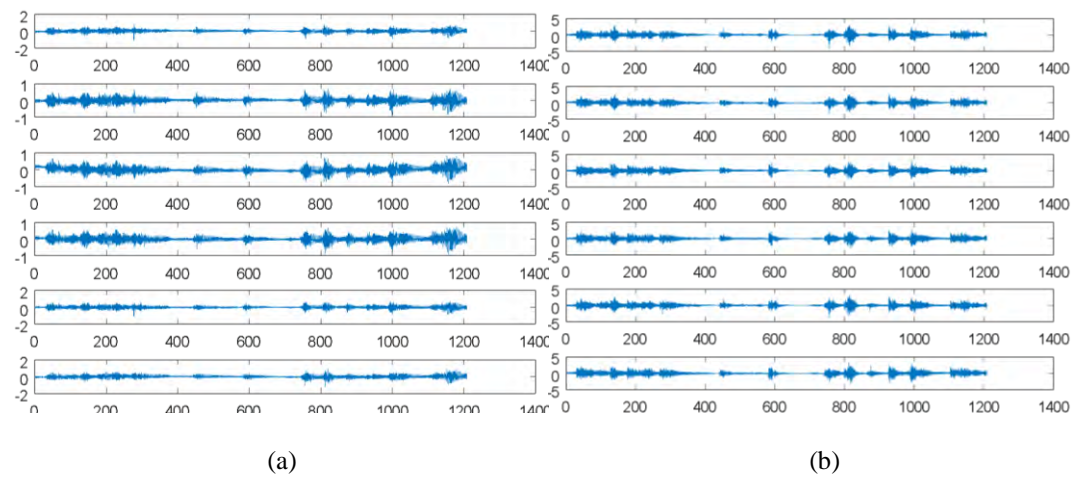


Figure 5.1.39 Active response time histories. The vertical axis is accelerations (m/s^2) and the horizontal is time (sec) (a) transverse (b) vertical sensors.

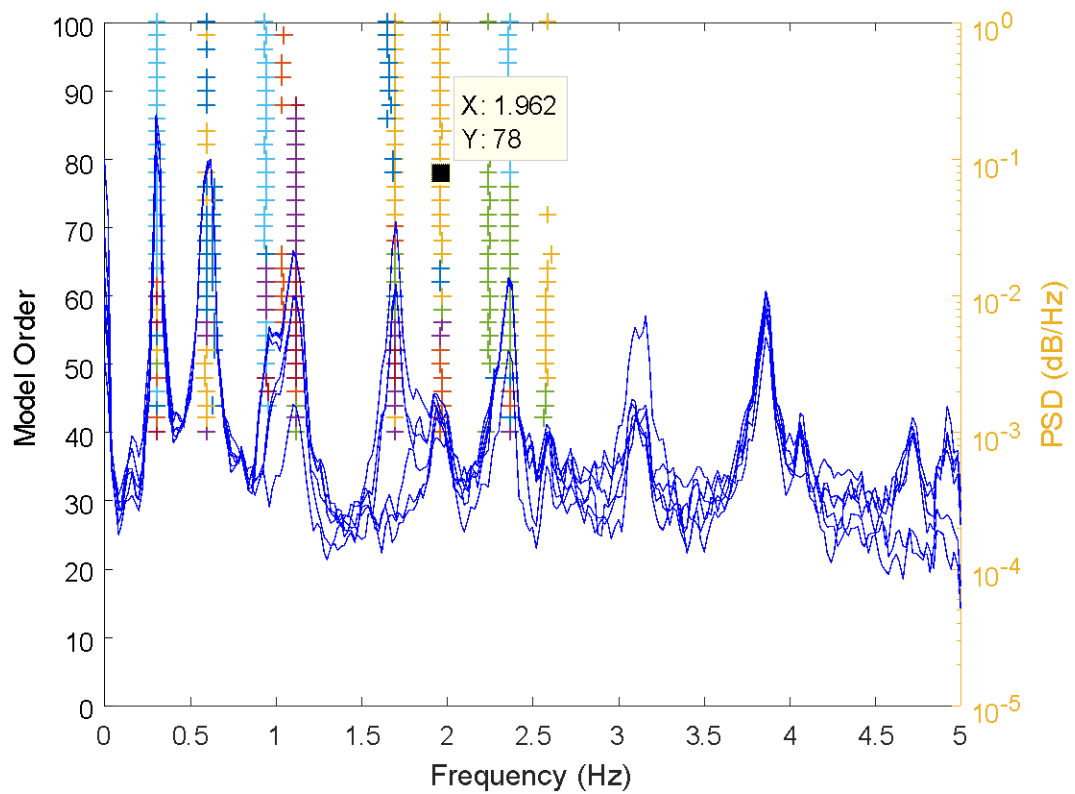


Figure 5.1.40. Modes after cluster merging depicted on the PSD-log scale (**transverse**)

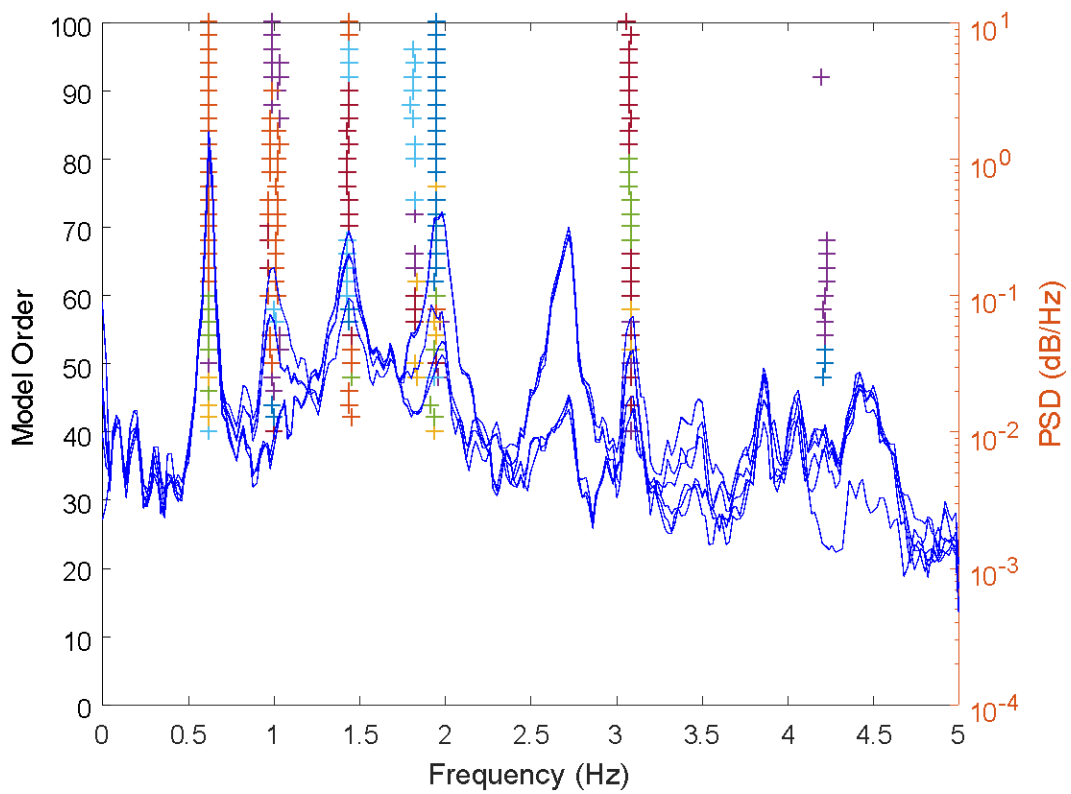


Figure 5.1.41. Modes after cluster merging depicted on the PSD-log scale (vertical)

Configuration 13 (18:30)			
Mode	Type	Frequency (Hz)	Damping ratio
1	Transverse	0.3058	0.0078
2	>>	0.5949	0.0339
3	>>	0.9400	0.0328
4	>>	1.1181	0.0211
5	>>	1.6970	0.0075
6	>>	1.9664	0.0189
7	>>	2.2458	0.0240
8	>>	2.3634	0.0088
9	>>	2.5792	0.0116
10	Vertical	0.6225	0.0103
11	>>	0.9866	0.0195
12	>>	1.4416	0.0269
13	>>	1.8269	0.0127
14	>>	1.9467	0.0161
15	>>	3.0809	0.0093
16	>>	4.2190	0.0052

Table 5.1.13. Identified modes and damping ratios of sensor configuration 13

The results included in the previous tables (5.1.1-5.1.13) are combined for every configuration and the mean value and the standard deviation of the modal frequencies and damping ratios are calculated and presented in a table in the following paragraph.

5.1.2. Results from Software 1

Using the previously presented *Software 1* (chapter 4), the modal frequencies and modal damping ratios of the bridge were extracted, and the mode shape components of each configuration were combined to produce the full mode shapes at all sensor locations covered by the 13 configurations [9]. Specifically, the first 20 modal frequencies and modal damping ratios of the bridge were successfully identified, along with 11 mode shapes. Due to the fact that the modal properties were identified from each of the 13 sensor configurations separately, their values vary slightly from one configuration to the other, so the mean value and standard deviation have to be taken into account. Table 5.1.14 presents the mean and standard deviation of the experimentally identified modal frequencies and modal damping ratios for all 20 identified modes of the Metsovo bridge. It also compares the identified frequencies and damping ratios with those produced by the developed software within this thesis. Finally, the identified modeshapes from Software 1 are presented in figures 5.1.42 - 5.1.46.

Table 5.1.14. First 20 experimentally identified modal frequencies and modal damping ratios of the Metsovo bridge (mean and standard deviation across all 13 configurations) by Software 1, compared to the results from the developed software

Software 1					Developed software			
	Frequency (Hz)		Damping ratio		Frequency (Hz)		Damping ratio	
Mode	Mean	Std	Mean	Std	Mean	Std	Mean	Std
1	0.3063	0.0018	0.0111	0.0025	0.3071	0.0017	0.0090	0.0023
2	0.6034	0.007	0.0178	0.0024	0.6155	0.0077	0.0106	0.0076
3	0.6227	0.0017	0.0085	0.0014	0.6232	0.0012	0.0073	0.0027
4	0.9646	0.0047	0.0136	0.0195	0.9561	0.0131	0.0192	0.0068
5	1.0468	0.0079	0.0194	0.0105	1.0367	0.0234	0.0187	0.0070
6	1.1389	0.0065	0.0106	0.0043	1.1271	0.0194	0.0176	0.0069
7	1.4280	0.0048	0.0143	0.0064	1.4329	0.0110	0.0182	0.0067
8	1.6967	0.0098	0.0161	0.0158	1.6831	0.0359	0.0096	0.0035
9	2.0053	0.0078	0.0113	0.0041	1.9874	0.0199	0.0133	0.0059
10	2.3034	0.0135	0.0085	0.0016	-	-	-	-
11	2.3666	0.0100	0.0083	0.0039	2.3672	0.0123	0.0088	0.0055
12	2.5901	0.0106	0.0080	0.0034	2.5760	0.0237	0.0084	0.0052
13	2.7226	0.0067	0.0109	0.0043	2.6990	0.595	0.0082	0.0055
14	3.0861	0.0126	0.0098	0.0043	3.0739	0.0536	0.0099	0.0045
15	3.1266	0.0154	0.0071	0.0015	3.1208	0.0218	0.0076	0.0053
16	3.4801	0.0159	0.0184	0.0021	3.4882	0.0133	0.0077	0.0023
17	3.8608	0.0056	0.0095	0.0023	3.8623	0.0082	0.0053	0.0014
18	4.0585	0.0116	0.0091	0.0085	4.0593	0.0120	0.0064	0.0023
19	4.2101	0.0105	0.0121	0.0032	4.1909	0.397	0.0047	0.0007
20	4.4102	0.0121	0.0084	0.0024	4.4428	0.0294	0.0075	0.0028

The following figures show the acquired mode shapes by Software 1.

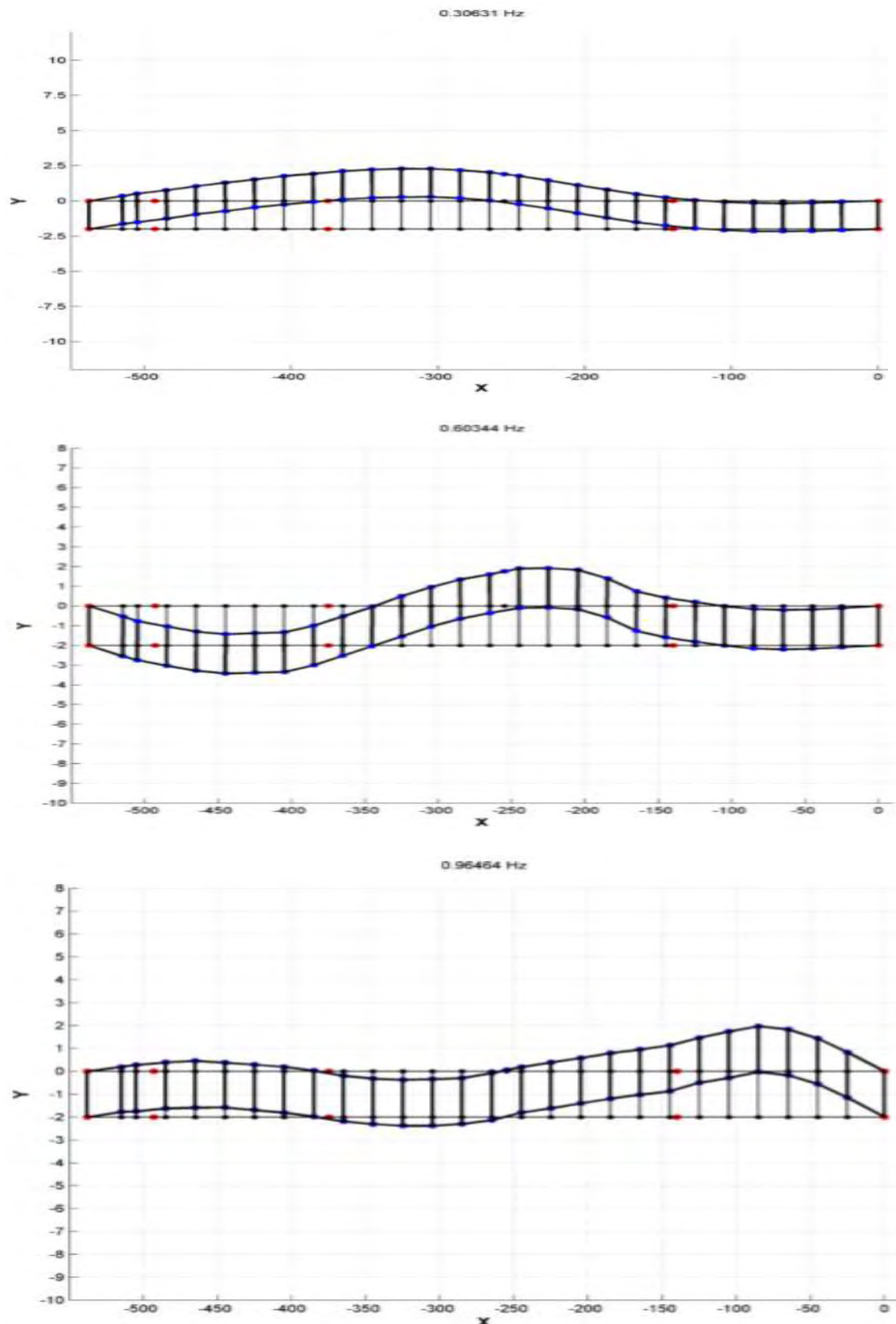


Figure 5.1.42. Modeshapes of the identified eigenfrequencies, by Software1, in the **transverse** direction. (Modes: 0.30631, 0.60344, 0.9646Hz)

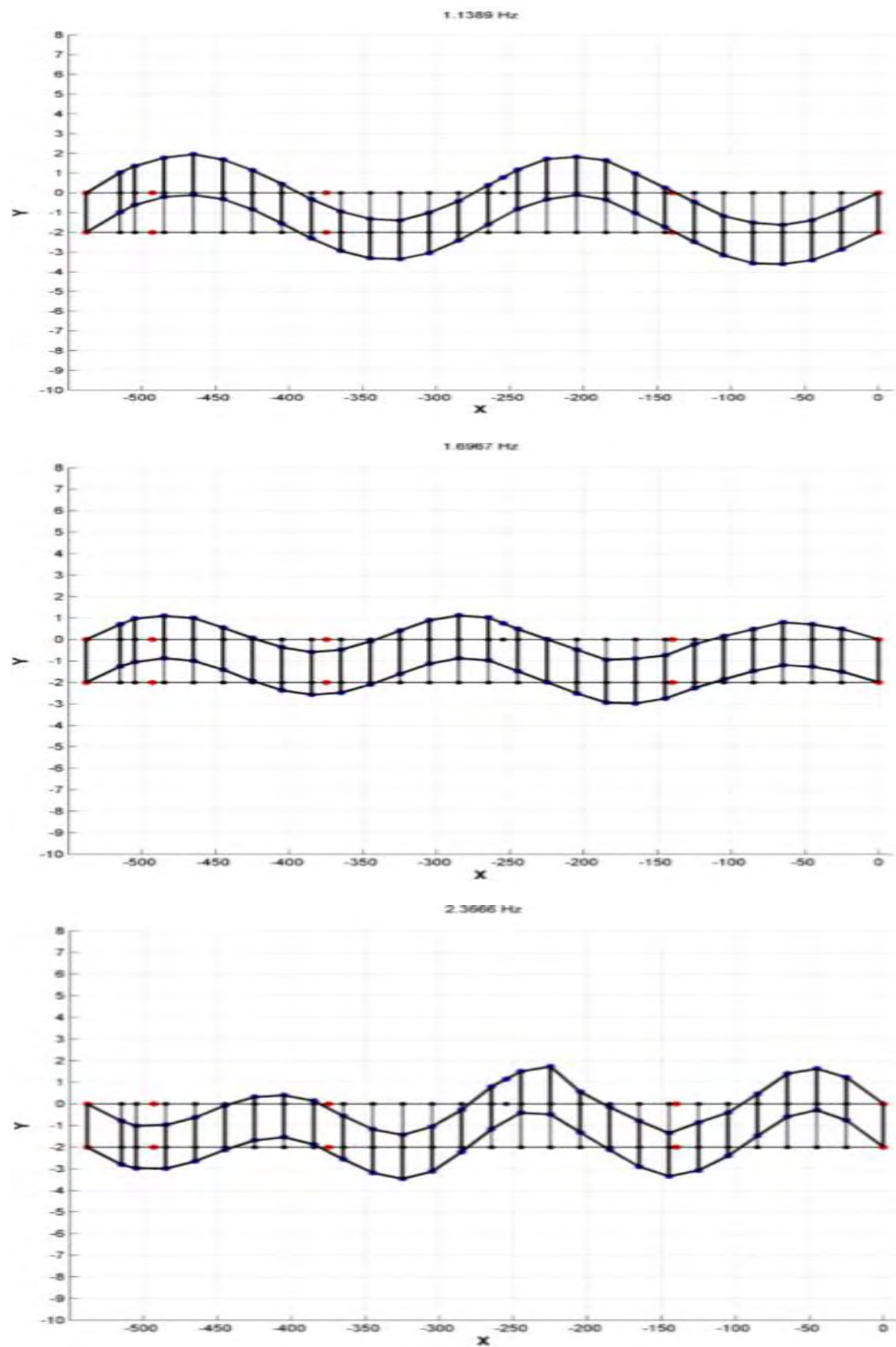


Figure 5.1.43. Modeshapes of the identified eigenfrequencies, by Software 1, in the **transverse** direction (Modes: 1.1389, 1.6967, 2.366 Hz)

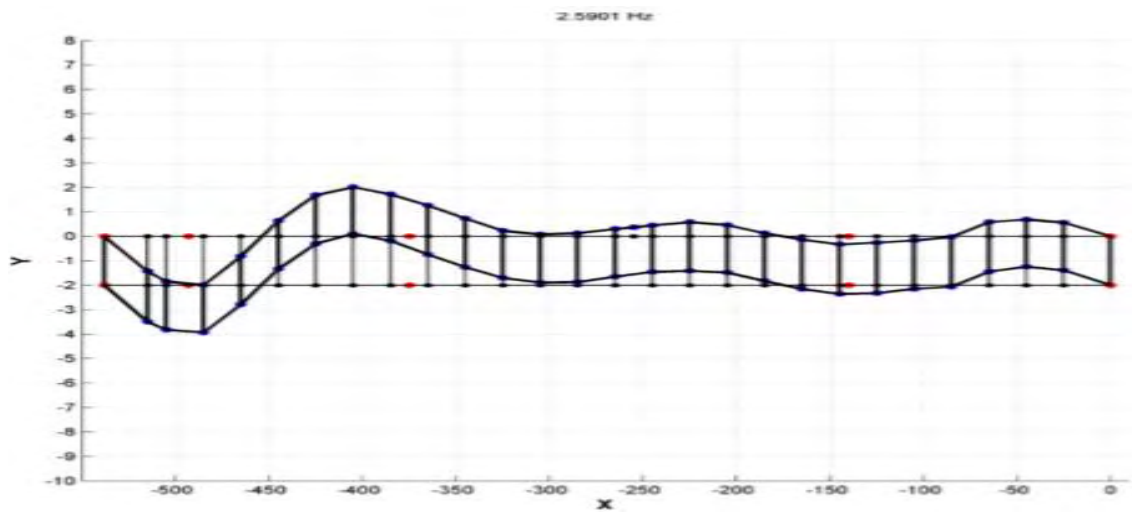


Figure 5.1.44. Modeshapes of the identified eigenfrequencies, by Software 1, in the **transverse** direction (Modes: 2.5901 Hz).

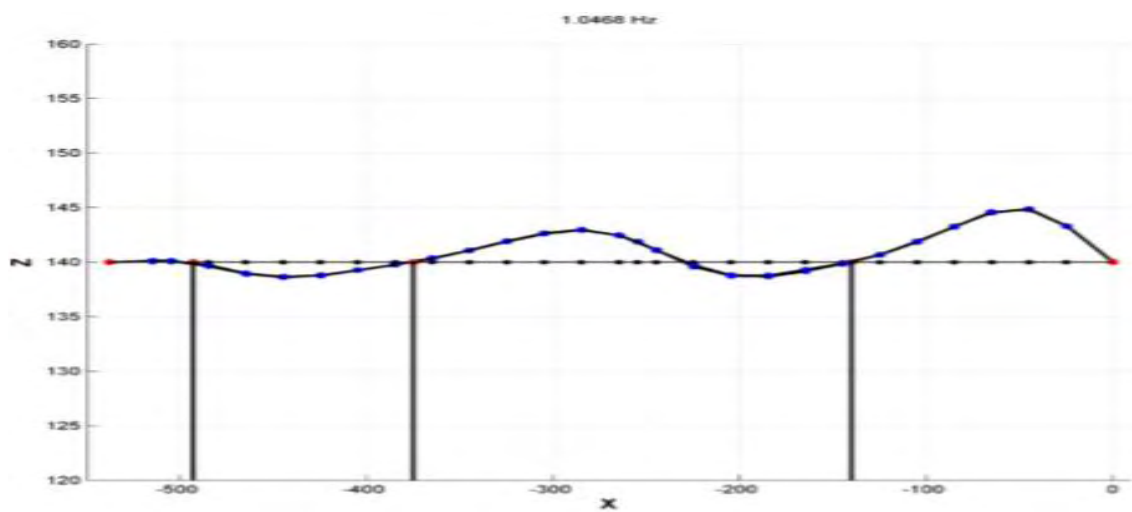
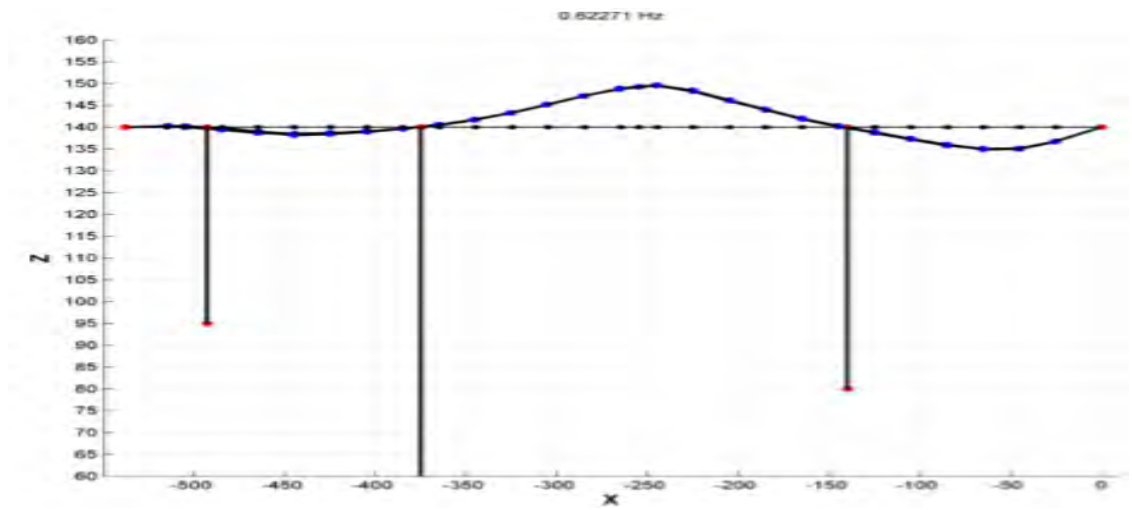


Figure 5.1.45. Modeshapes of the identified eigenfrequencies, by Software1, in the **vertical** direction (Modes: 0.6227, 1.0468 Hz)

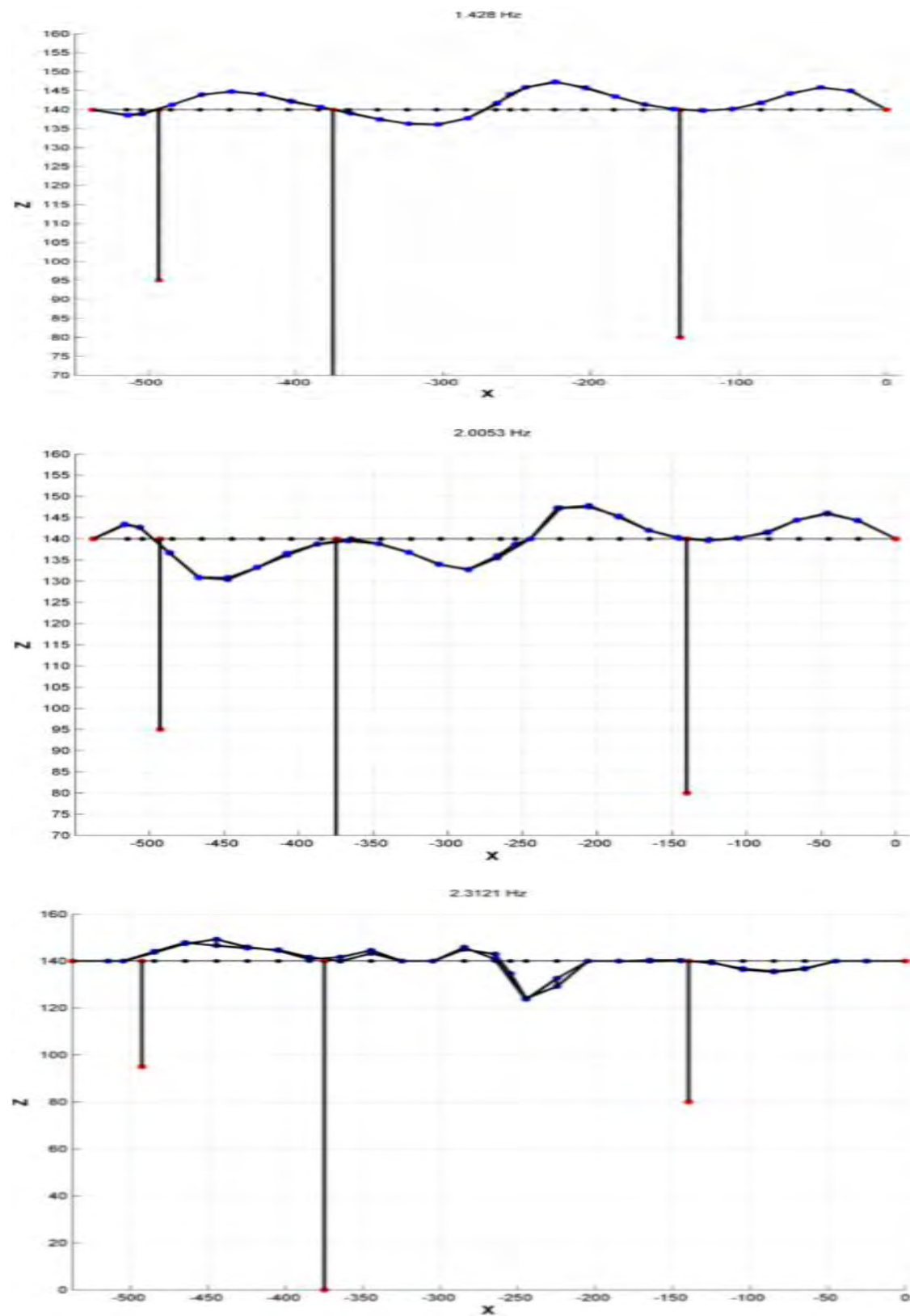


Figure 5.1.46. Modeshapes of the identified eigenfrequencies, by Software 1, in the **vertical** direction (Modes: 1.428, 2.0053, 2.3121 Hz)

5.1.3. Conclusions

By observing and comparing the results of the software, important conclusions can be deduced about the number of the produced modes, their type and the similarity between the values of their modal properties.

First of all, we notice that the number of modes that are identified by using the developed, in the context of this thesis, software, changes from one configuration to another. We don't get a clear and steady modal number in every configuration from the developed software. For example, in configuration 10, there are 20 modes identified, whereas in configuration 11, there are noted 22 identified modes. Probably, this happens, due to the fact that the developed software is sensitive to new input and needs special adjustment and selection of parameters in order to achieve the most accurate output. Despite all that, the differences between the results are faint and most of the identified modes by the one software are also identified by the other. Furthermore, the identified type for the modes by software 1 agrees with the type that the developed software indicates. However, only a few of the modes can be clearly categorized by type, since some of the modes appear in both types, when using the within developed software and also the available results by software 1 have only 11 mode types identified as. The modes, whose type has been identified, are presented in the following table:

Mode number	Mode(Hz)	Type	Comment
1	0.30631	Transverse	Both software
2	0.6034	Transverse	Both software
3	0.6227	Vertical	Both software
4	0.9646	Transverse	Both software
5	1.0468	Vertical	Both software
6	1.1389	Transverse	Both software
7	1.428	Vertical	Both software
8	1.6967	Transverse	Both software
9	2.0053	Vertical	Both software
10	2.3121	Vertical	Only software 1
11	2.3666	Transverse	Both software
12	2.5901	Transverse	Both software

Table 5.1.15The identified types of some of the modes

As we can see, mode 10, 2.3121Hz, has not been identified, by the developed software. It hasn't appeared in any configuration's results. This is one more mismatch between the software.

Although the mode, 2.3121 Hz, has not been acquired by the developed software, the other identified, modal frequencies are close to each other as it can be clearly seen by observing *Table 5.1.14*. As far as the damping ratios are concerned, it can be deduced that there are similar enough values between the computed damping ratios and all of them have values below 2%.

Finally, the results of the complex modeshapes by the developed software define the damping type of the bridge. Since the blue points in the complex modeshape diagrams are following or are close to a straight line, then Bridge 1 is classically damped.

5.2. Bridge 2

The available input data for the second bridge, were extracted from vibration measurements on it with 6 accelerometer units. The vibration measurements refer to no heavy truck running on the bridge. In order to cover the whole deck of the bridge, 3 different sensor configurations were made on it. Each configuration was recording for 20 minutes at a sampling rate of 200 Hz. These sensor configurations are presented below (fig.5.2. 2) along with some information about the position, in which each sensor unit was placed. The geometry of the bridge is also shown in fig.5.2.1.

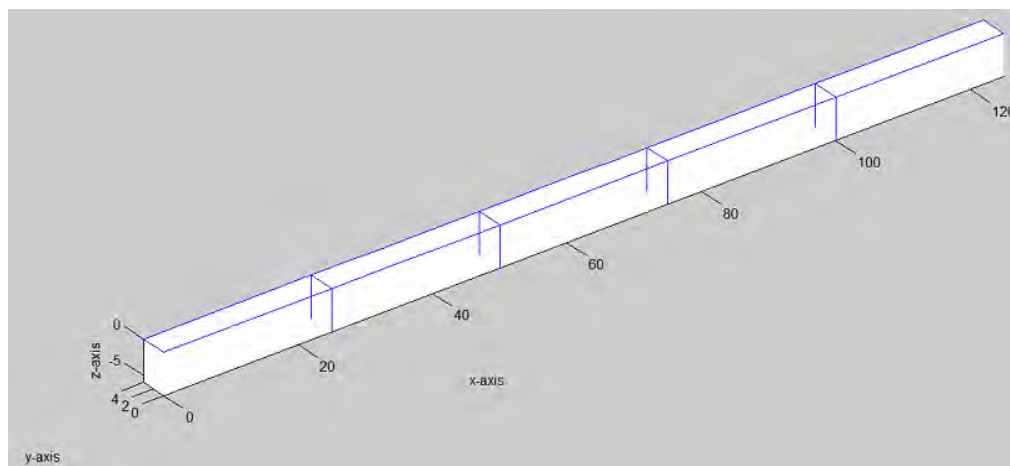


Figure 5.2.1. The geometry of the bridge

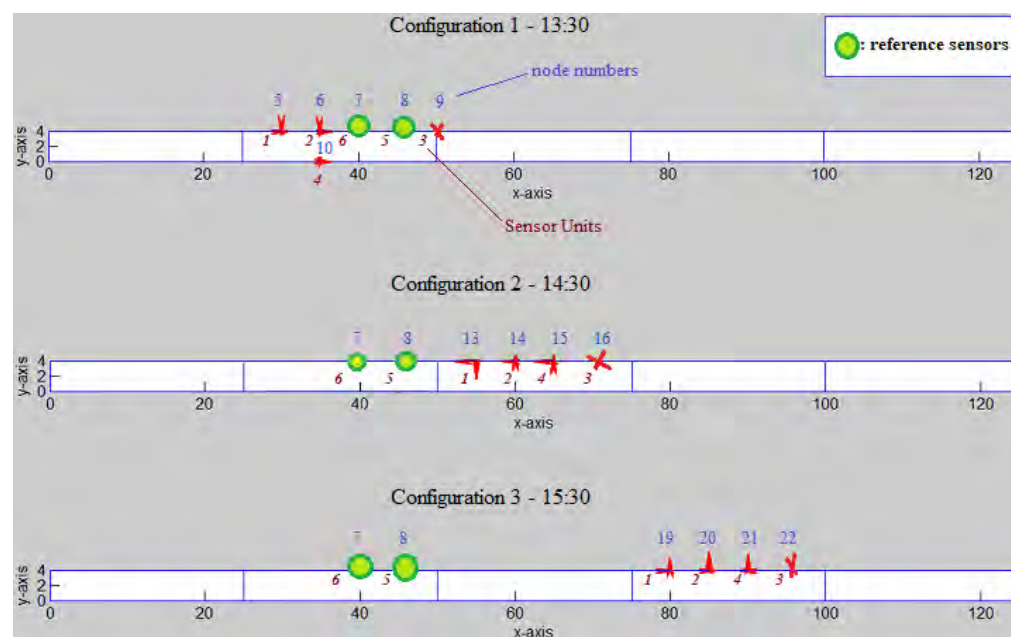


Figure 5.2.2. All sensor configurations for Bridge 2

As we can understand by looking at Figure 5.2.2 the different locations of the sensor units in each configuration, cover the three spans of the bridge. In this way, we can have an assembled global modeshape of the whole structure.

Here, we should note a technical issue that arose during the vibration test. The GPS module of sensor unit 3 was not synchronized with the other sensors during the experimental measurements, so the data from Unit 3 were not taken into account.

5.2.1. Results from the developed software

Using the **developed software** (chapter 4), the modal frequencies and modal damping ratios of the bridge were extracted, and the mode shape components of each configuration were combined to form and illustrate the assembled modeshapes.

Configuration 1 (time 13:30)

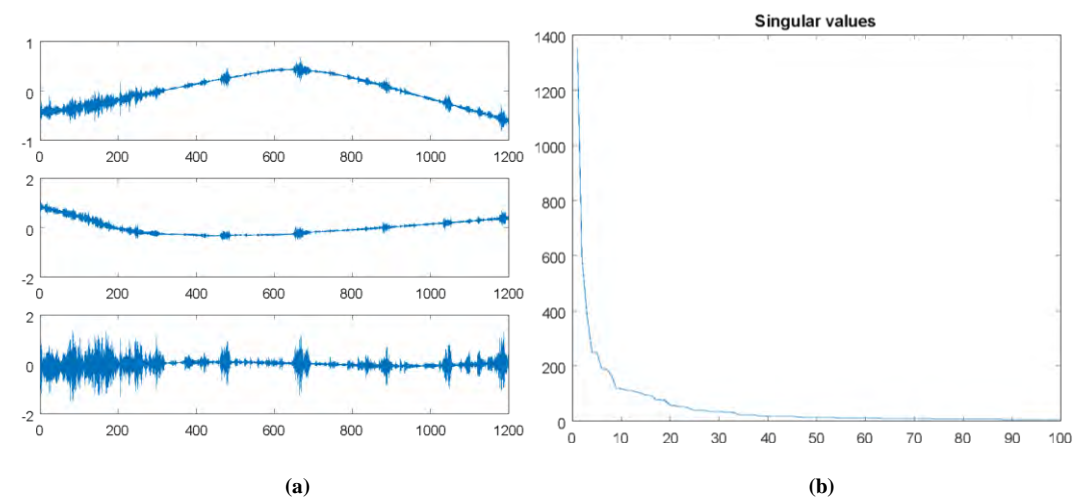


Figure 5.2.3. (a) Representative active response time histories. The vertical axis is accelerations (m/s²) and the horizontal is time (sec). (b) Singular values

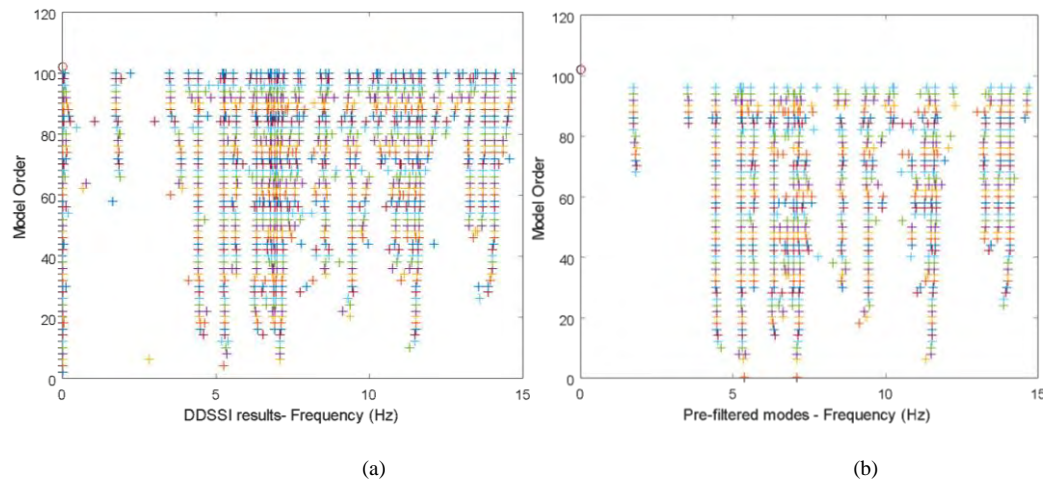


Figure5.2.4. (a) The DD-SSI modal analysis results (b) Results after filtering with the hard validation criteria.

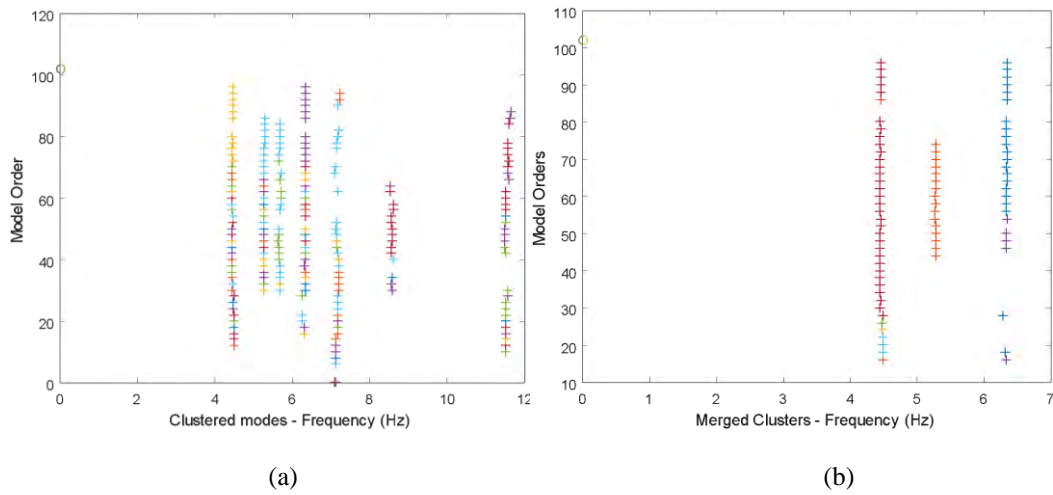


Figure5.2.5. (a) Results after the modes clustering (b) Results after the cluster merging procedure and the elimination of the clusters with less modes than 50% of the total model order

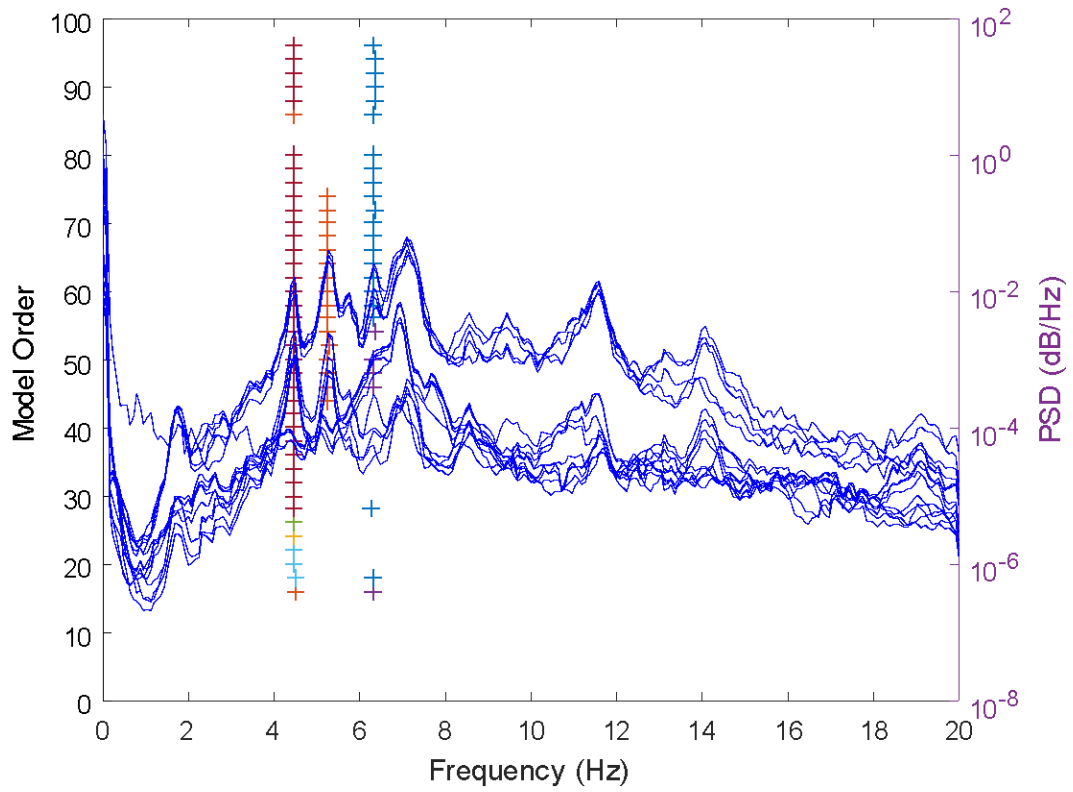


Figure 5.2.6 Modes after cluster merging depicted on the PSD (log scale)

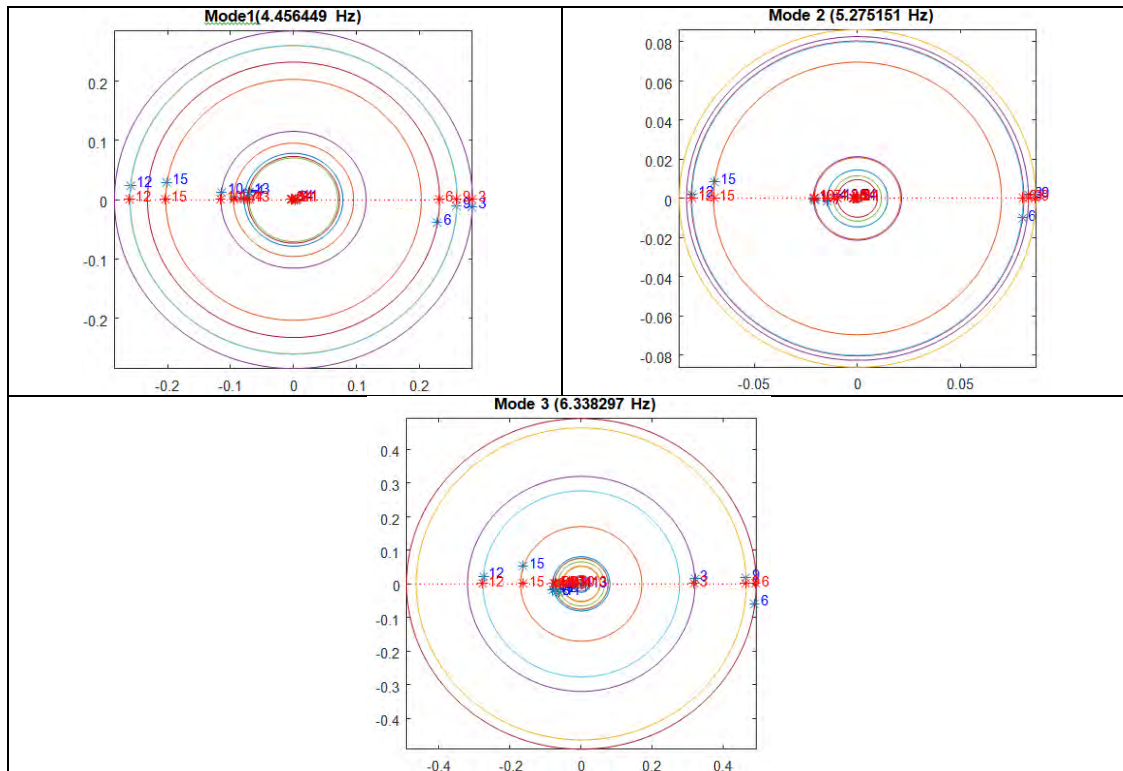


Figure 5.2.7. Diagrams of the complex modeshapes (blue color) and the corresponding real modeshapes (red color) of the identified modes. Blue points in a straight line demonstrate that the bridge is classically damped.

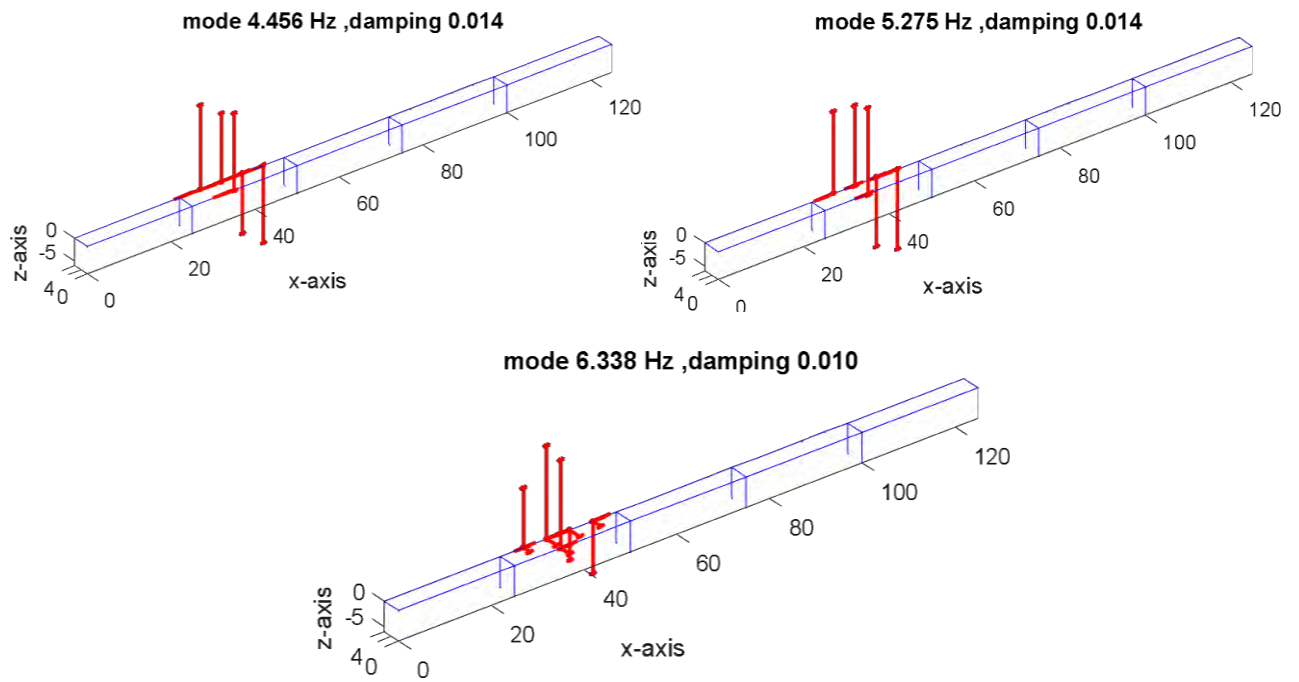


Figure 5.2.8.Real modeshapes of the identified modes, plotted on the geometry of the bridge for configuration 1.

Configuration 2 (time 14:30)

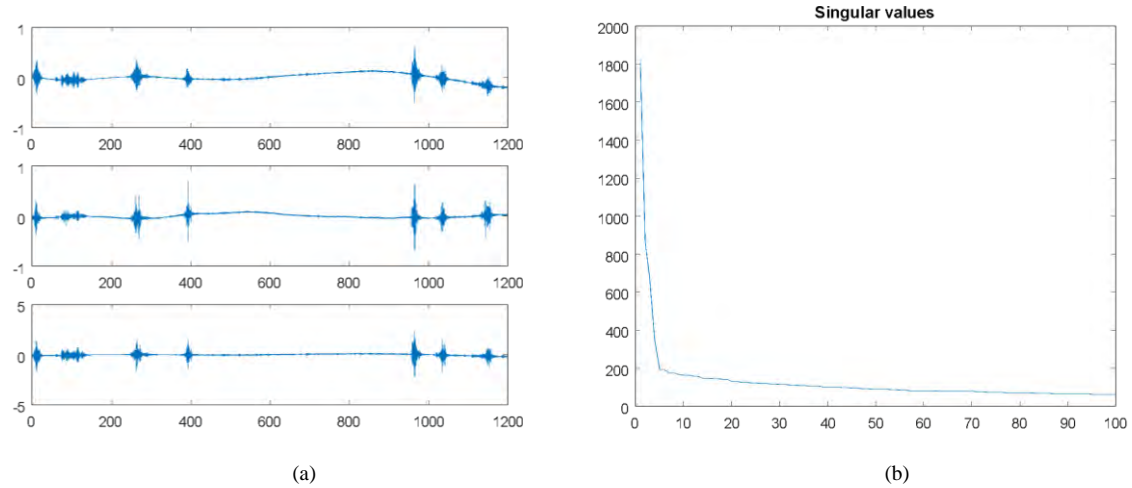


Figure 5.2.9.(a) Representative response time histories. The vertical axis is accelerations (m/s^2) and the horizontal is time (sec). (b) Singular values

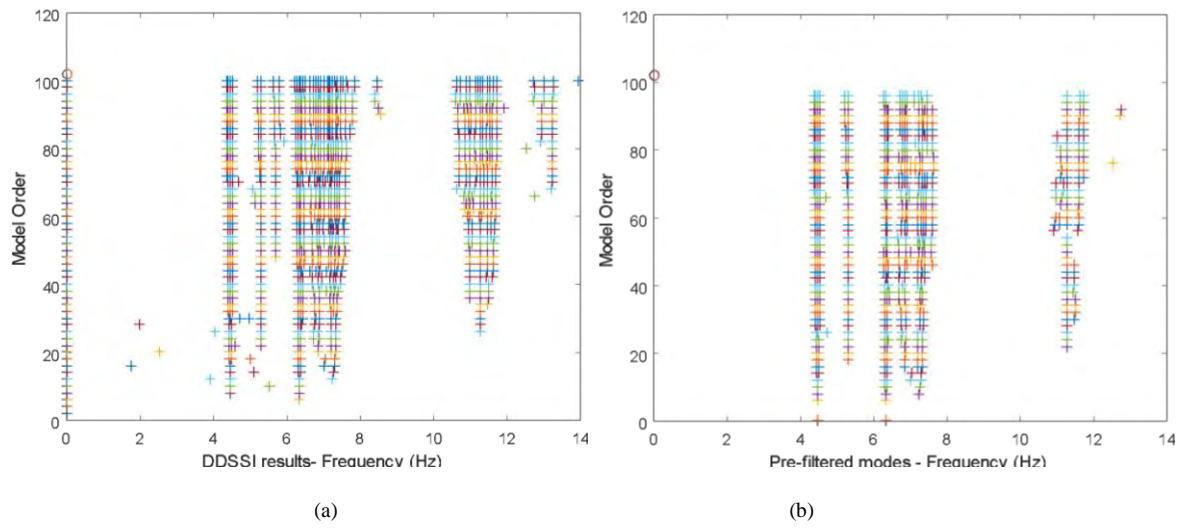


Figure 5.2.10.(a) The DD-SSI modal analysis results (b) Results after filtering with the hard validation criteria

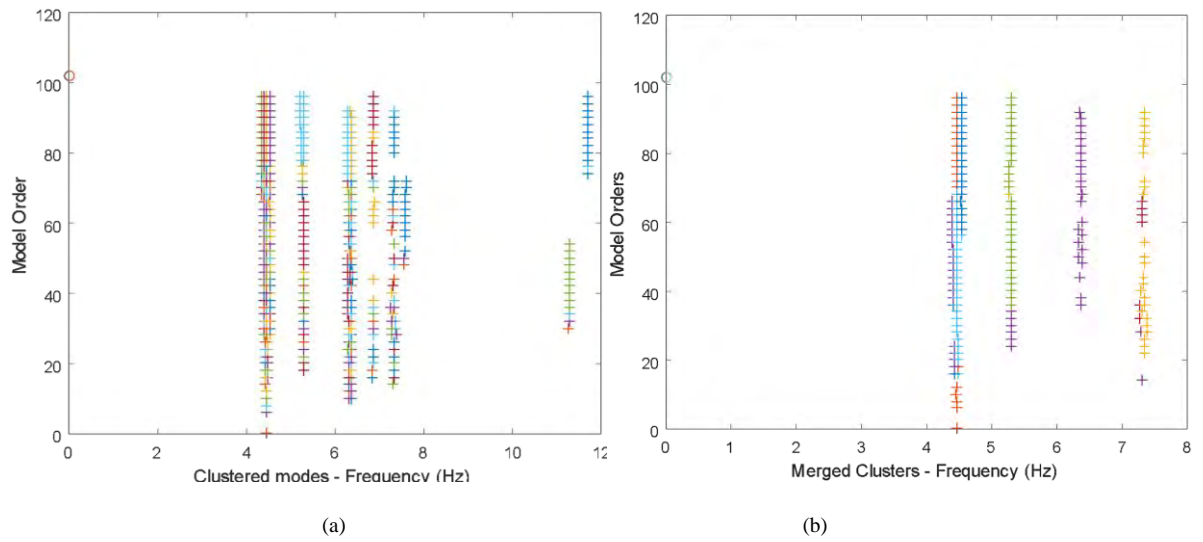


Figure5.2.11. (a) Results after the modes clustering (b) Results after the cluster merging procedure

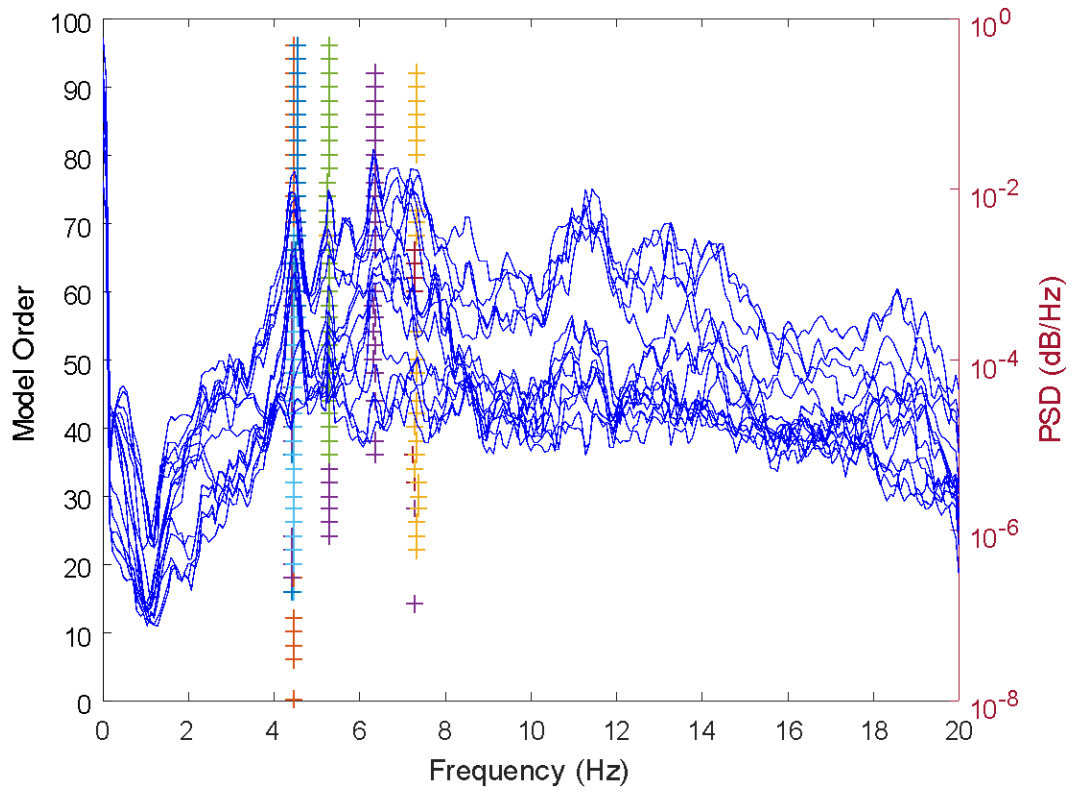


Figure 5.2.12 Modes after cluster merging depicted on the PSD

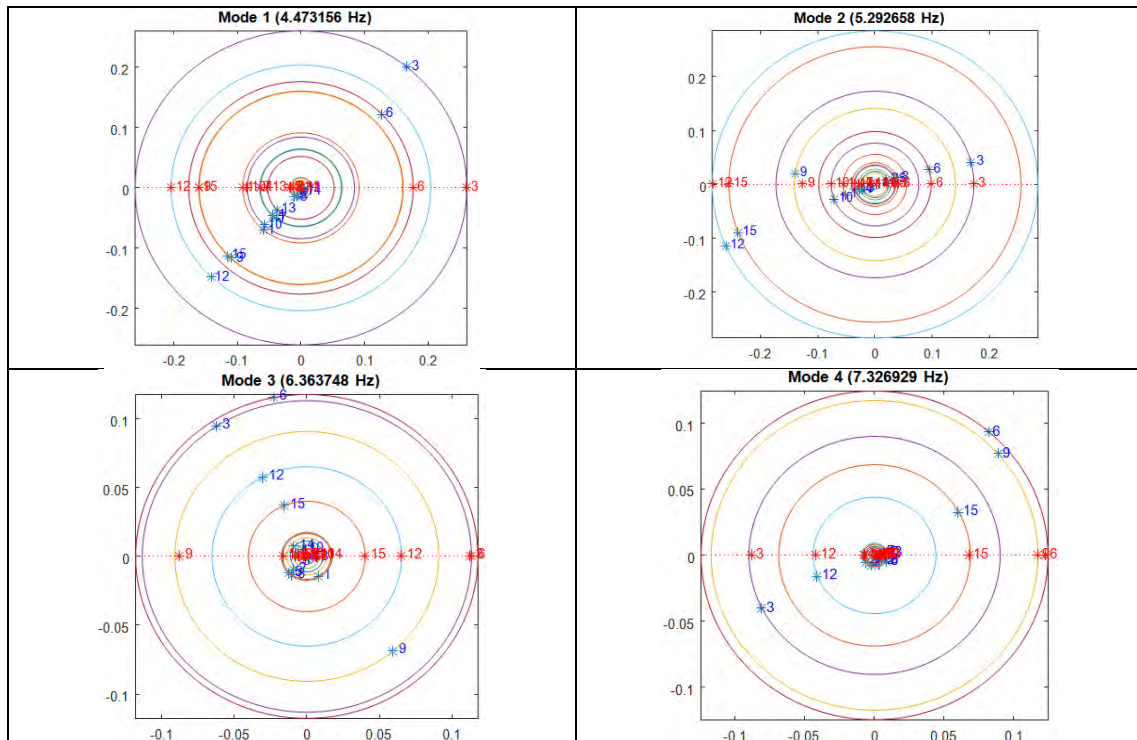


Figure 5.2.13. Diagrams of the complex modeshapes (blue color) and the corresponding real modeshapes (red color) of the identified modes. Blue points in a straight line demonstrate that the bridge is classically damped.

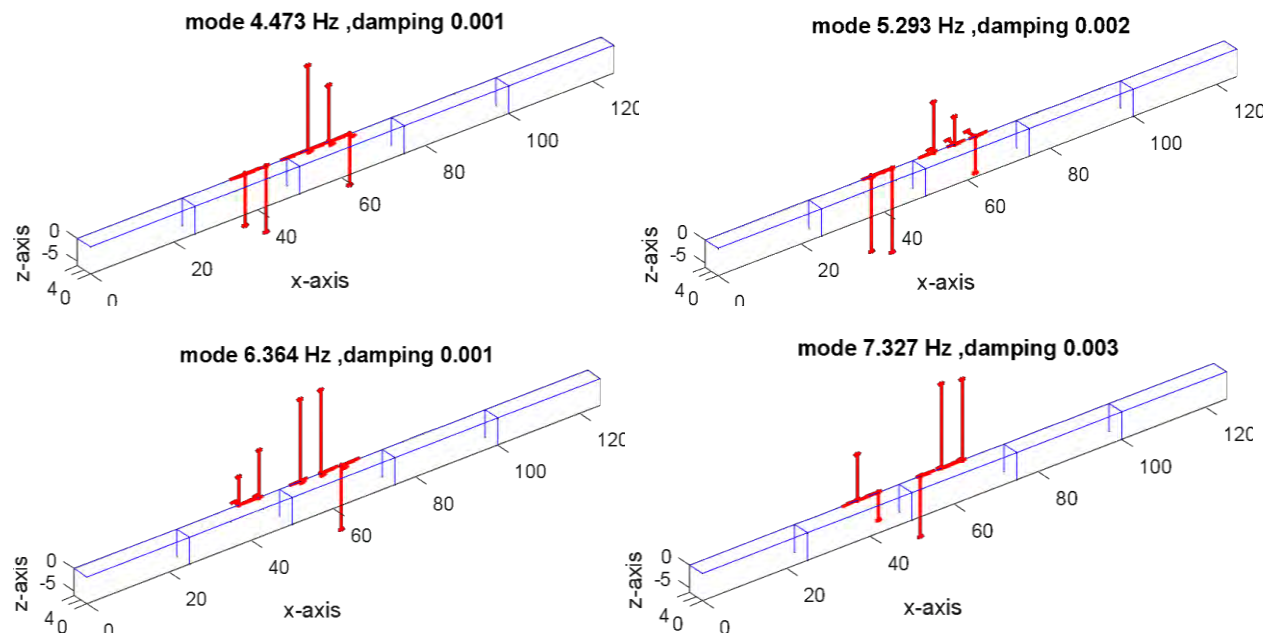


Figure 5.2.14. Real modeshapes of the identified modes, plotted on the geometry of the bridge

Configuration 3 (time 15:30)

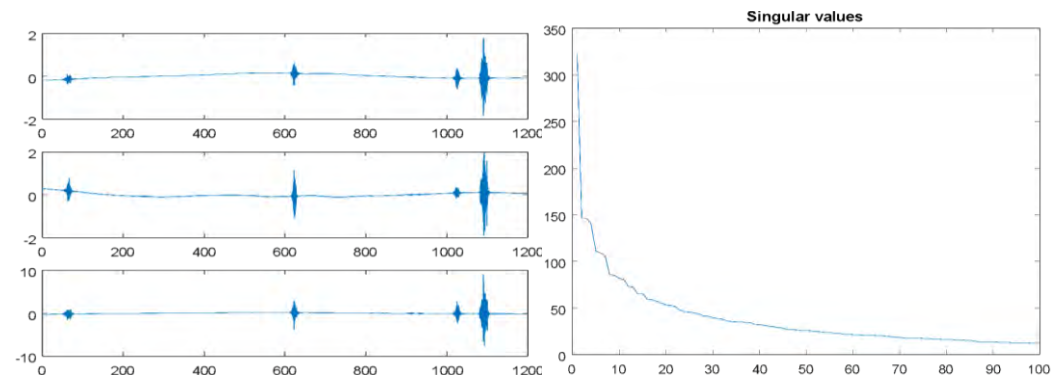


Figure 5.2.15. (a) Representative active response time histories. The vertical axis is accelerations (m/s^2) and the horizontal is time (sec). (b) Singular values

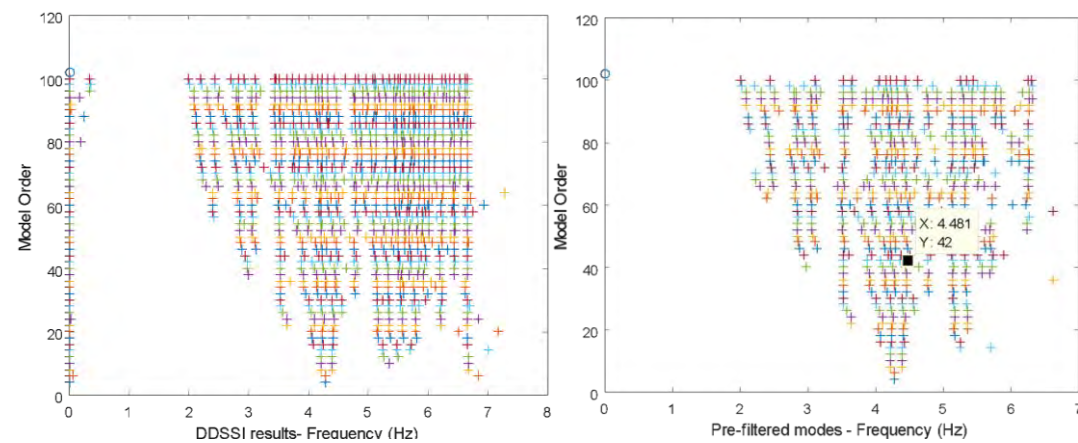


Figure 5.2.16 (a) The DD-SSI modal analysis results (b) Results after filtering with the hard validation criteria

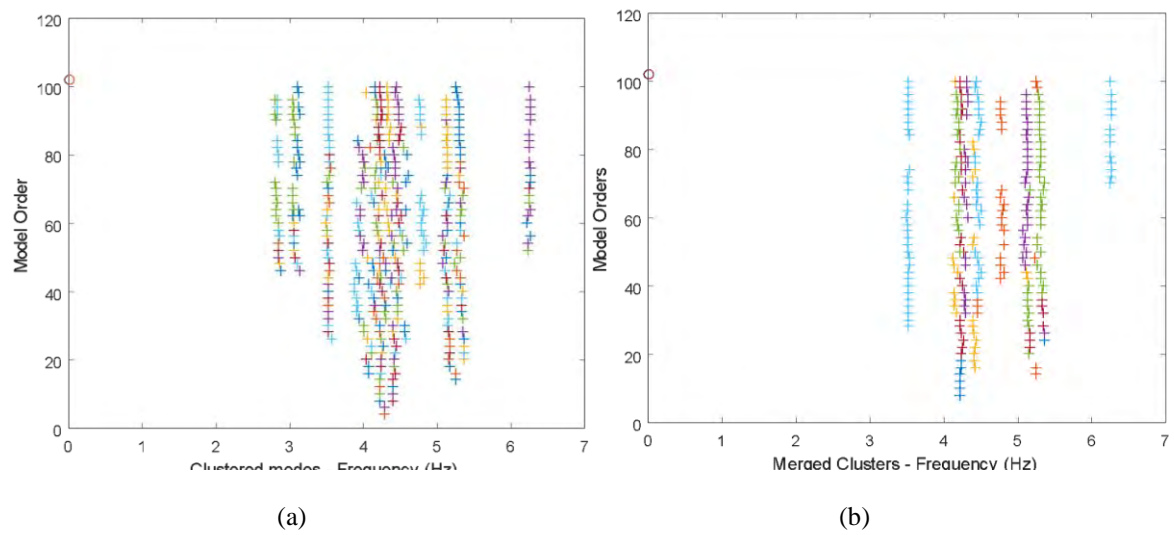


Figure 5.2.17.(a) Results after the modes clustering (b) Results after the cluster merging procedure

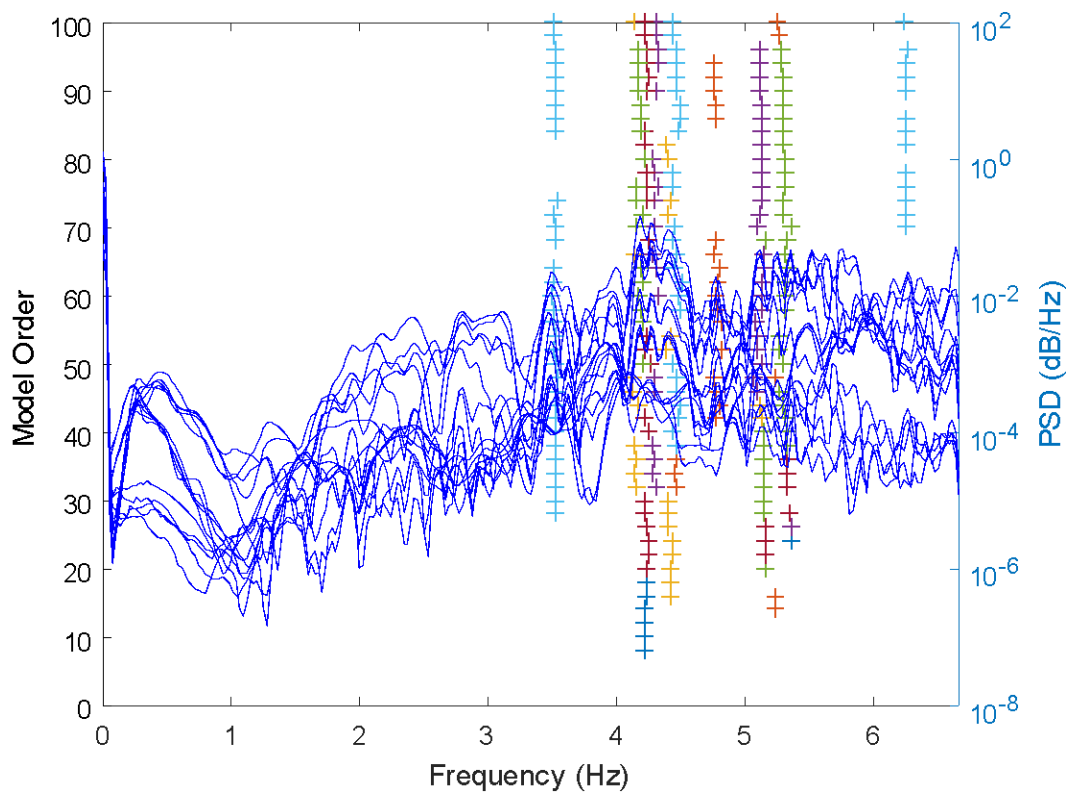


Figure 5.2.18. Modes after cluster merging depicted on the PSD

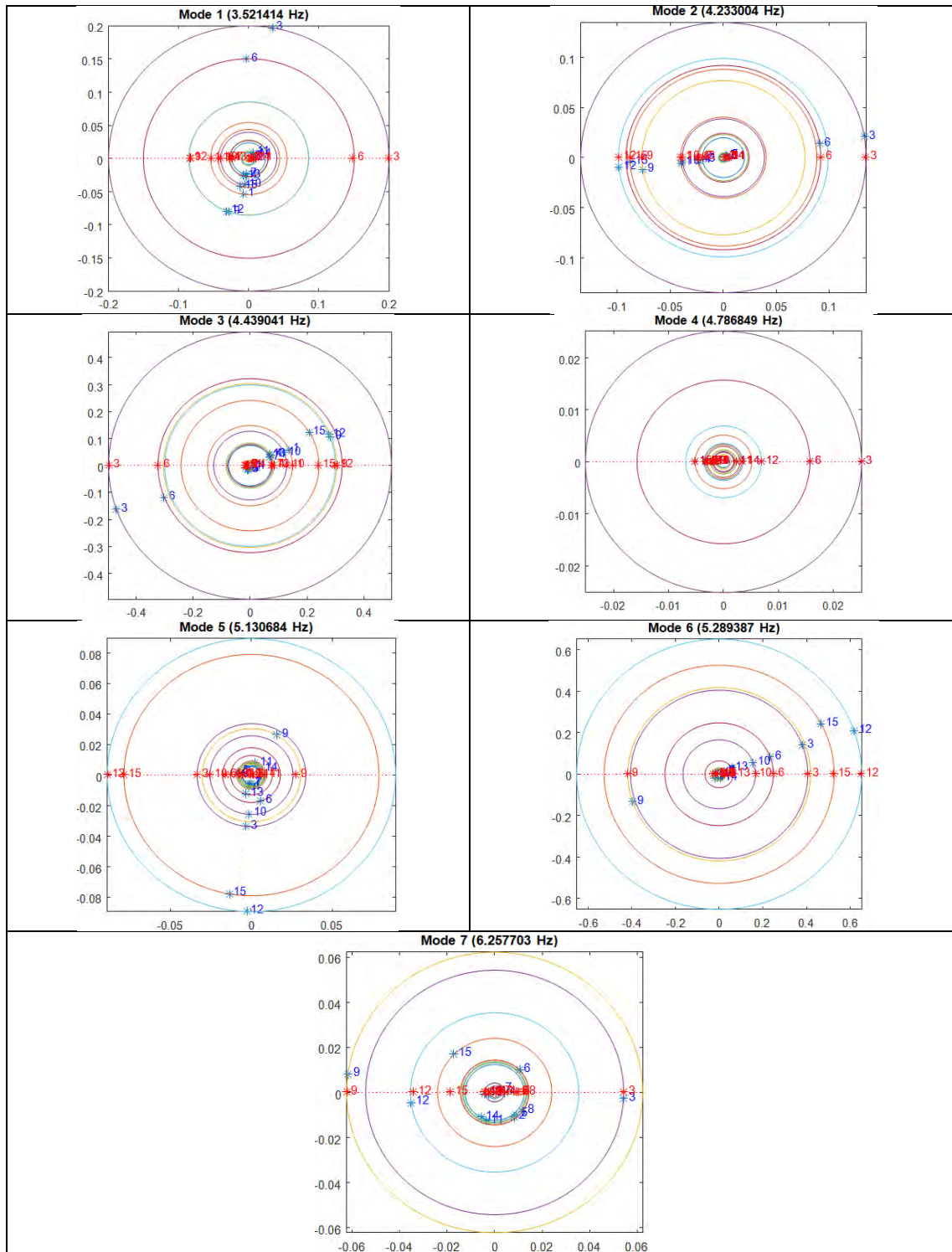


Figure 5.2.19. Diagrams of the complex modeshapes (blue color) and the corresponding real modeshapes (red color) of all the identified modes. Blue points in a straight line demonstrate that the bridge is classically damped.

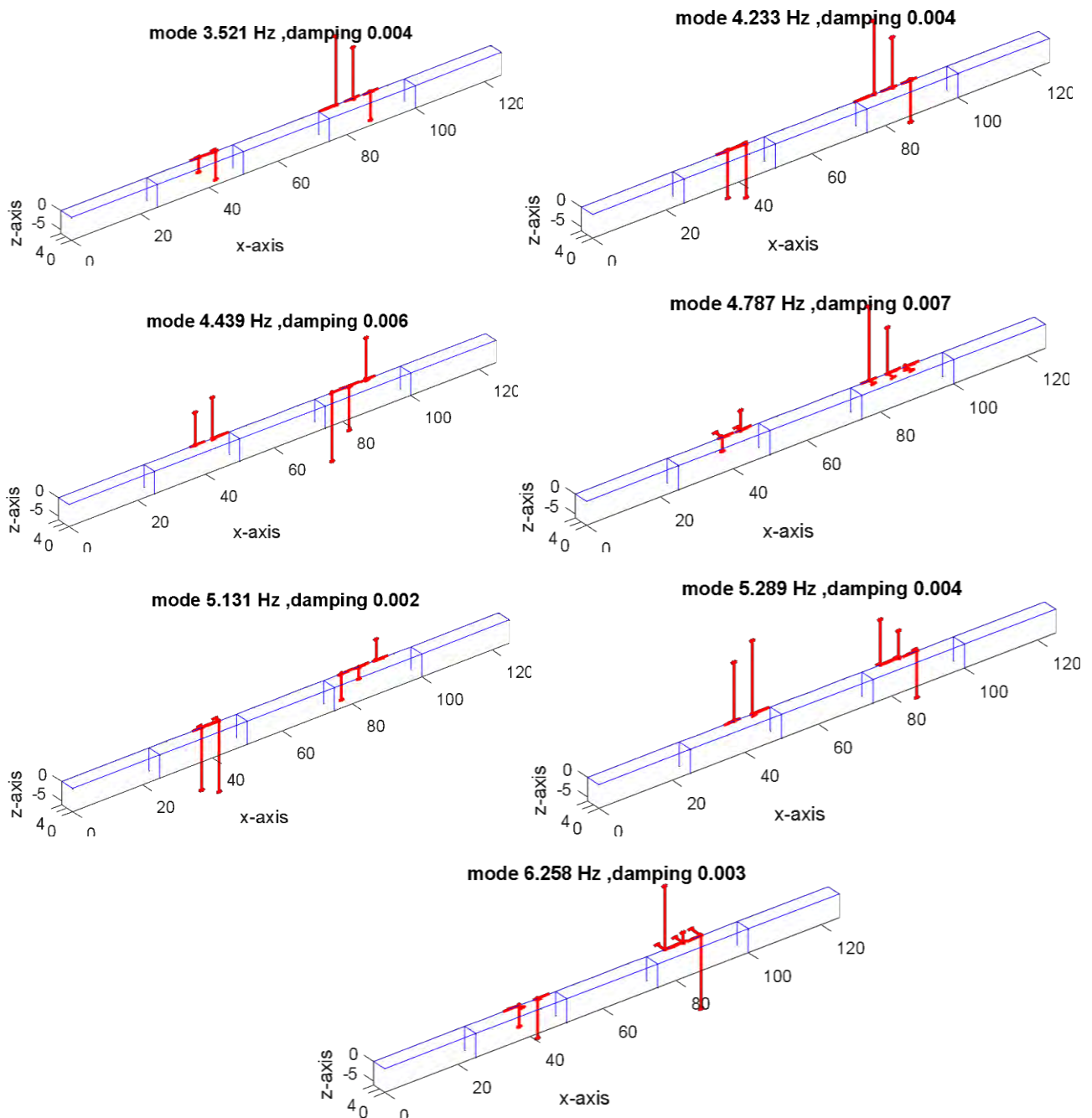


Figure 5.2.20. Real modeshapes of all the identified modes plotted on the geometry of the bridge

The above identified modeshapes were combined for the modes, which are common in each configuration and the assembled modeshapes are following. The common identified modes are presented in the next table:

Configuration	Common identified modes		
1	4.456	5.275	6.338
2	4.47	5.293	6.364
3	4.439	5.289	6.258

Table 5.2.1. Common modes for each configuration

Assembled modeshapes

- **Mode 1**

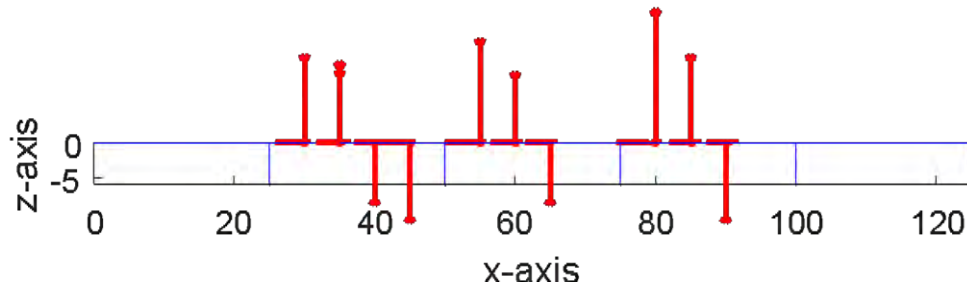
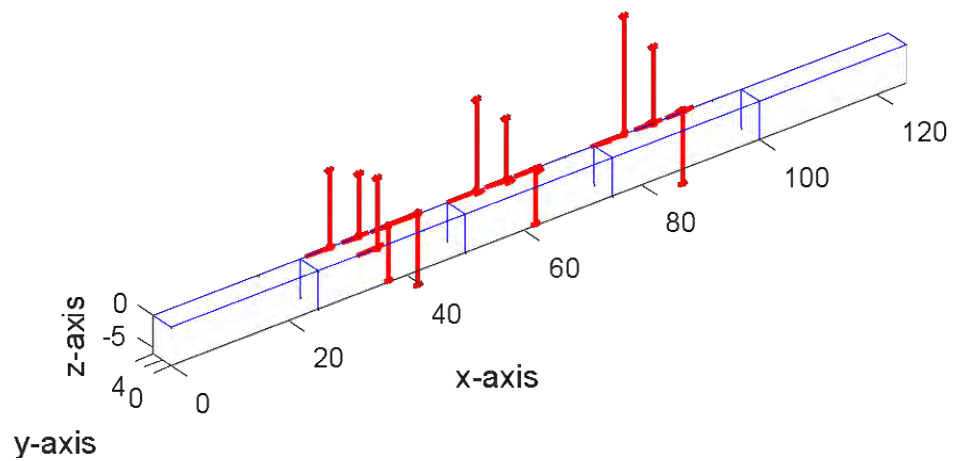


Figure5.2.21. **Mode 1 – Vertical (4.456 Hz, 4.47 Hz, 4.439 Hz).** Span 2, 3 and 4 deflect vertically. Motion is exactly the same. Within each span the “second simply supported” mode is excited. The longitudinal deflection is significant. Deflection in transverse direction is very small.

- **Mode 2**

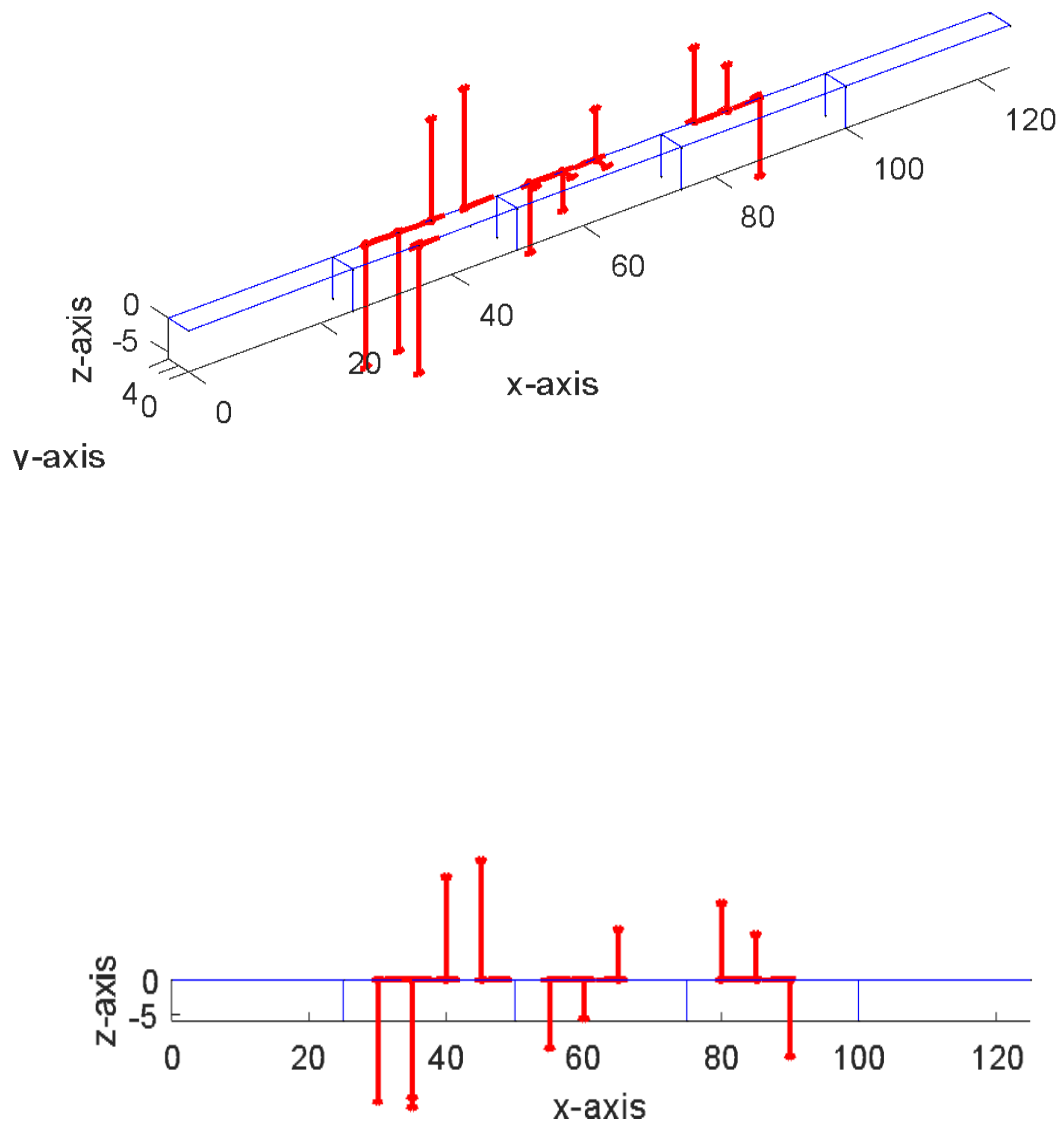


Figure 5.2.22. **Mode 2 – Vertical (5.275 Hz, 5.293 Hz, 5.289 Hz):** Span 2, 3 and 4 deflect vertically. Motion in span 2 and 3 is similar. Deflection in span 3 is less than deflection in span 2. Deflection in span 4 is in opposite direction than deflection in span 2 or 3. Within each span the “second simply supported” mode is excited. The longitudinal deflection is significant. Deflection in transverse direction is relatively small.

- **Mode 3**

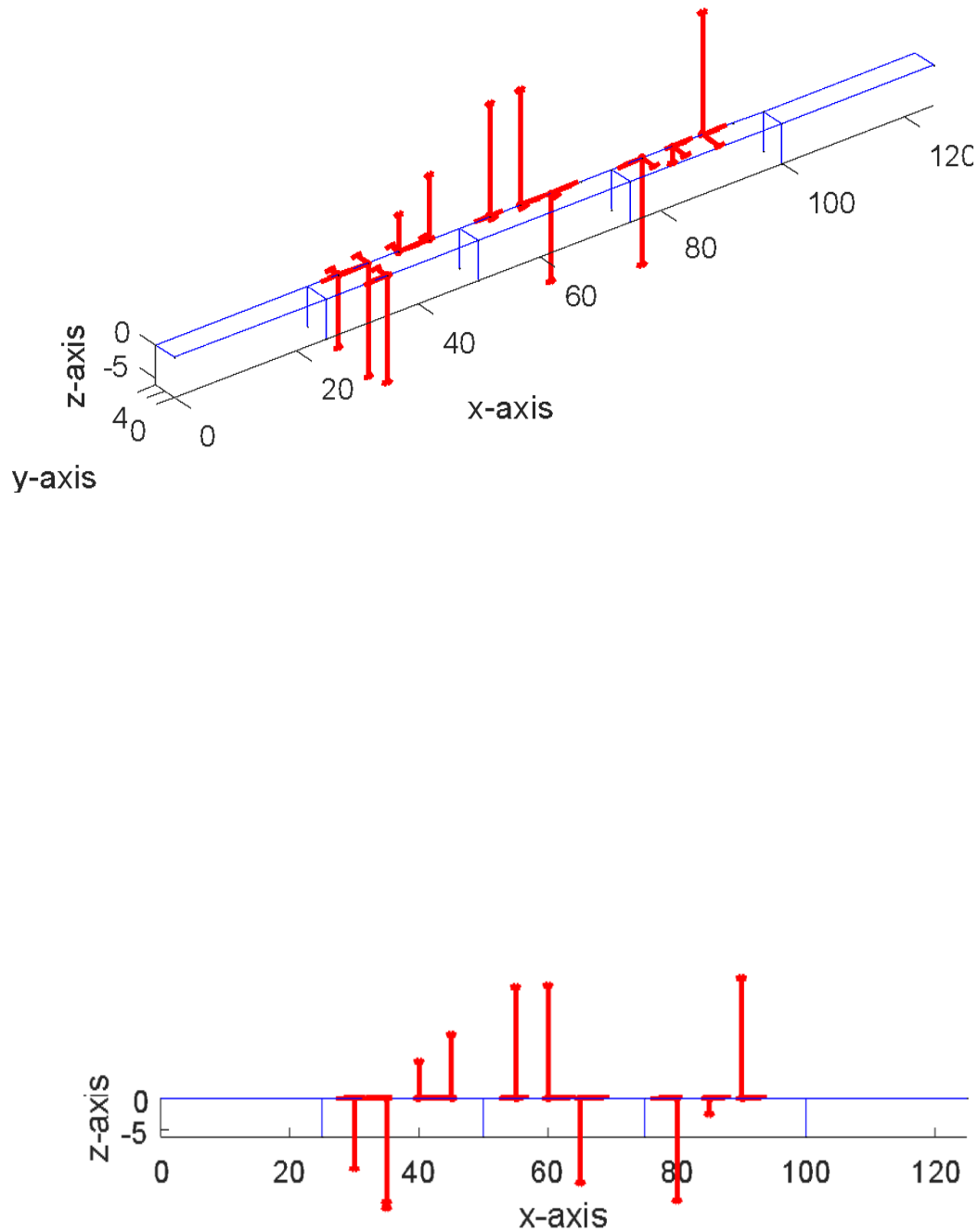


Figure 5.2.23. **Mode 3 – Vertical (6.338 Hz, 6.364 Hz, 6.258 Hz):** Span 2, 3 and 4 deflect vertically. Motion in span 2 and 4 is similar. Deflection in span 3 is in opposite direction that deflection in span 2 or 4. Within each span the “second simply supported” mode is excited. The longitudinal deflection is significant. There is some small deflection in the transverse direction.

5.2.2. Results from Software 2

Using the previously presented **Software 2** (chapter 4), which is based on the peak picking approach on the power spectral densities, the modal frequencies and modal

damping ratios of the bridge were extracted, and the mode shapes were constructed for each configuration separately as well as the assembled ones. The following table contains the acquired results. An example of the acquired results from Software 2, in further detail, is presented in Appendix B.

Table5.2.2. First 3 experimentally identified modal frequencies (vertical) and modal damping ratios of the second bridge, by Software 2 compared to the results from the developed software.

Software 2				
Mode	Modal Frequency (Hz) Damping Ratio Conf_13:30	Modal Frequency (Hz) Damping Ratio Conf_14:30	Modal Frequency (Hz) Damping Ratio Conf_15:30	Mean values for all configurations
1	4.471 0.0083	4.456 0.0112	4.528 0.0095	4.485 0.0096
2	5.332 0.0105	5.302 0.0029	5.336 0.0032	5.323 0.0055
3	6.347 0.0184	6.33 0.0048	6.413 0.0070	6.363 0.0101
Developed software				
Mode	Modal Frequency (Hz) Damping Ratio Conf_13:30	Modal Frequency (Hz) Damping Ratio Conf_14:30	Modal Frequency (Hz) Damping Ratio Conf_15:30	Mean values for all configurations
1	-	-	3.5214 0.004	-
2	-	-	4.133 0.004	-
3	4.4565 0.014	4.4732 0.001	4.439 0.006	4.4562 0.007
4	-	-	5.13 0.002	-
5	5.2752 0.014	5.2927 0.002	5.2894 0.004	5.2858 0.0067
6	6.3383 0.010	6.3637 0.001	6.2577 0.003	6.3199 0.00467
7	-	7.3269 0.003	-	-

The assembled modeshapes of the identified modes from Software 2, are given in the following figures:

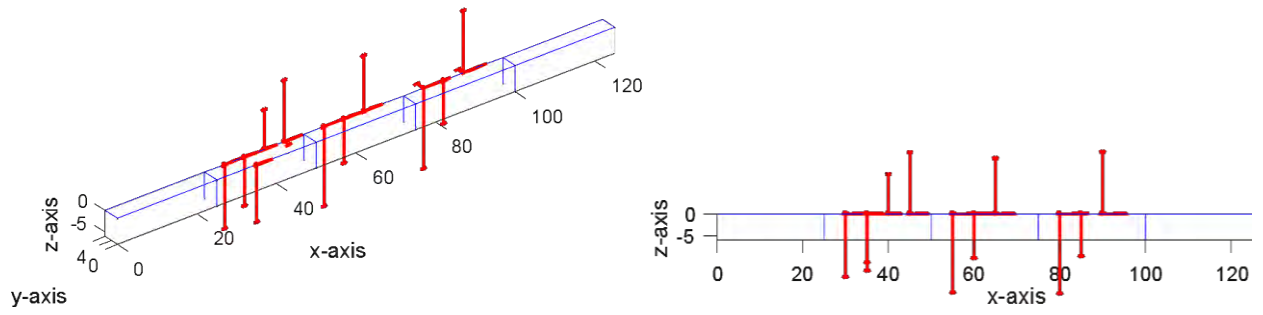


Figure5.2.24. **Mode 1** – Vertical (4.47 Hz, 4.46 Hz, 4.52 Hz) by Software 2.

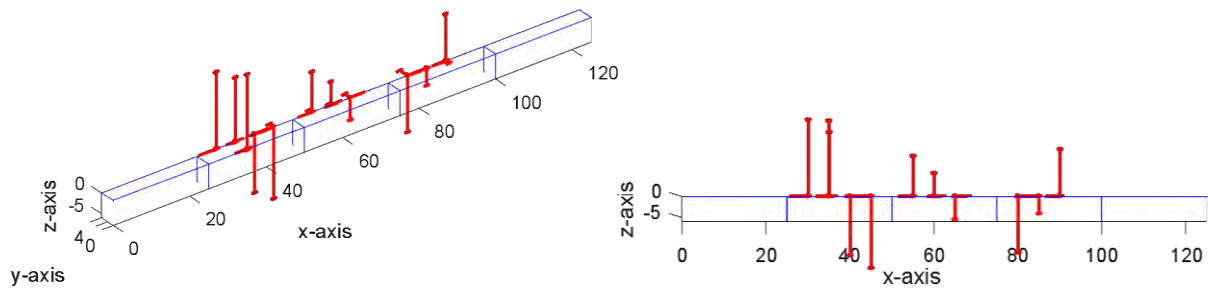


Figure5.2.25. **Mode 2** – Vertical (5.33 Hz, 5.30 Hz, 5.34 Hz) by Software 2.

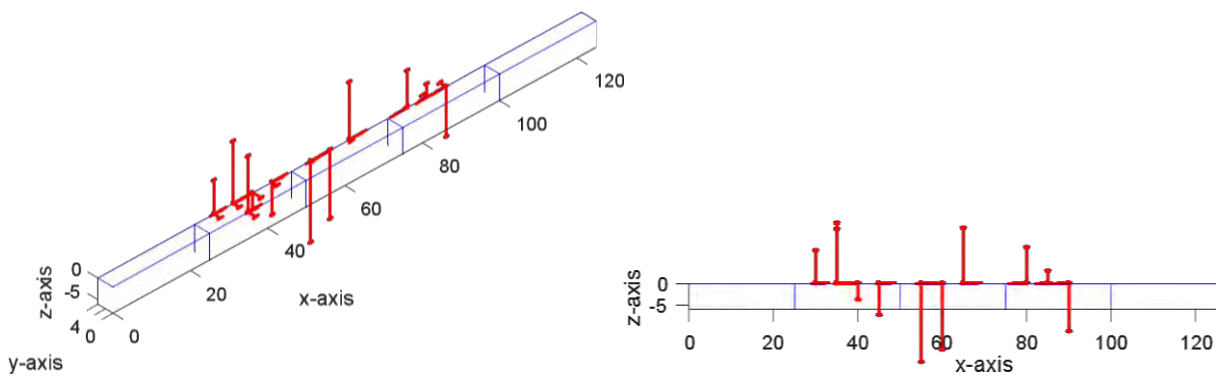


Figure5.2.26. **Mode 3** – Vertical (6.35 Hz, 6.33 Hz, 6.41 Hz) by Software 2.

5.2.3. Conclusions

The previously presented results by both software, show us some interesting information about the structure and the software themselves. To begin with, the developed software has once more given, as an output, different modes for each configuration but also common modes between the configurations. The common modes, among the configurations, are 4.4562, 5.2858 and 6.3199 (mean values) and are in the vertical direction. In addition, these modes are the second simply supported modes of the structure's spans. The complex modeshapes that are presented for most of the modes, consist of blue points in a straight line, something that shows that the bridge is classically damped. The complex modeshapes, which are not close to a straight line, probably, indicate that the mode they correspond to is not real.

Moreover, Software 2 produces results, which match, significantly, the results of the developed software. In addition, the real modeshapes that occur for every identified mode after plotting, show the same motion for the bridge, as in the developed software. However, the vectors on the plots have completely opposite directions. For example, in Figures 5.2.21, 5.2.24. The opposite direction does not indicate that the modeshape is different, but it is simply the same solution in the opposite phase. As far as the damping ratios are concerned, there is a slight mismatch between the values that correspond to the common frequencies.

To sum up, the results of both software match each other well and the produced assembled modeshapes by the developed software, as well as Software 2, predict, exactly the same deformation for the bridge.

5.3. Bridge 3

Within the health monitoring of the third bridge, measurements were made on two spans of it. The intention was to compare the healthy operating one (span 15) with the one suspected to have mechanical damage (span 14). Geometry of both spans is depicted in one picture in figure 5.3.1, because geometry is the same for both of them.

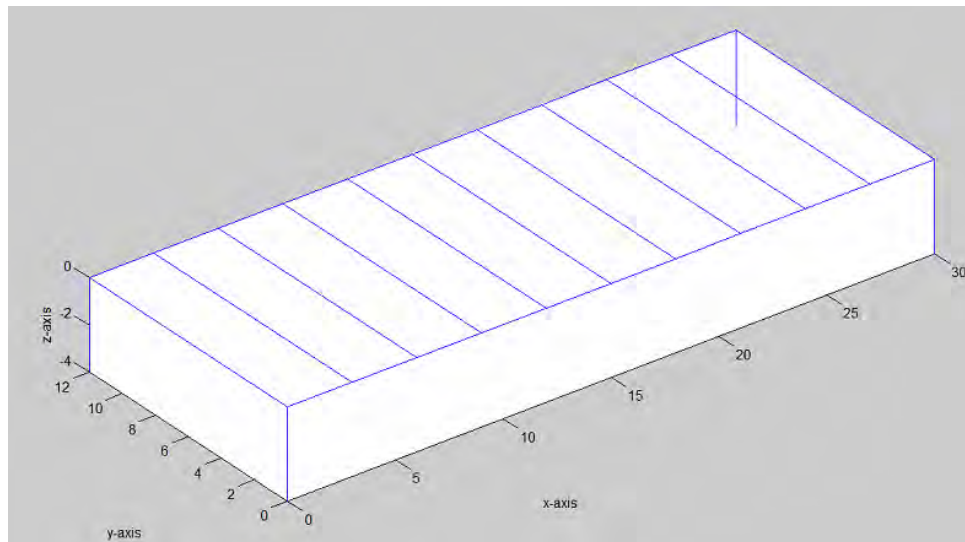


Figure 5.3.1 The geometry of the spans (both are 30m long)

Changes in the mechanical properties of the bridge (failures) are expected to change the dynamical characteristics of the bridge, mostly its modal frequencies and the damping ratios. The comparison between the modal properties of the two neighboring spans (span 14, 15) is expected to give us information about the mechanical state of span 14 in relation to possible fractures or damages. A damage in span 14 of the bridge, will modify the eigenfrequencies of the span (reduction is expected) and probably, the damping ratios (increase is expected). These comparisons were made for different states of load on the bridge, which consist of the following cases: no load on the span and loads of 2,3,4 heavy trucks on the span.

The positioning of heavy trucks with masses comparable to the mass of the bridge is expected to change the dynamic characteristics of the bridge. The loading of the span with heavy vehicles is expected to cause the reduction of the eigenfrequencies if the dynamical characteristics of the trucks are considered to be insignificant. On the other hand, if the dynamic characteristics of the trucks are not ignored, then it is not possible to predict what will happen to the eigenfrequencies.

The accelerometers measured for 10 minutes with a sampling frequency of 200Hz, since the sampling time was $dt = 0,005s$. The number of the sensor configurations made on this bridge are shown in Table 5.3.1, as well as the span, on which they took place and the load case they refer to.

Configuration	Time	Span	Comments
1	9:30	15	Ignored
2	9:50	15	>>
3	10:10	15	NO TRUCKS ON THE SPAN
4	10:30	15	Ignored
5	10:50	15	>>
6	11:10	15	2 TRUCKS ON THE SPAN
7	11:30	15	Ignored
8	11:50	15	>>
9	12:10	15	3 TRUCKS ON THE SPAN
10	12:30	15	Ignored
11	12:50	15	>>
12	13:10	15	4 TRUCKS ON THE SPAN
13	13:30	15	NO TRUCKS ON THE SPAN
14	13:50	14	NO TRUCKS ON THE SPAN
15	14:10	14	2 TRUCKS ON THE SPAN
16	14:30	14	Ignored
17	14:50	14	3 TRUCKS ON THE SPAN
18	15:10	14	4 TRUCKS ON THE SPAN
19	15:30	14	Ignored
20	15:50	14	NO TRUCKS ON THE SPAN

Table 5.3.1. Table with the sensor configurations information.

Not all from the above configurations have been analyzed. The results for each span and configuration, are presented on the following figures. Firstly, for the healthy operating one (span 15) and then for span 14, which is supposed to have a mechanical damage. The load of each span during each sensor configuration can be distinguished in five cases:

Case 1: Span loaded with no trucks

Case 2: Span loaded with 2 trucks

Case 3: Span loaded with 3 trucks

Case 4: Span loaded with 4 trucks

Case 5: Span loaded with no trucks- measurements made after the loading with 2, 3, 4 vehicles

Measurements towards the longitudinal and the transverse direction of the bridge's spans are not used, since there is no significant motion in these directions, so this information is not useful. The most important motion is across the vertical direction, which is used for the definition of four, vertical, bending modes with eigenfrequencies less than 7 Hz.

5.3.1. Results from the developed software

Using the within this thesis **developed software** (chapter 4), the modal frequencies and modal damping ratios of the bridge were extracted as well as the complex mode shapes, which are illustrated in the following diagrams.

SPAN 15 – Case 1: No trucks on span - Configuration 3 (time 10:10)

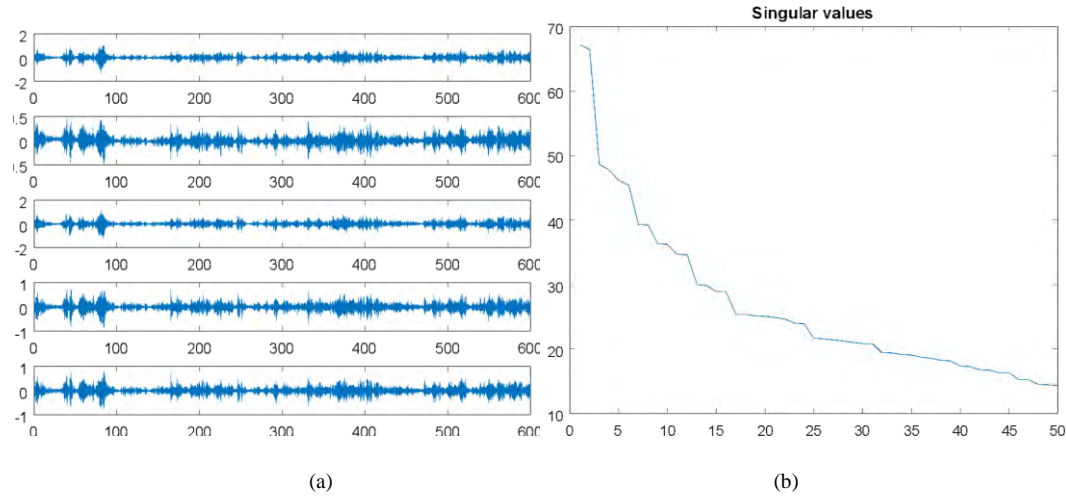


Figure 5.3.2.(a) Active response time histories. The vertical axis is accelerations (m/s²) and the horizontal is time (sec). (b) Singular values.

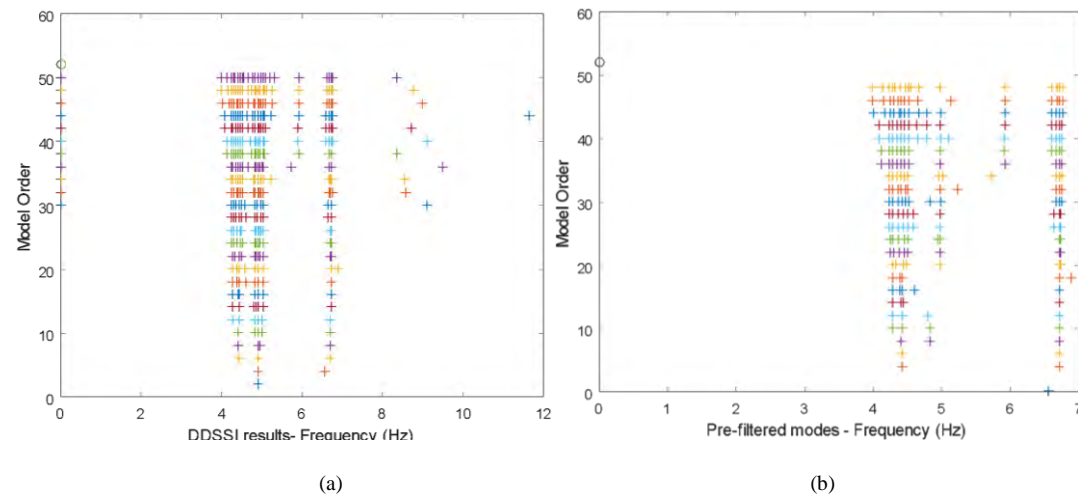


Figure 5.3.3 (a) The DD-SSI modal analysis results (b) Results after filtering with the hard validation criteria

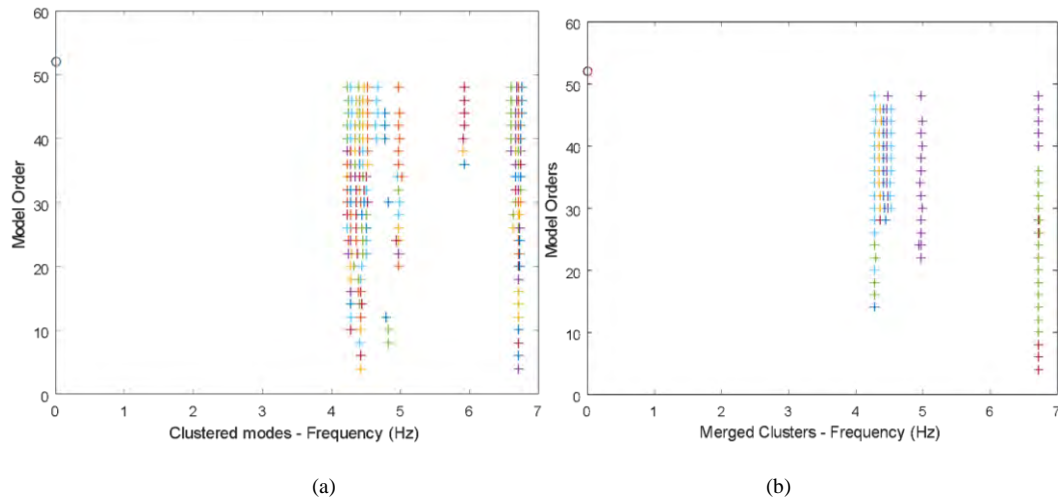


Figure 5.3.4 (a) Results after the modes clustering (b) Results after the cluster merging procedure

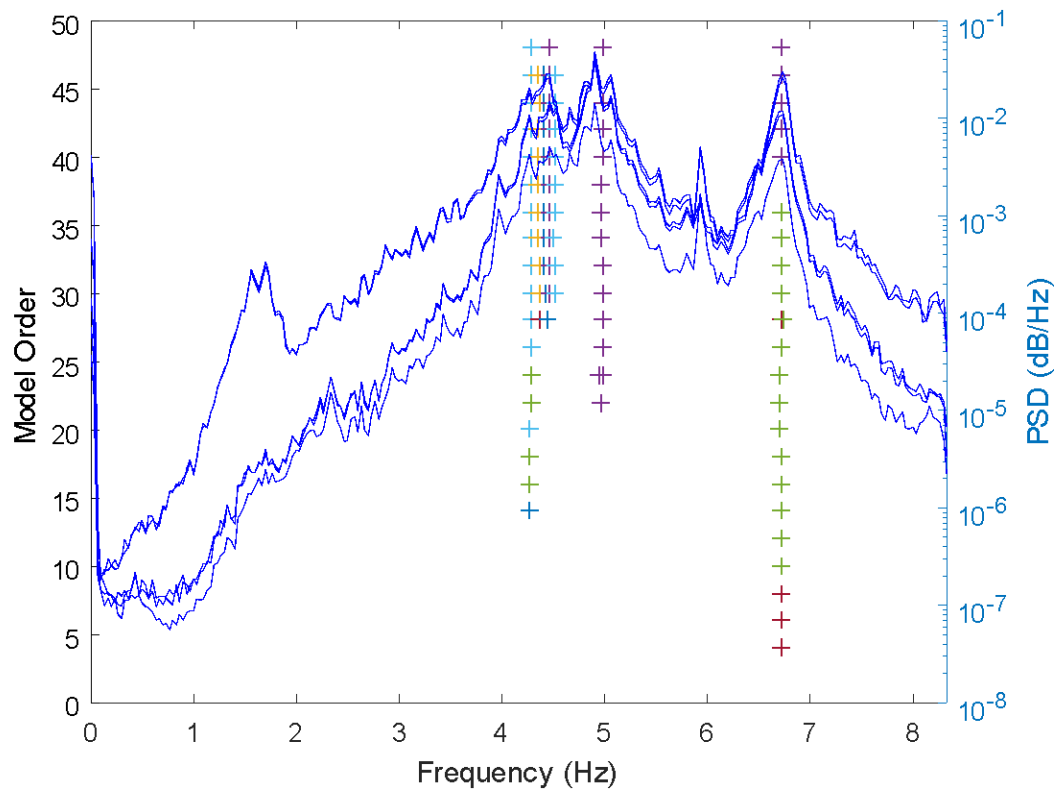


Figure 5.3.5 Modes after cluster merging depicted on the PSD

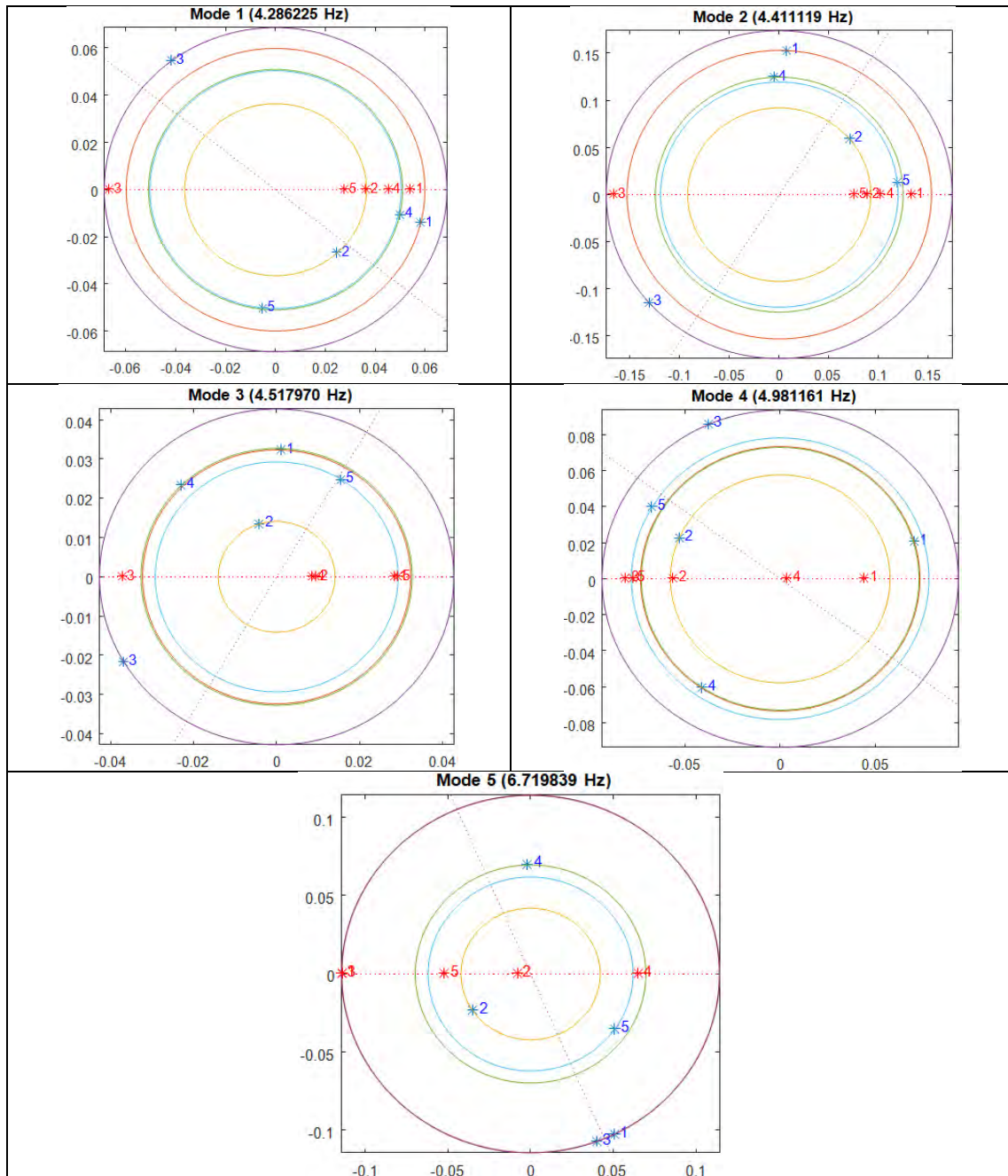


Figure 5.3.6 Diagrams of the complex modeshapes (blue color) and the corresponding real modeshapes (red color). Blue points in no straight line demonstrate that the bridge is non-classically damped.

SPAN 15 – Case 2: Two trucks on span - Configuration 6 (time 11:10)

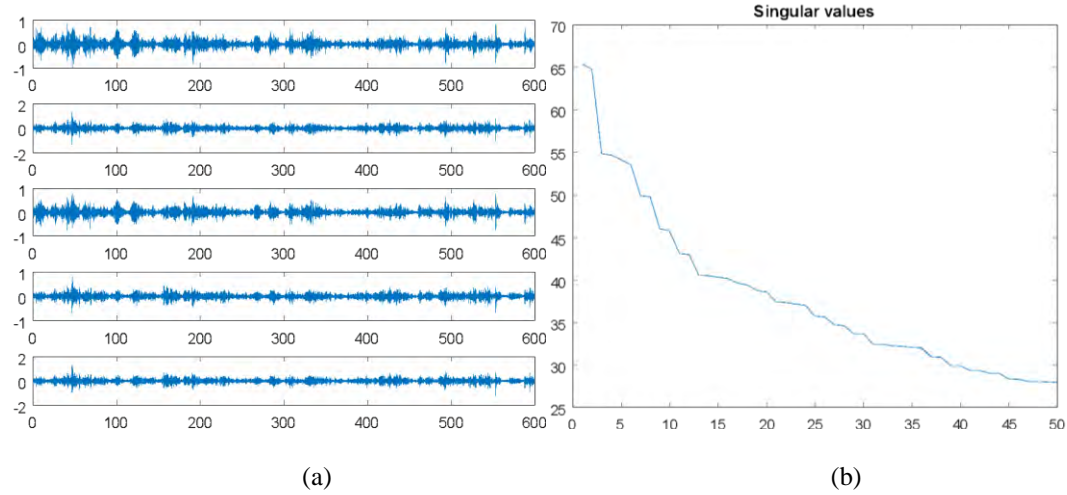


Figure 5.3.7(a) Active response time histories. The vertical axis is accelerations (m/s²) and the horizontal is time (sec). (b) Singular Values

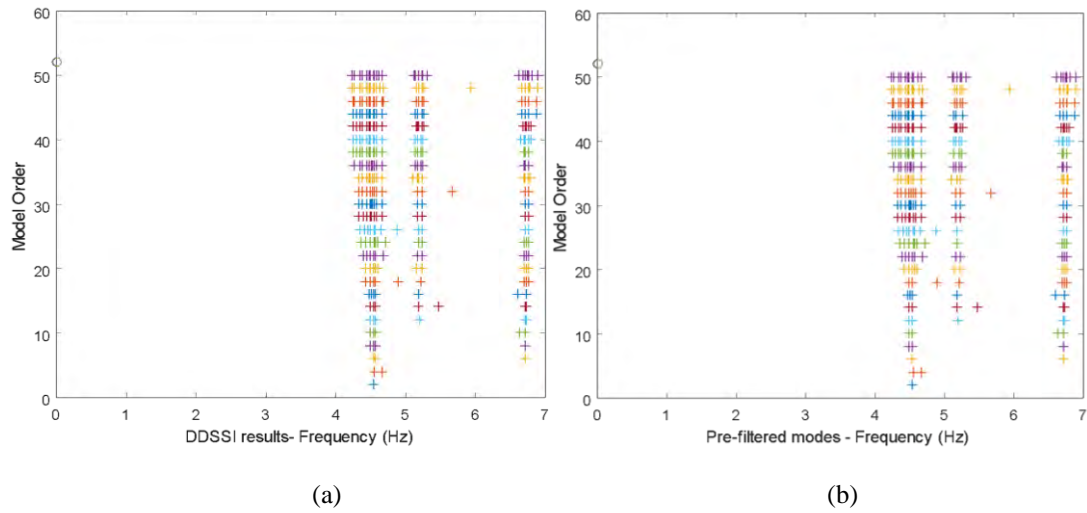


Figure 5.3.8 (a) The DD-SSI modal analysis results (b) Results after filtering with the hard validation criteria

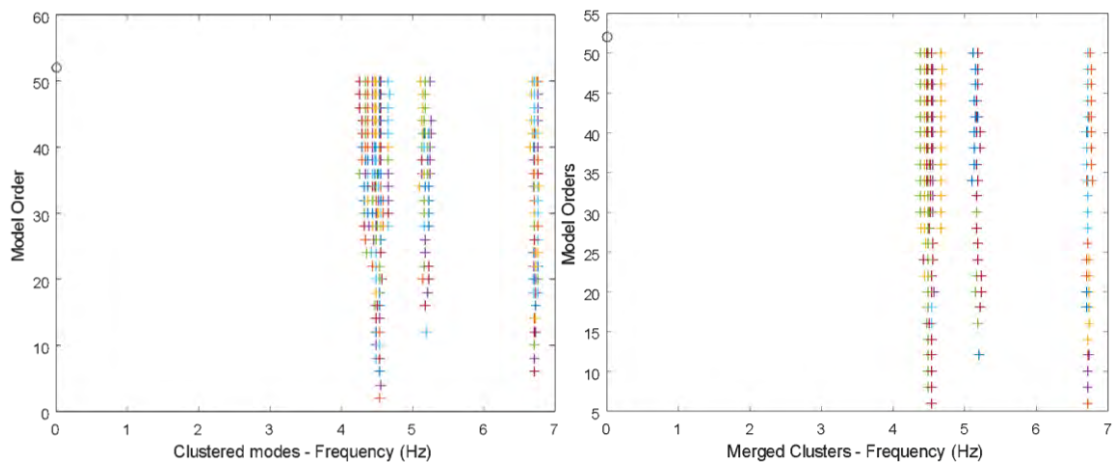


Figure 5.3.9 (a) Results after the modes clustering (b) Results after the cluster merging procedure

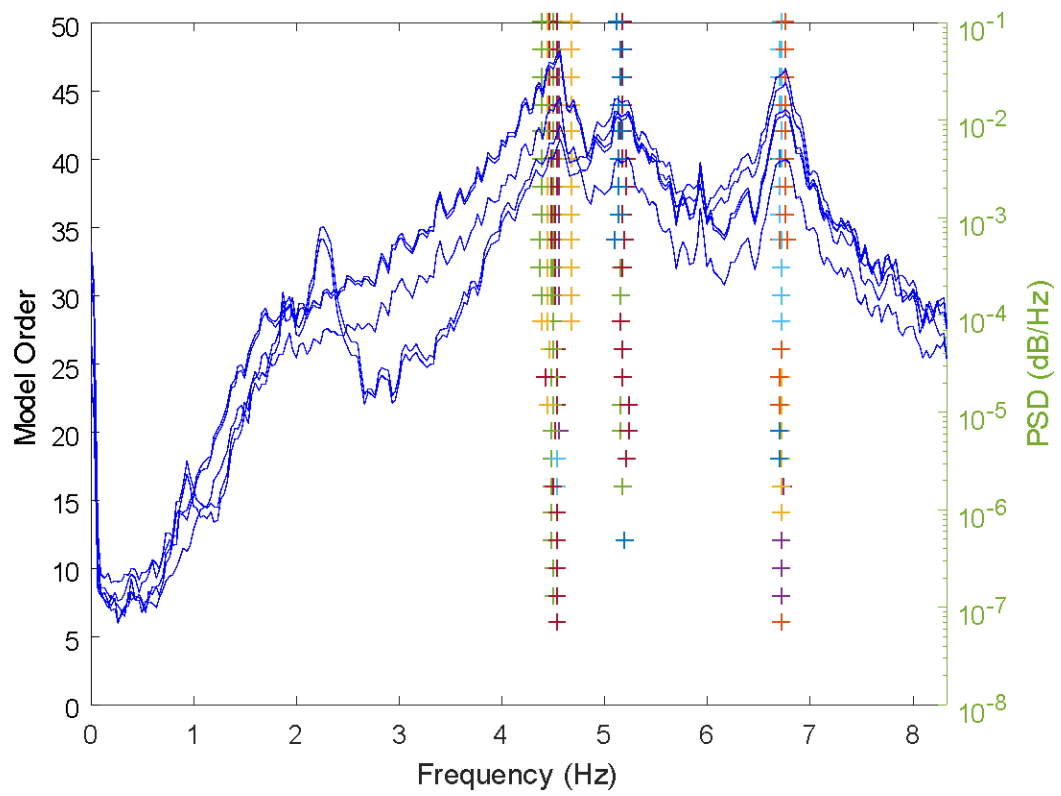
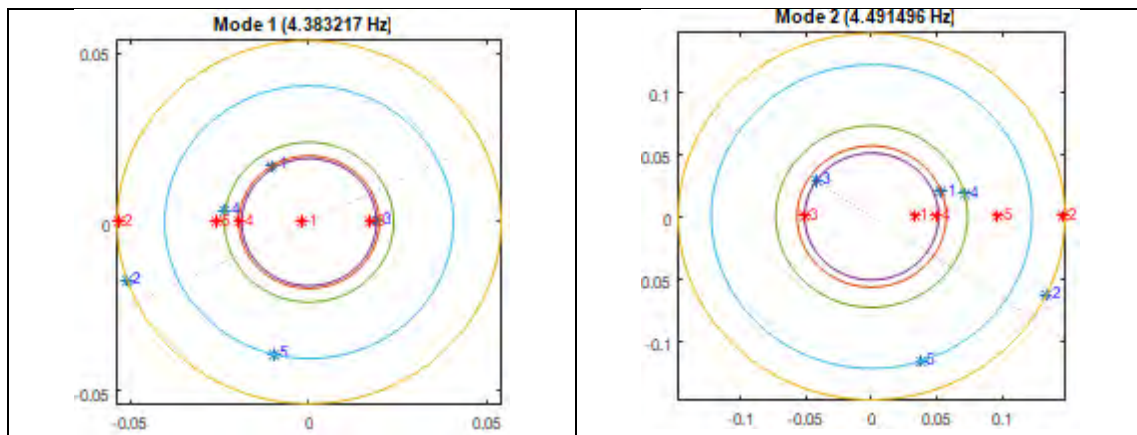


Figure5.3.10. Modes after cluster merging depicted on the PSD



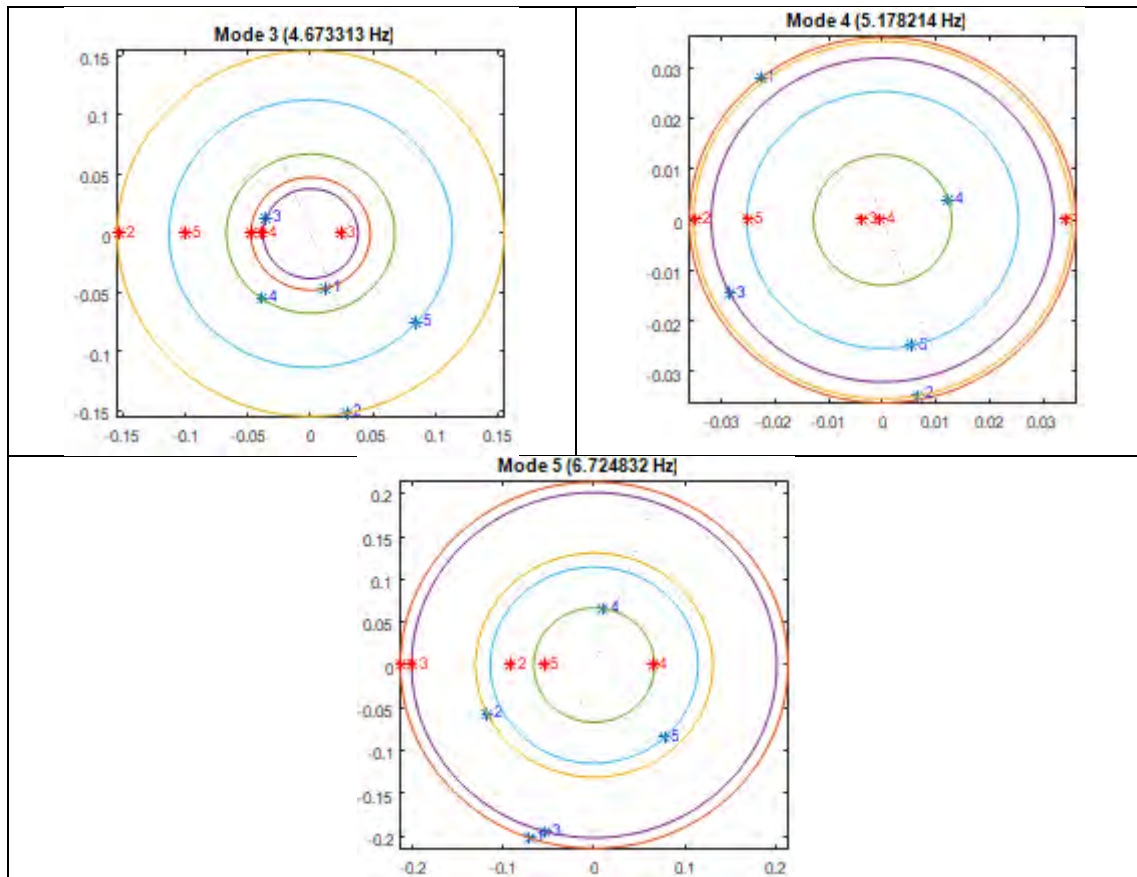


Figure 5.3.11. Diagrams of the complex modeshapes (blue color) and the corresponding real modeshapes (red color). Blue points in no straight line demonstrate that the bridge is non-classically damped

SPAN 15 – Case 3: Three trucks on span - Configuration 9 (time 12:10)

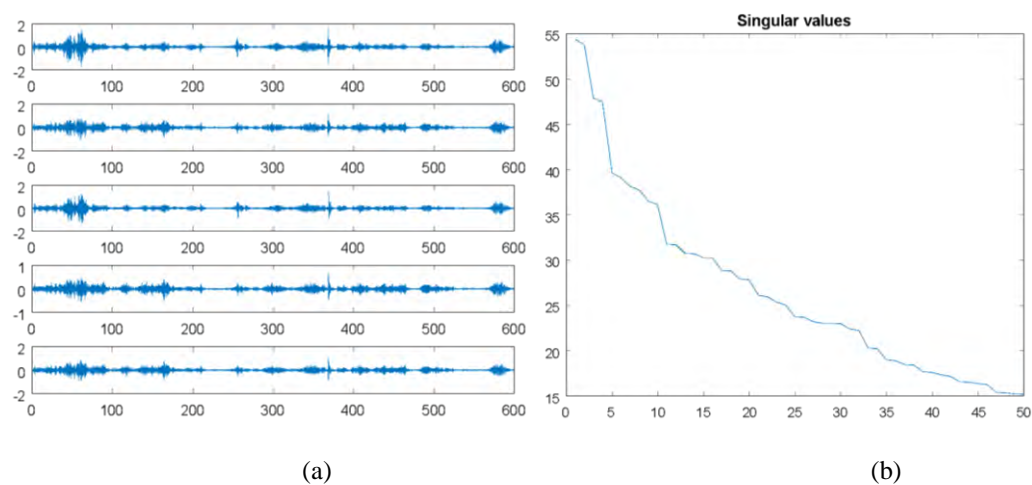


Figure 5.3.12.(a) Active response time histories. The vertical axis is accelerations (m/s^2) and the horizontal is time (sec). (b) Singular values

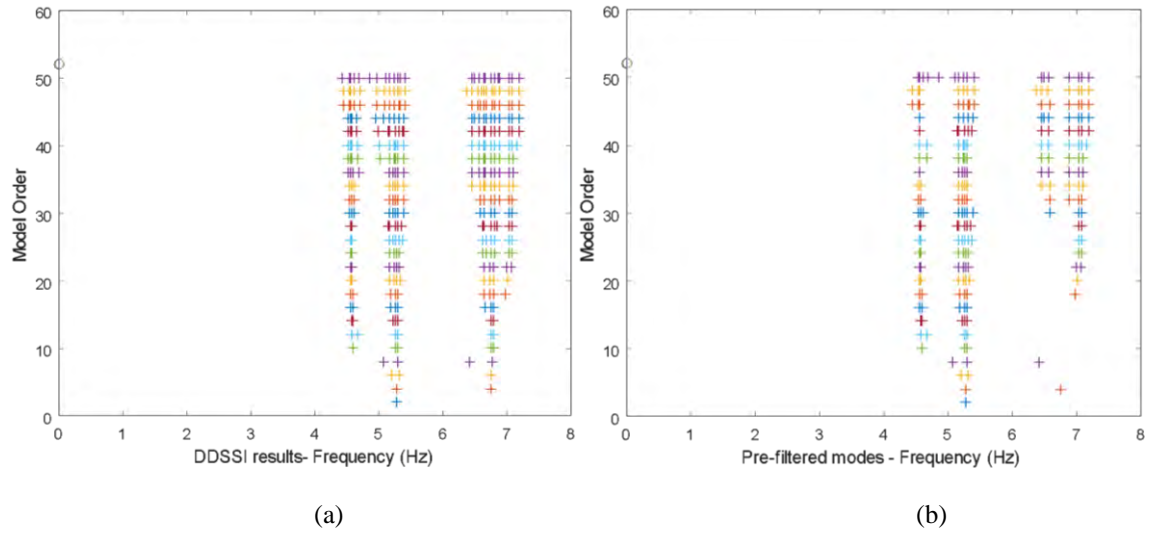


Figure5.3.13. (a) The DD-SSI modal analysis results (b) Results after filtering with the hard validation criteria

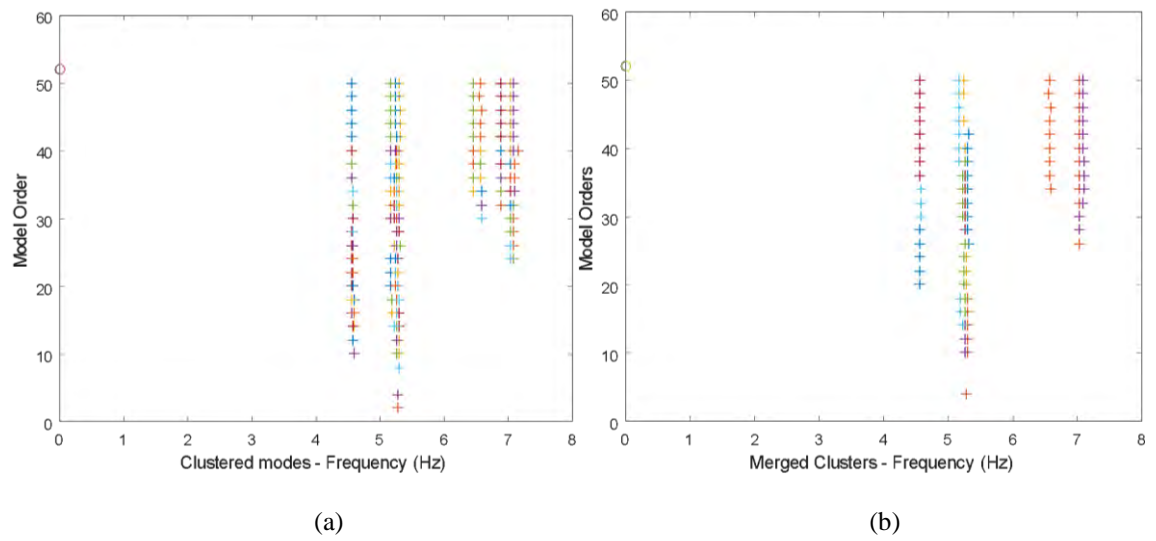


Figure5.3.14. (a) Results after the modes clustering (b) Results after the cluster merging procedure

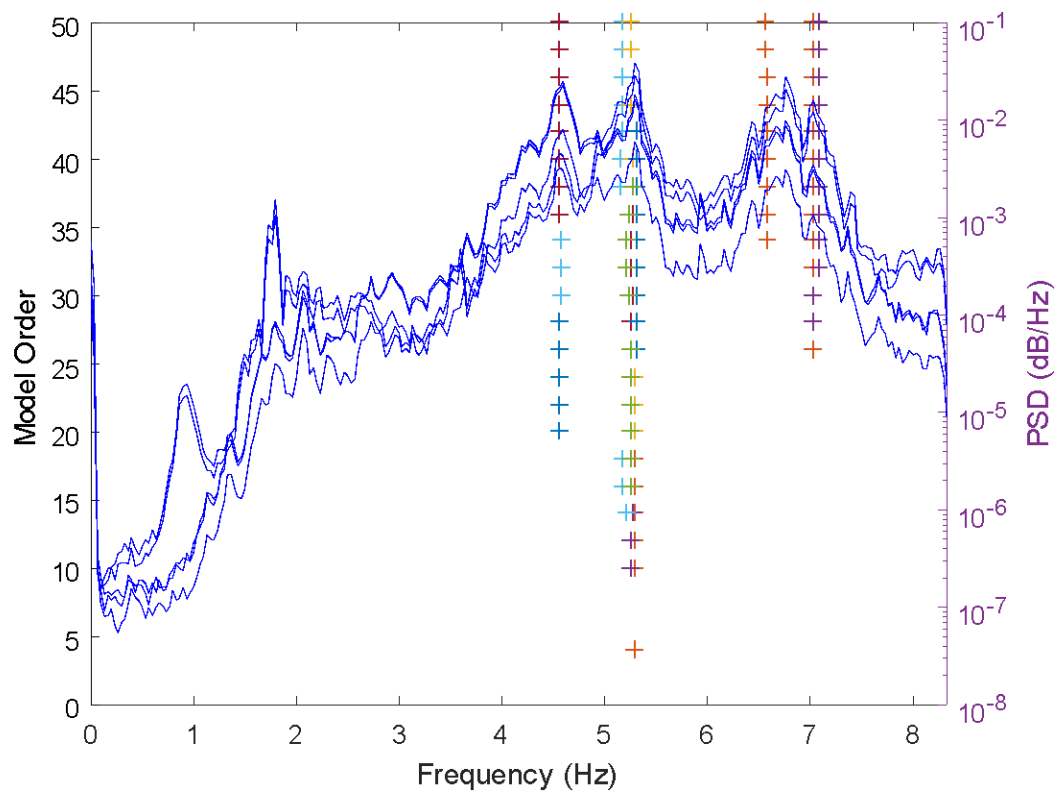
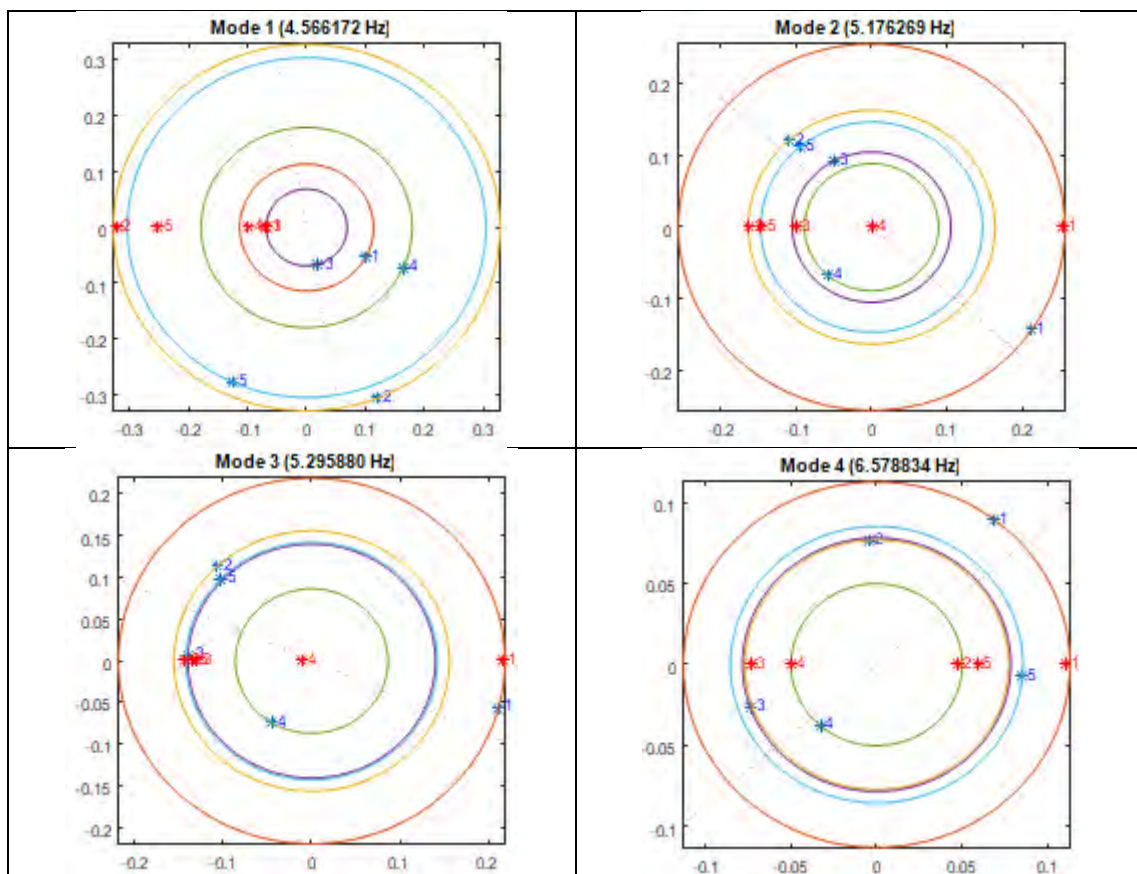


Figure5.3.15. Modes after cluster merging depicted on the PSD



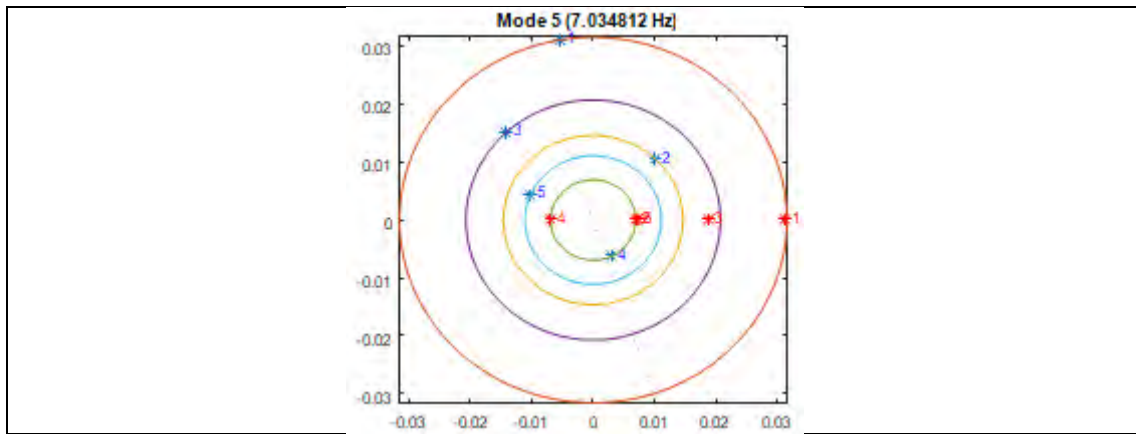


Figure5.3.16. Diagrams of the complex modeshapes (blue color) and the corresponding real modeshapes (red color). Blue points in no straight line demonstrate that the bridge is non-classically damped.

SPAN 15 – Case 4: Four trucks on span - Configuration 12 (time 13:10)

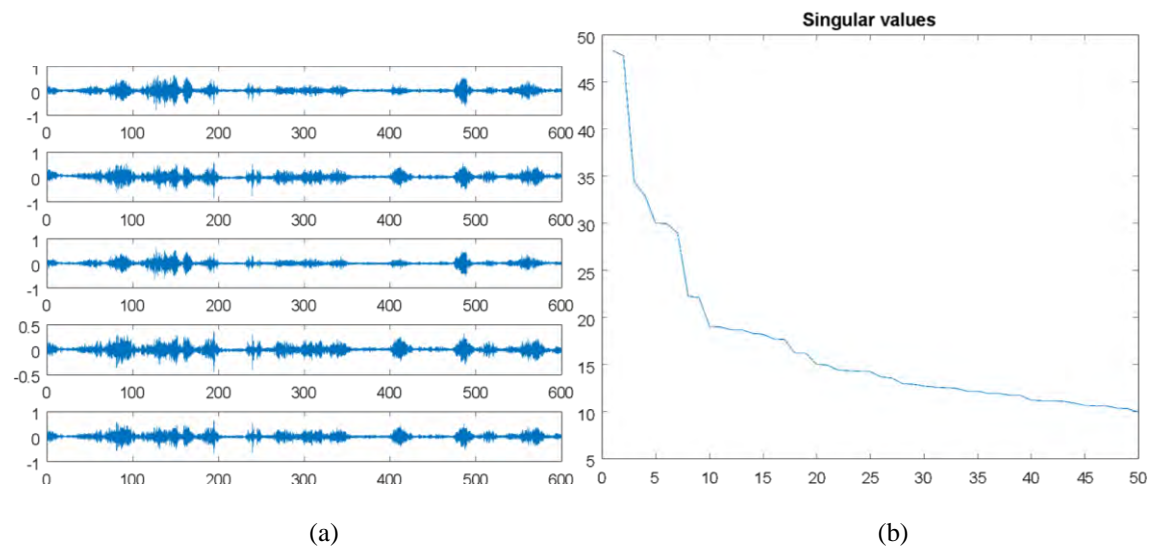


Figure5.3.17.(a) Active response time histories. The vertical axis is accelerations (m/s²) and the horizontal is time (sec). (b) Singular values

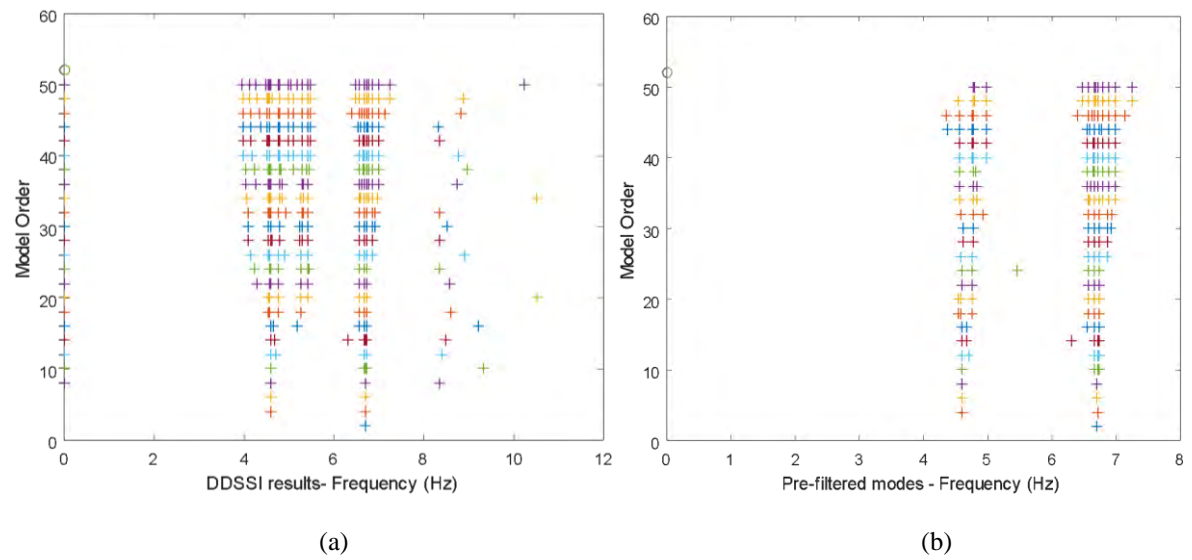


Figure5.3.18. (a) The DD-SSI modal analysis results (b) Results after filtering with the hard validation criteria.

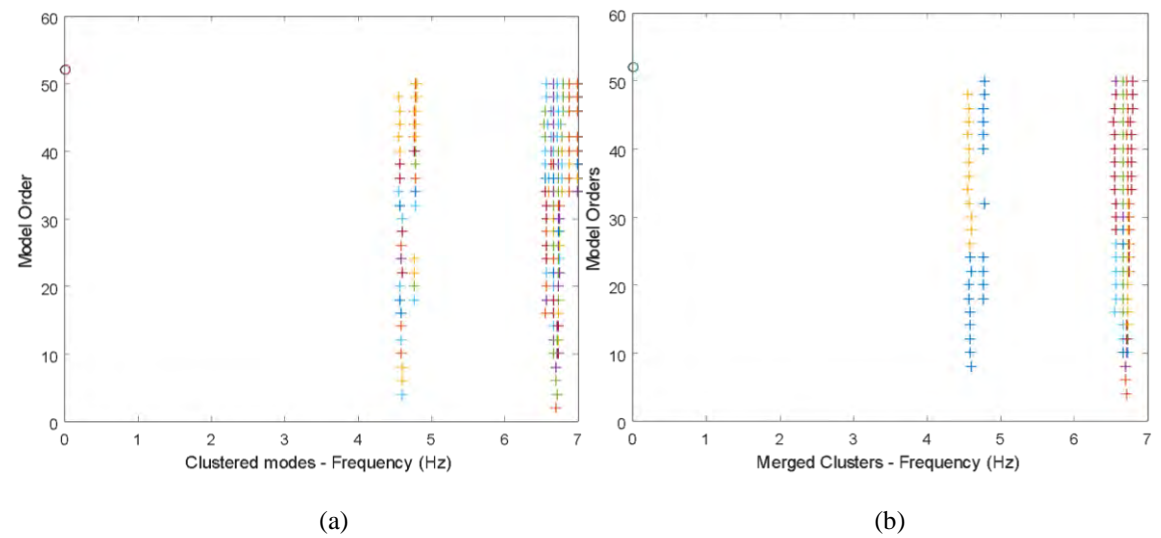


Figure5.3.19. (a) Results after the modes clustering (b) Results after the cluster merging procedure

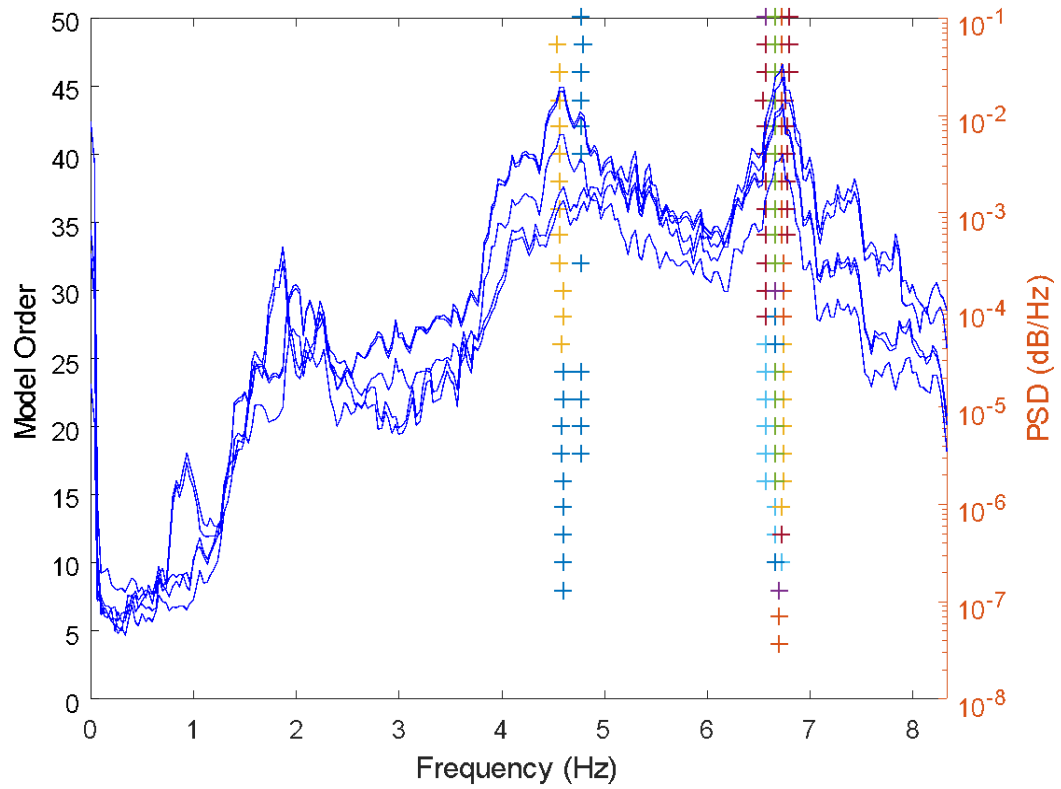


Figure5.3.20. Modes after cluster merging depicted on the PSD

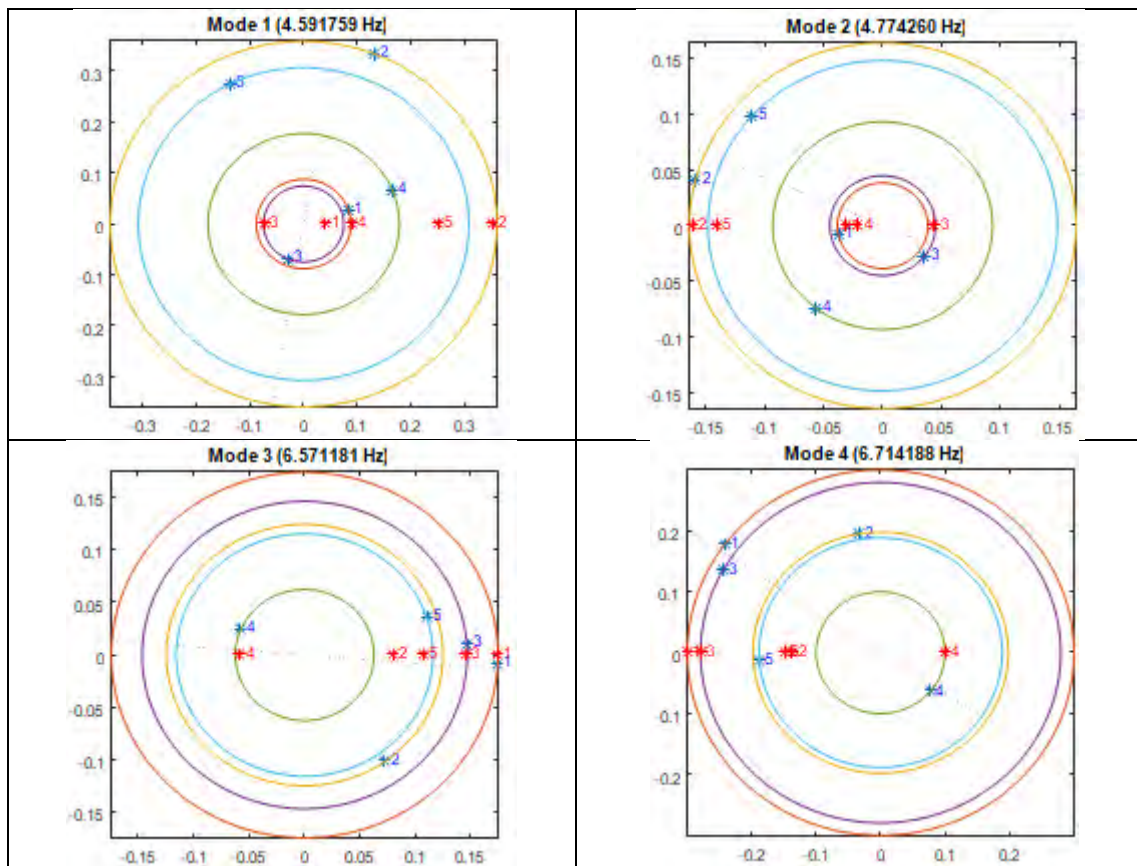


Figure5.3.21. Diagrams of the complex modeshapes (blue color) and the corresponding real modeshapes (red color). Blue points in no straight line demonstrate that the bridge is non-classically damped.

SPAN 15 – Case 5: No trucks on span - Configuration 13 (time 13:30)

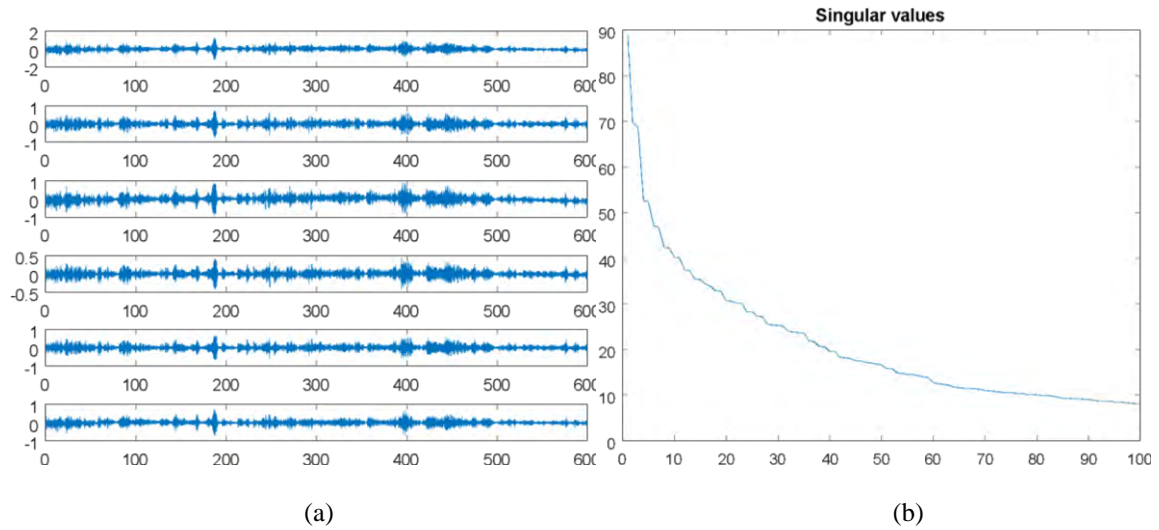


Figure 5.3.22. (a) Active response time histories. The vertical axis is accelerations (m/s²) and the horizontal is time (sec). (b) Singular values

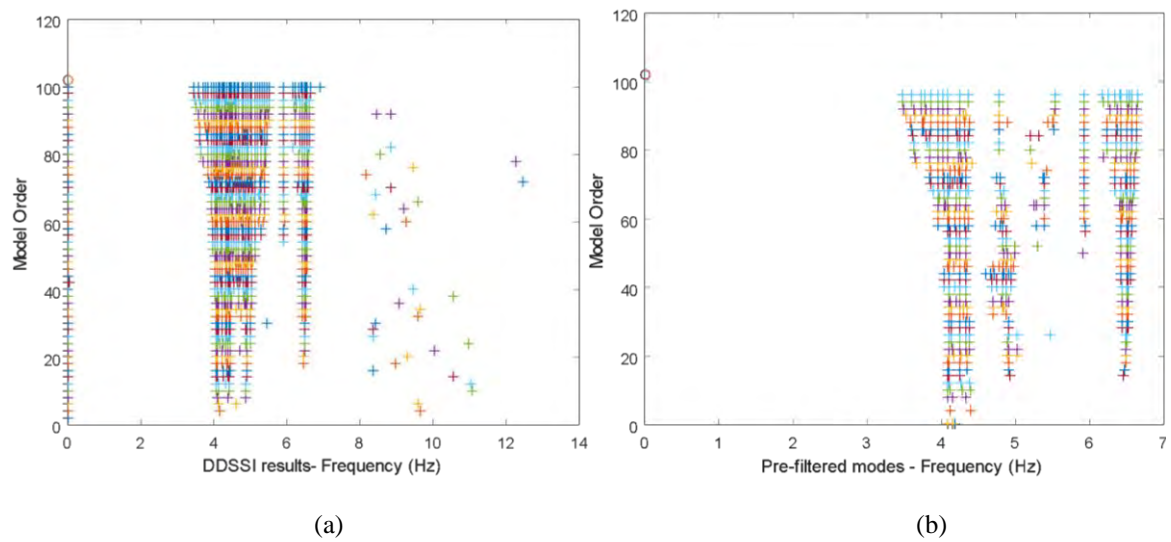


Figure 5.3.23. (a) The DD-SSI modal analysis results (b) Results after filtering with the hard validation criteria

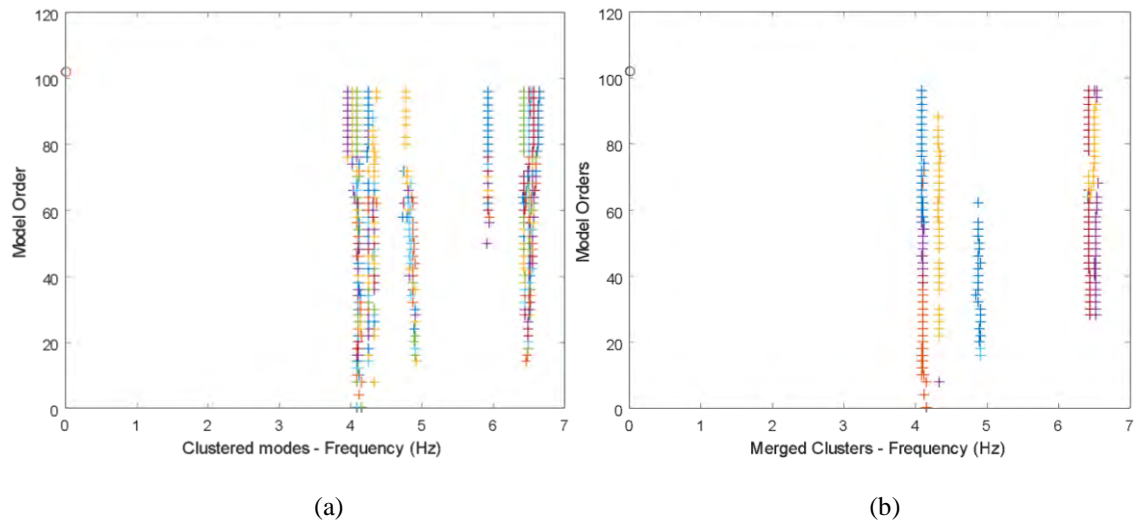


Figure5.3.24.(a) Results after the modes clustering (b) Results after the cluster merging procedure

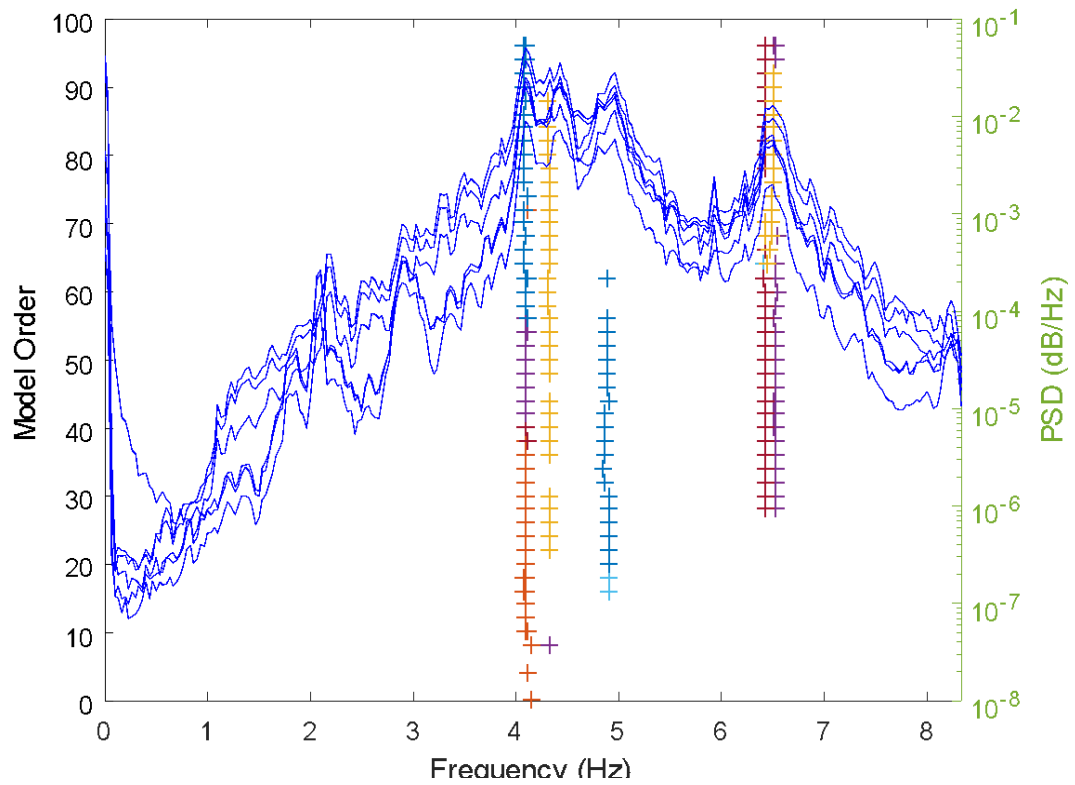
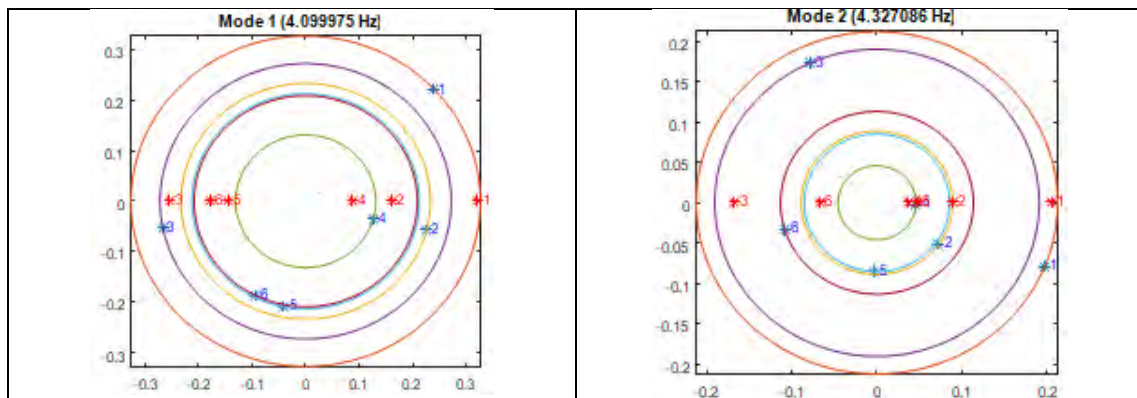


Figure5.3.25. Modes after cluster merging depicted on the PSD



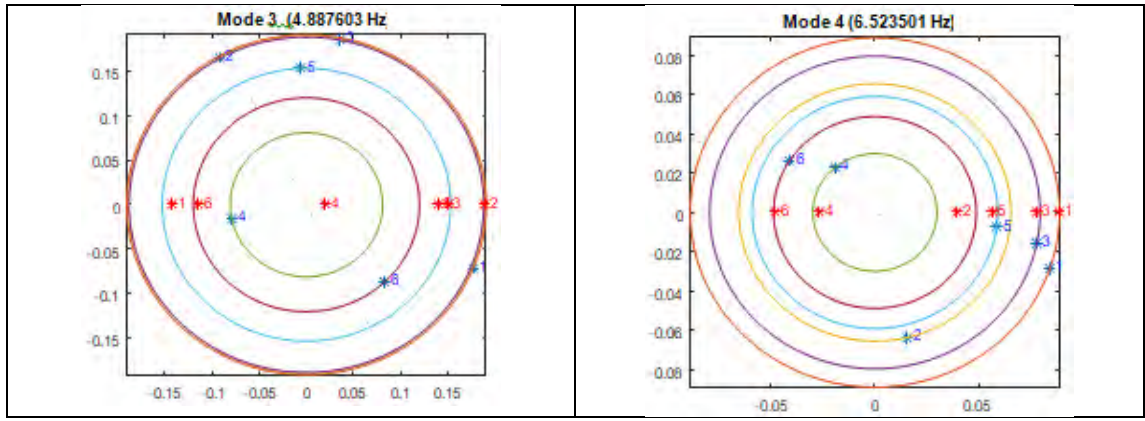


Figure 5.3.26. Diagrams of the complex modeshapes (blue color) and the corresponding real modeshapes (red color). Blue points in no straight line demonstrate that the bridge is non-classically damped.

SPAN 14 - Case 1: No trucks on span - Configuration 14 (time 13:50)

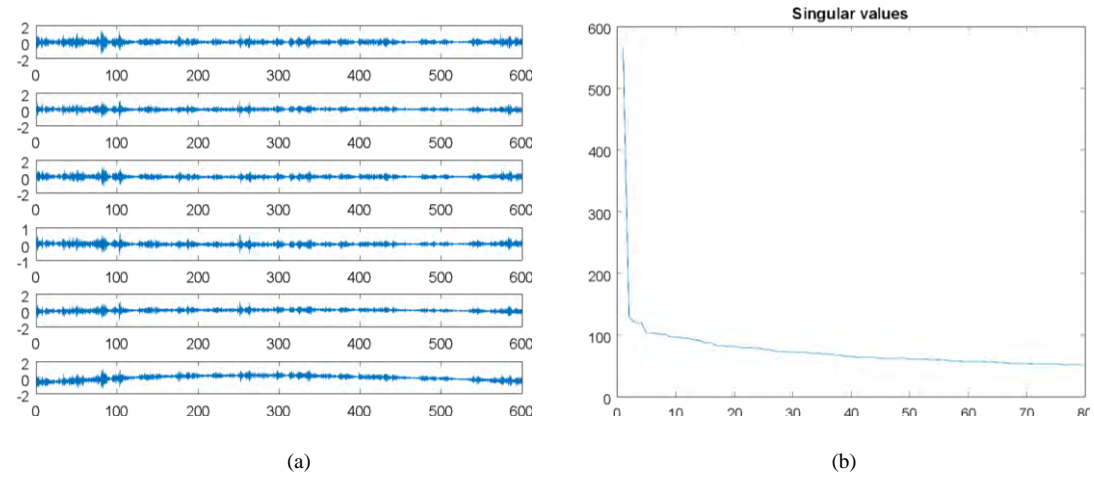


Figure 5.3.27. (a) Active response time histories of the 6 sensors measuring the vertical dimension. The vertical axis is accelerations (m/s²) and the horizontal is time (sec). (b) Singular values

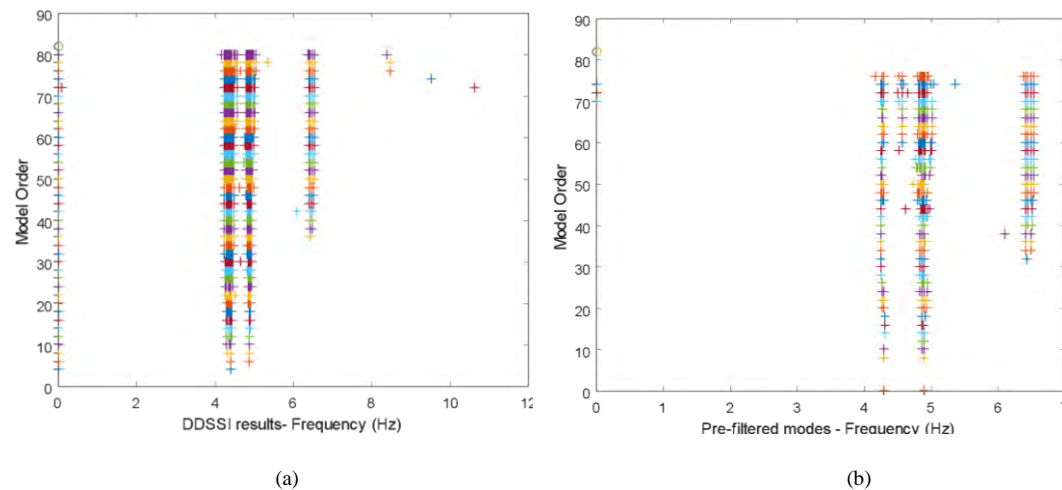


Figure 5.3.28. (a) The DD-SSI modal analysis results (b) Results after filtering with the hard validation criteria

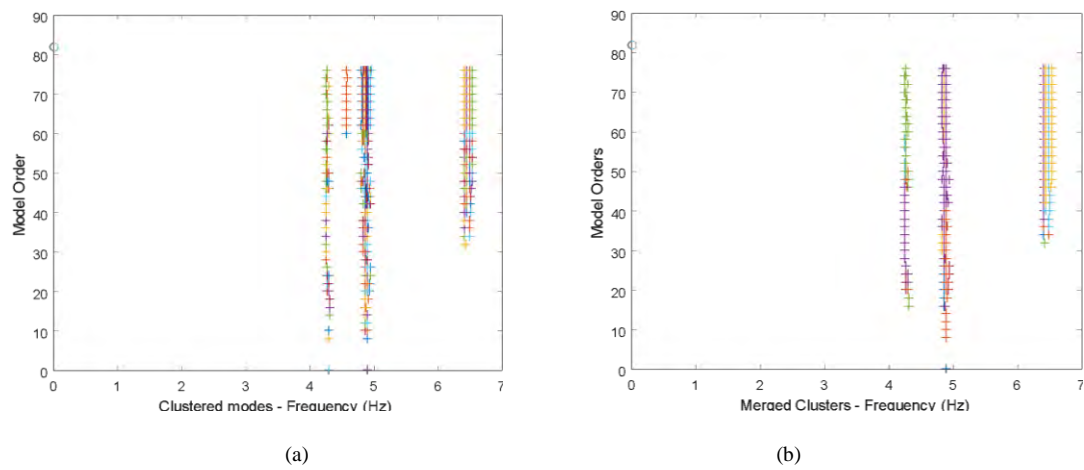


Figure5.3.29.(a) Results after the modes clustering (b) Results after the cluster merging procedure

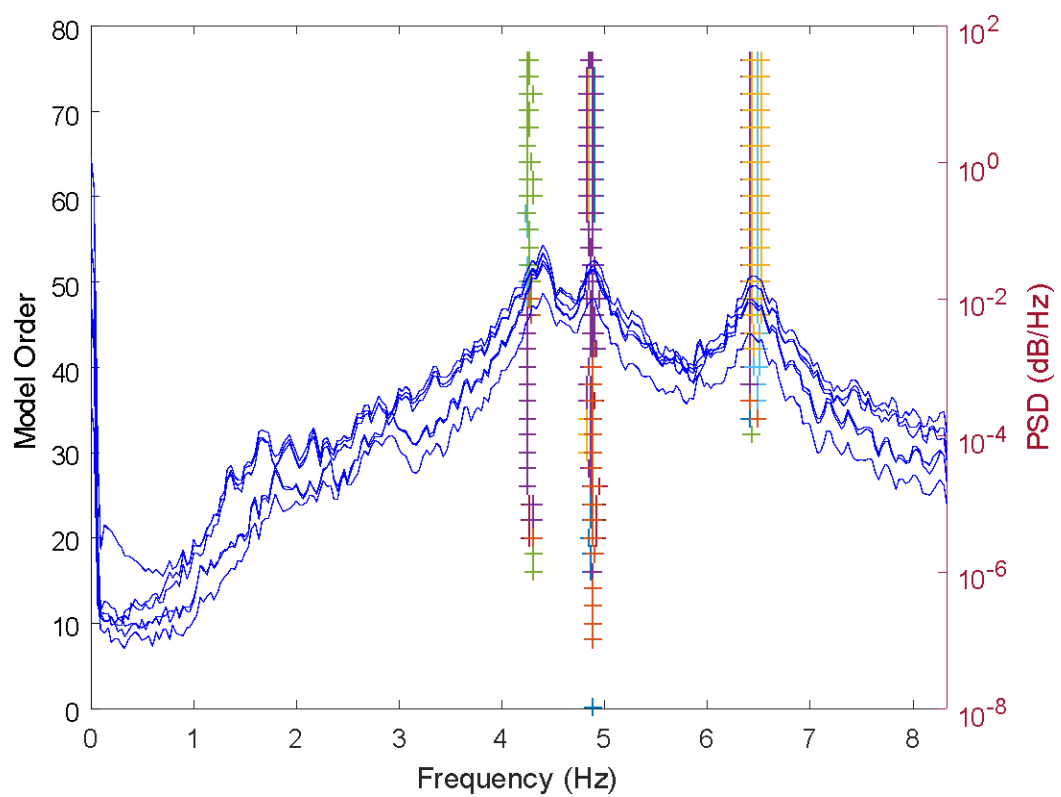
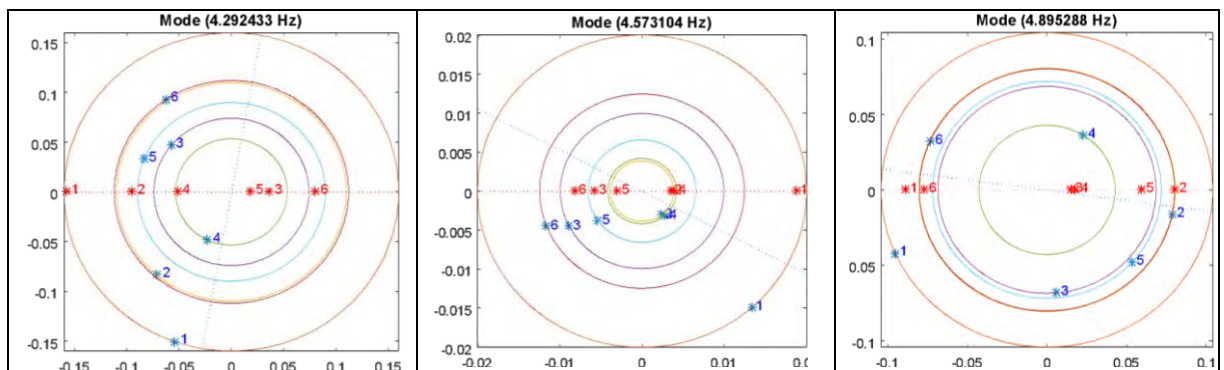


Figure5.3.30. Modes after cluster merging depicted on the PSD



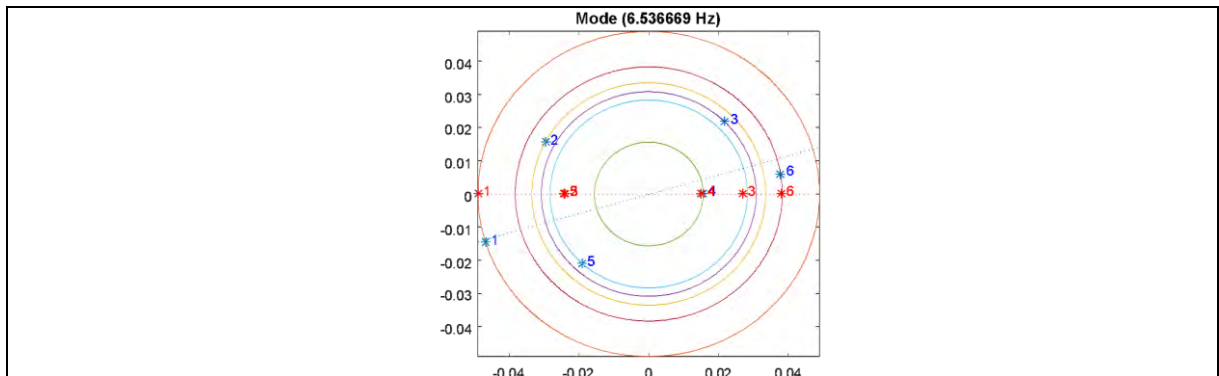


Figure5.3.31. Diagrams of the complex modeshapes (blue color) and the corresponding real modeshapes (red color). Blue points in no straight line indicate that the bridge is non- classically damped.

SPAN 14 - Case 2: Two trucks on span - Configuration 15 (time 14:10)

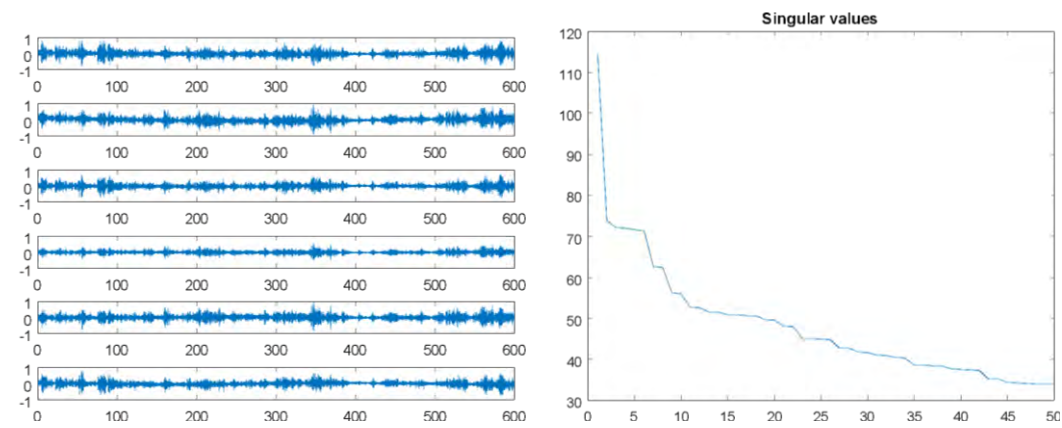


Figure5.3.32.(a) Active response time histories. The vertical axis is accelerations (m/s^2) and the horizontal is time (sec). (b) Singular values

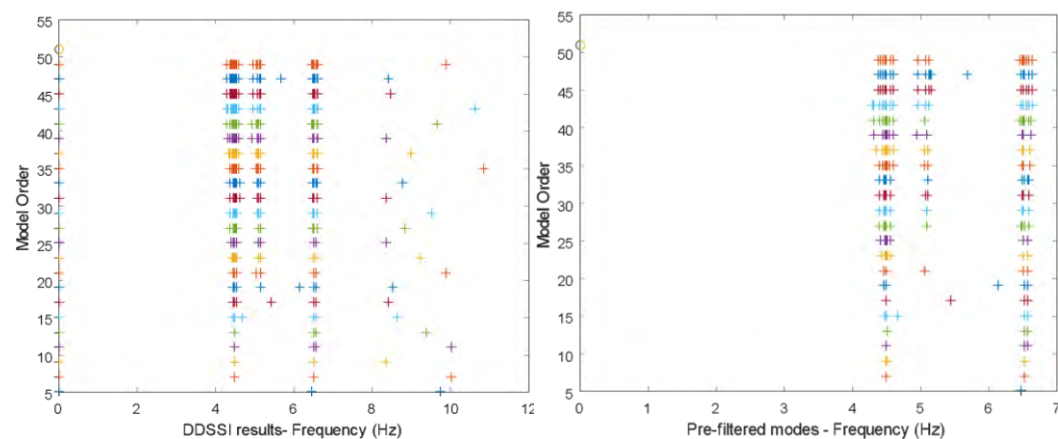


Figure5.3.33. (a) The DD-SSI modal analysis results (b) Results after filtering with the hard validation criteria

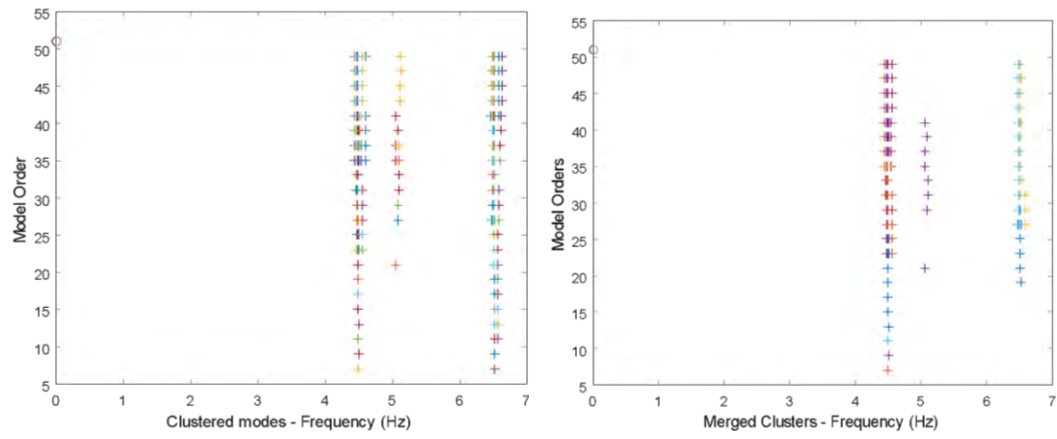


Figure 5.3.34. (a) Results after the modes clustering (b) Results after the cluster merging procedure (30% elimination)

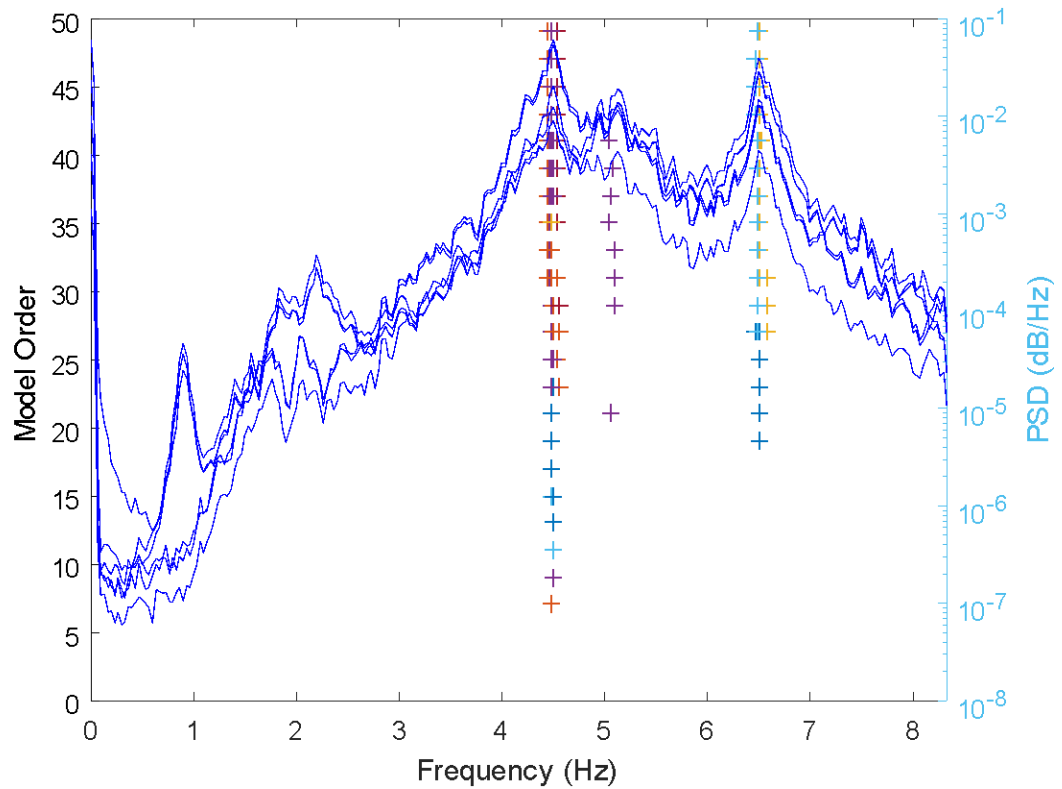
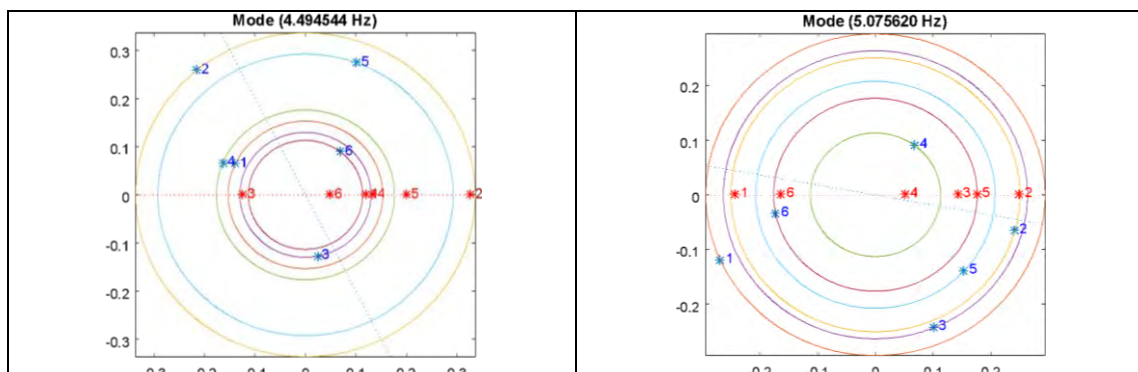


Figure 5.3.35. Modes after cluster merging depicted on the PSD



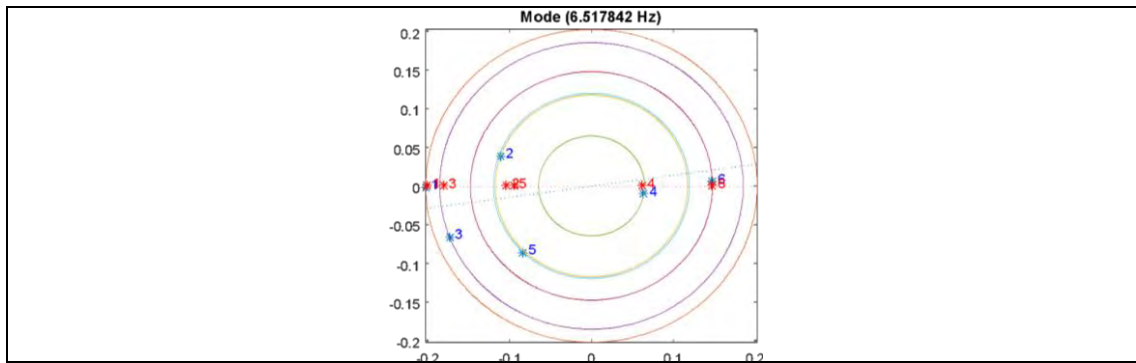


Figure5.3.36. Diagrams of the complex modeshapes (blue color) and the corresponding real modeshapes (red color). Blue points in no straight line indicate that the bridge is non- classically damped.

SPAN 14 – Case 3: Three trucks on span - Configuration 17 (time 14:50)

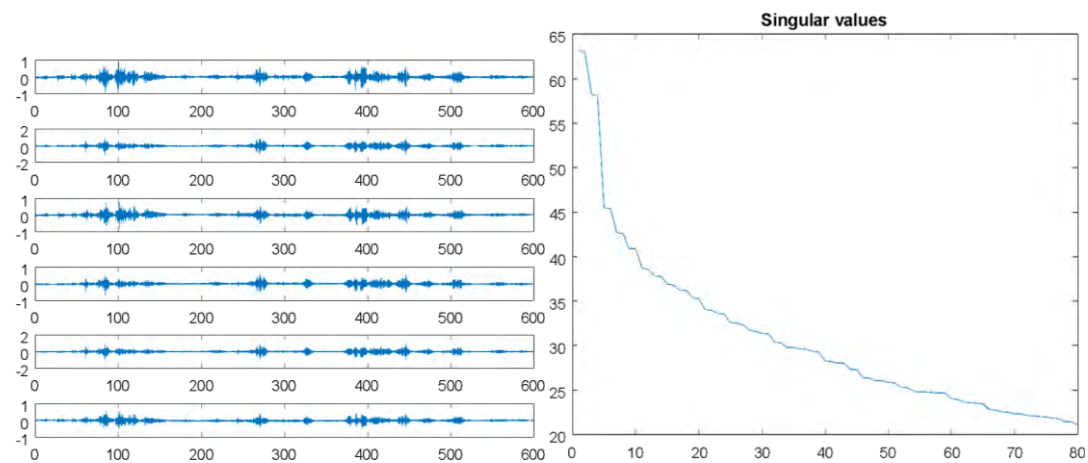


Figure5.3.37.(a) Active response time histories. The vertical axis is accelerations (m/s^2) and the horizontal is time (sec). (b) Singular values

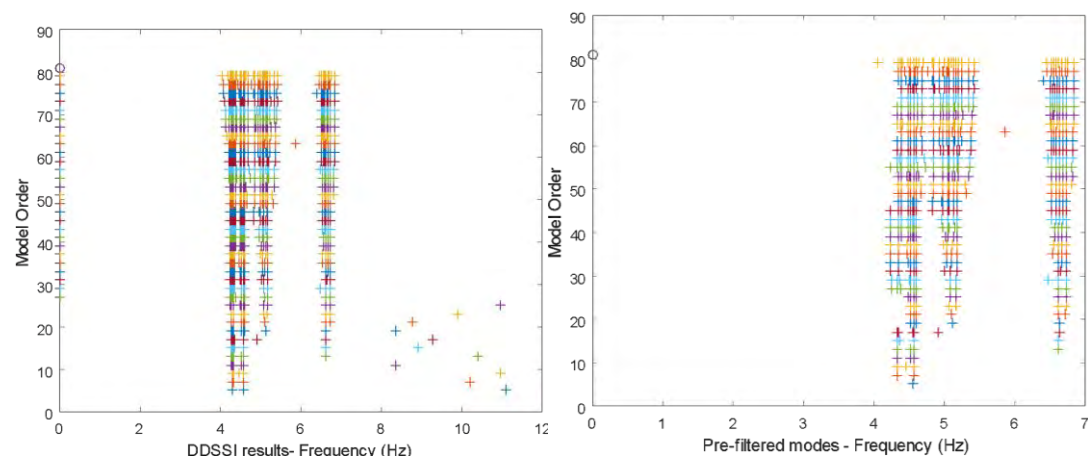


Figure 5.3.38. (a) The DD-SSI modal analysis results (b) Results after filtering with the hard validation criteria

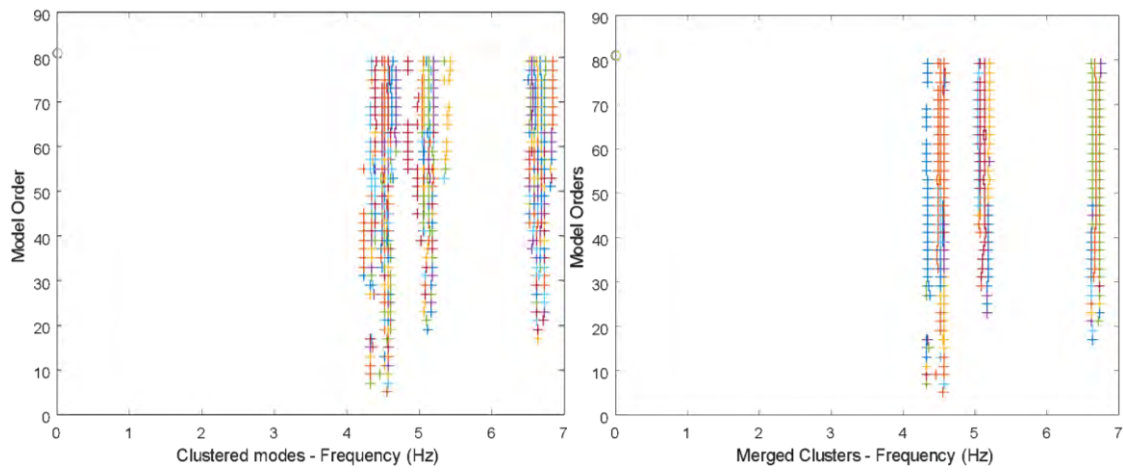


Figure5.3.39. (a) Results after the modes clustering (b) Results after the cluster merging procedure

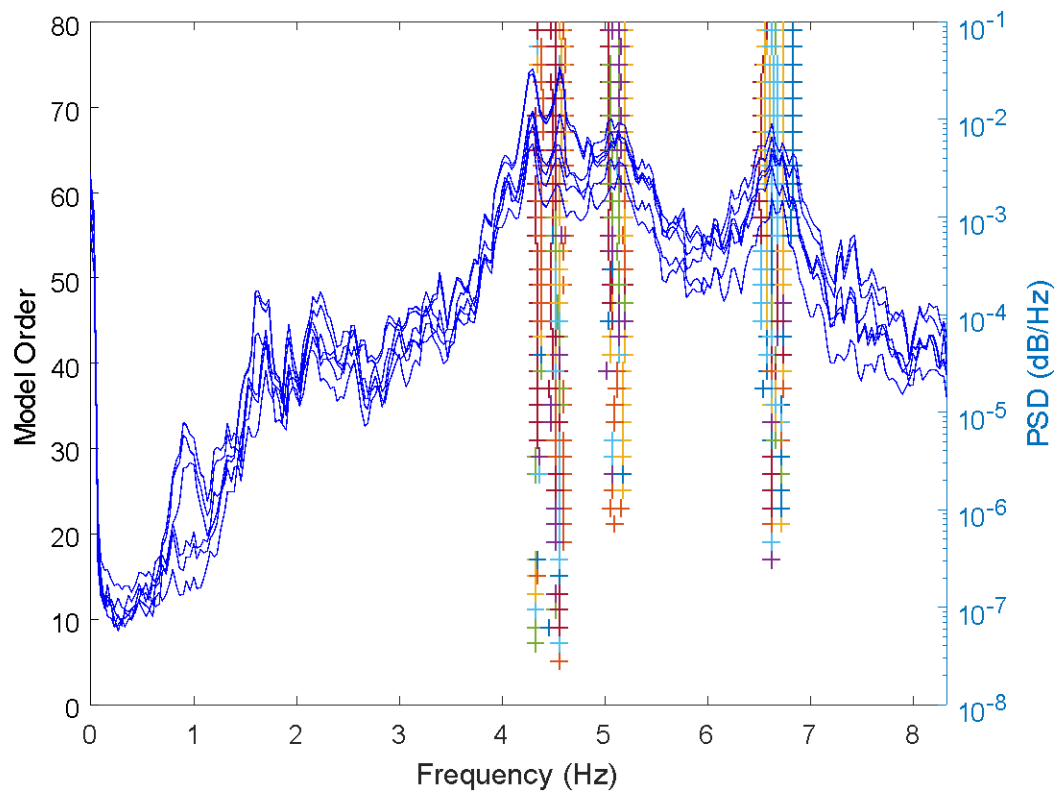


Figure5.3.40. Modes after cluster merging depicted on the PSD

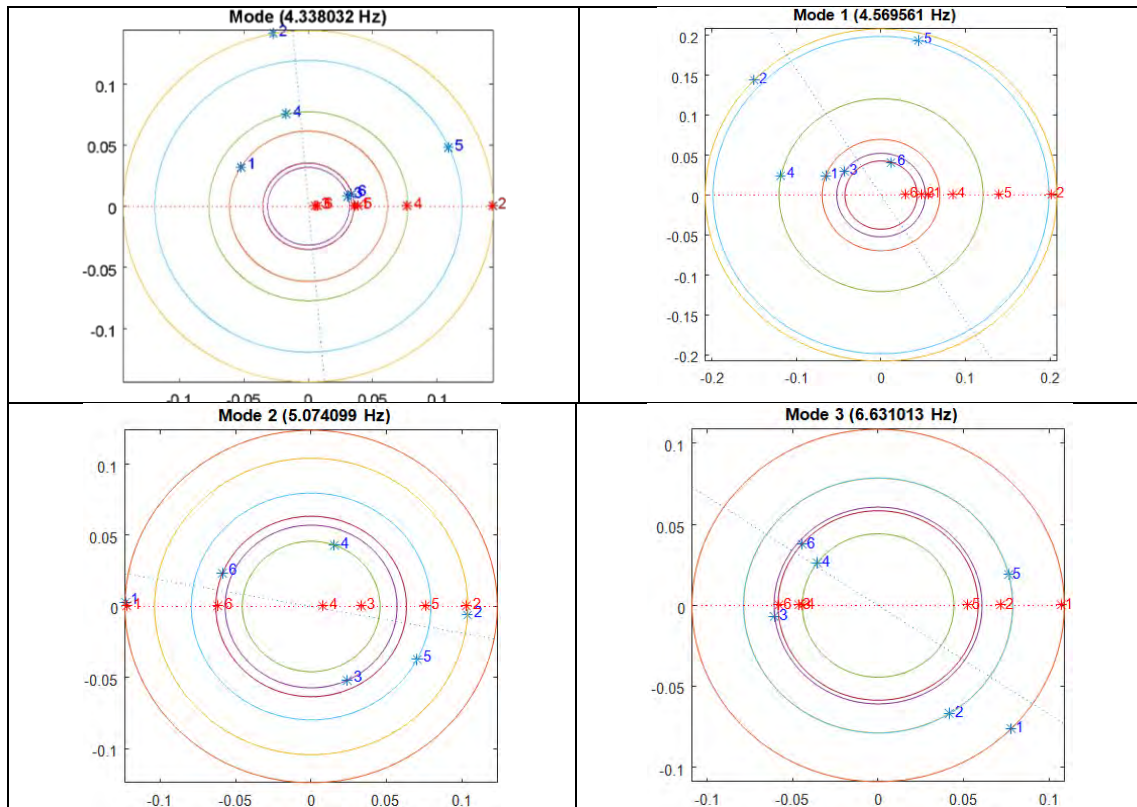


Figure 5.3.41. Diagrams of the complex modeshapes (blue color) and the corresponding real modeshapes (red color). No straight line demonstrates that the bridge is non-classically damped.

SPAN 14 – Case 4: Four trucks on span - Configuration 18 (time 15:10)

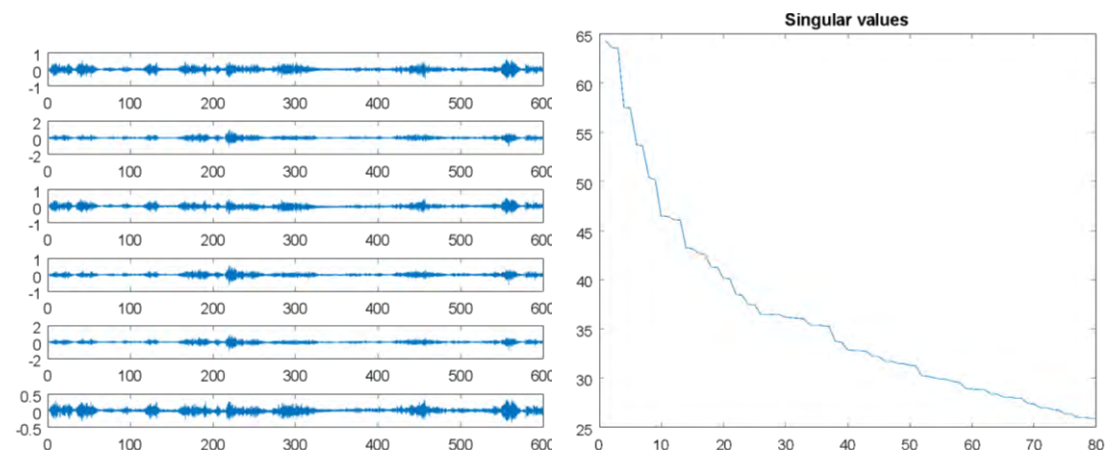


Figure 5.3.42. (a) Active response time histories. The vertical axis is accelerations (m/s^2) and the horizontal is time (sec). (b) Singular values

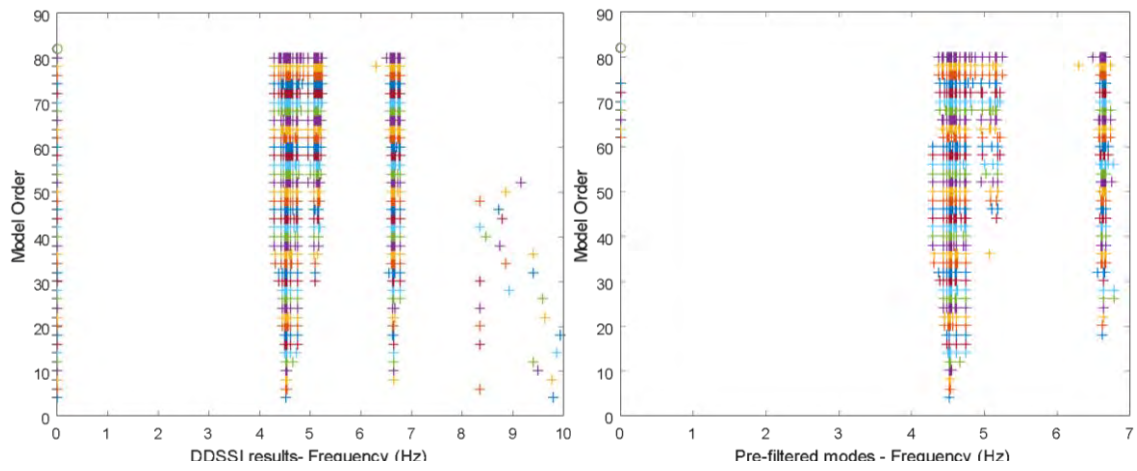


Figure 5.3.43.(a) The DD-SSI modal analysis results (b) Results after filtering with the hard validation criteria

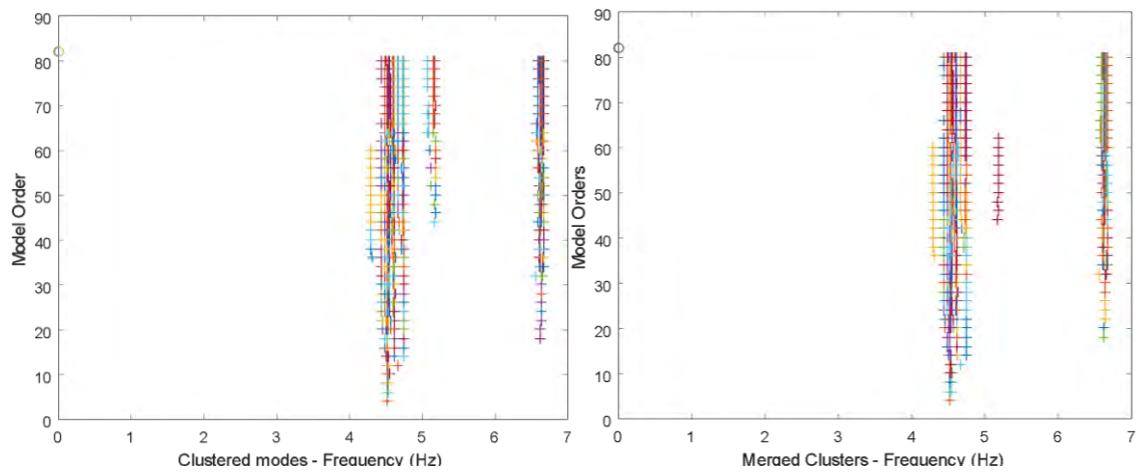


Figure 5.3.44.(a) Results after the modes clustering (b) Results after the cluster merging procedure(20% elimination)

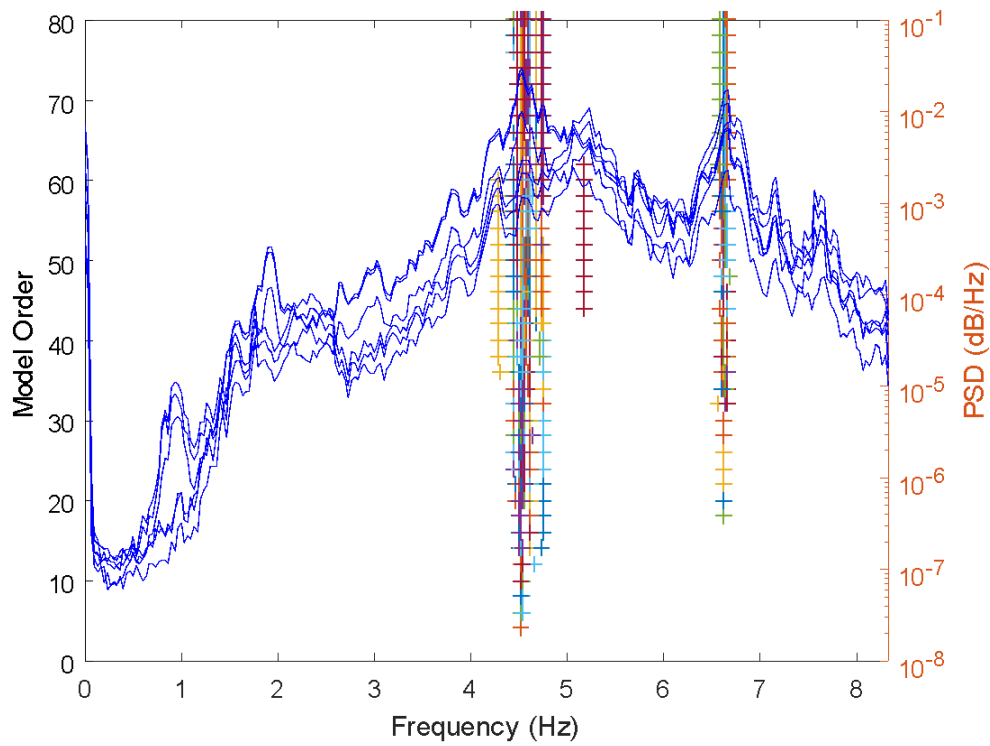


Figure5.3.45. Modes after cluster merging depicted on the PSD

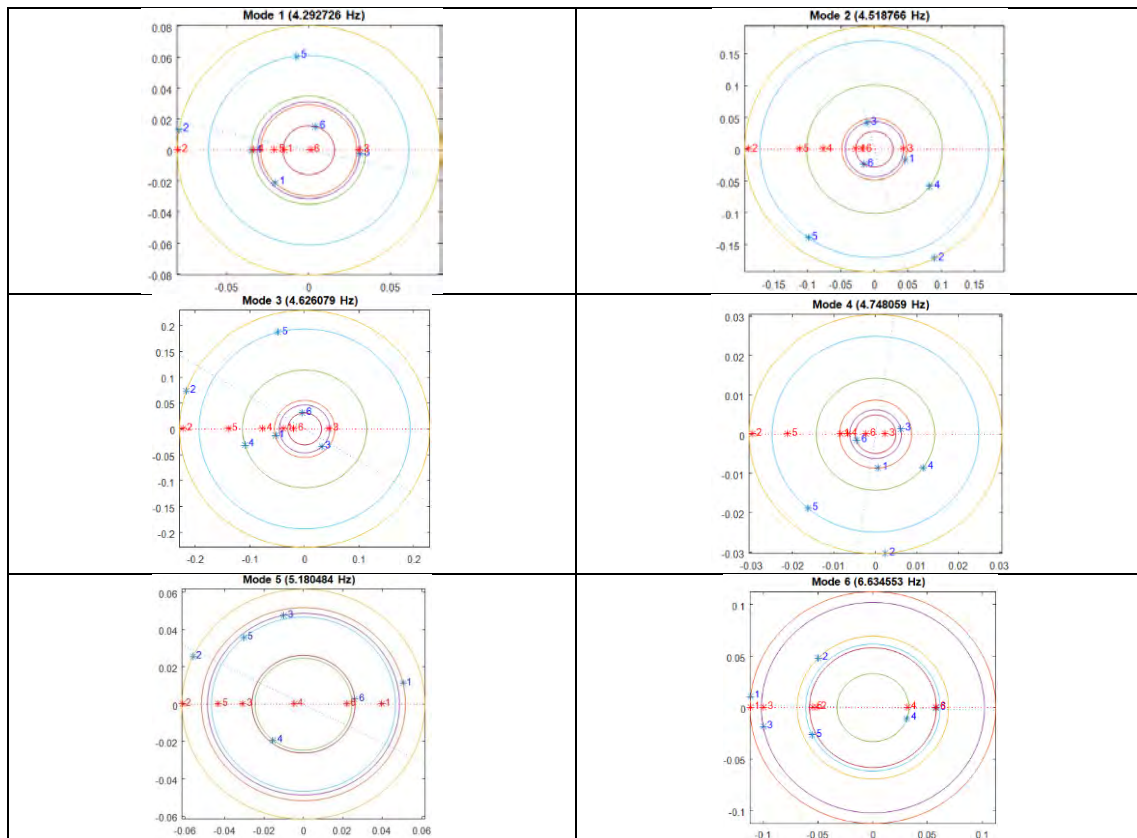


Figure 5.3.46. Diagrams of the complex modeshapes (blue color) and the corresponding real modeshapes (red color). No straight line demonstrates that the bridge is non- classically damped.

SPAN 14 – Case 5: No trucks on span - Configuration 20 (time 15:50)

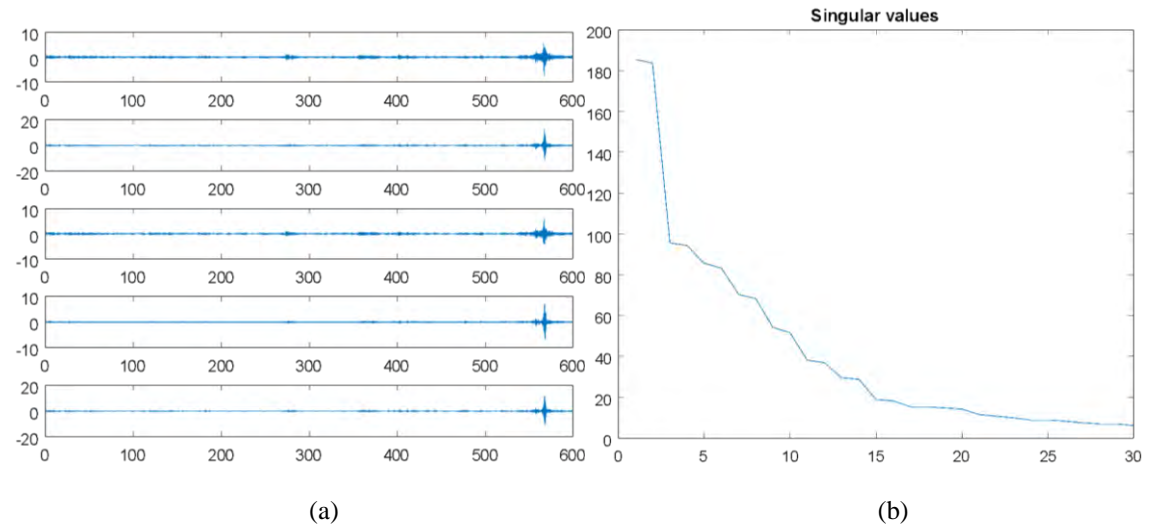


Figure 5.3.47. (a) Active response time histories. The vertical axis is accelerations (m/s²) and the horizontal is time (sec). (b) Singular values.

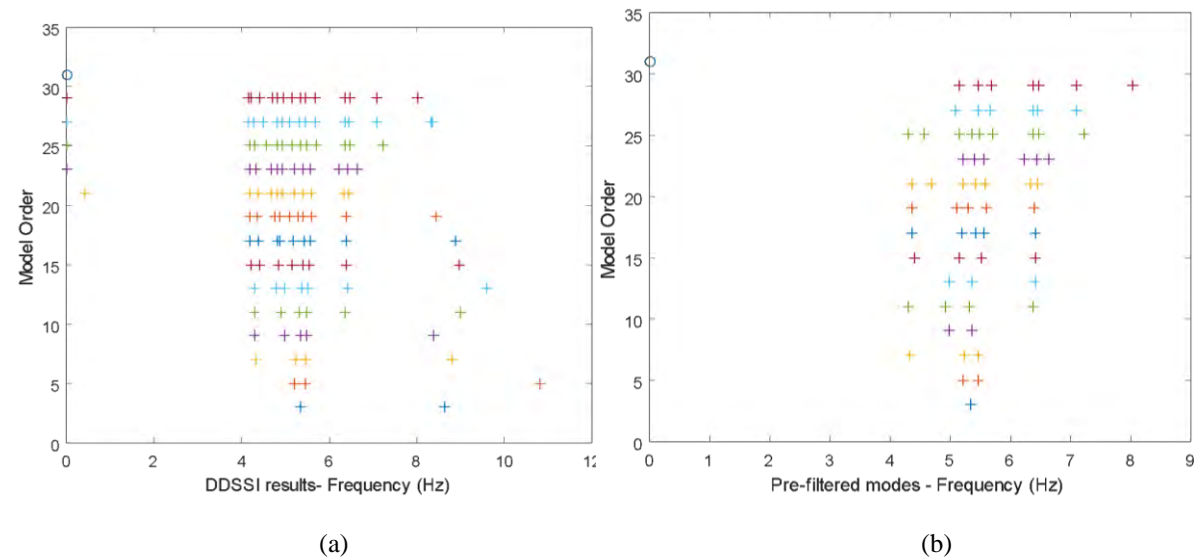


Figure 5.3.48. (a) The DD-SSI modal analysis results (b) Results after filtering with the hard validation criteria

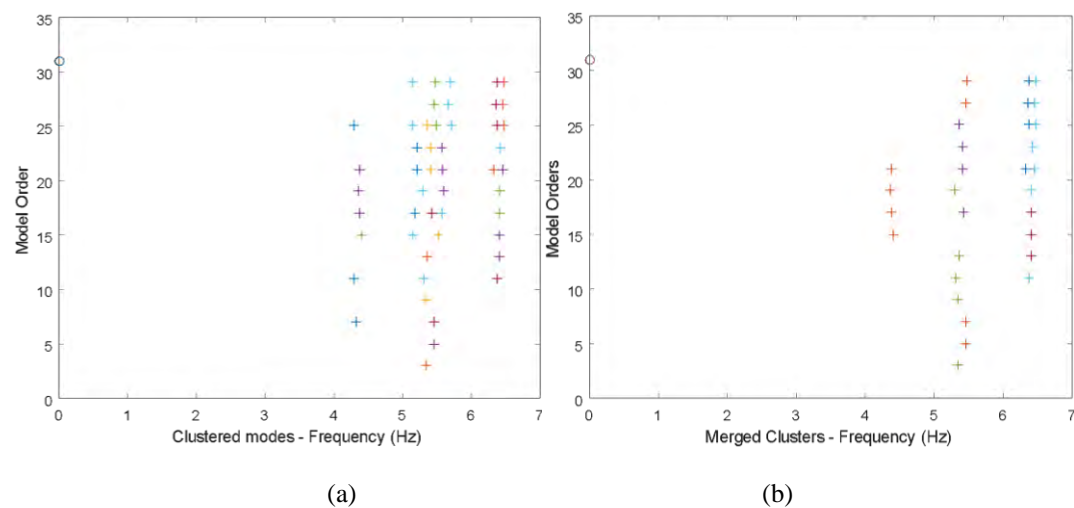


Figure5.3.49.(a) Results after the modes clustering (b) Results after the cluster merging procedure

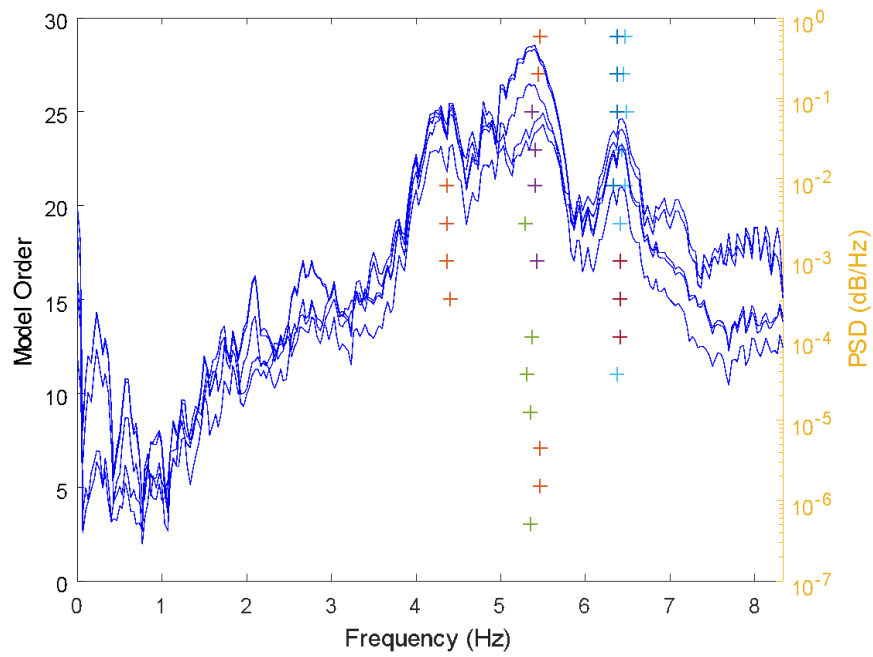


Figure5.3.50.Modes after cluster merging depicted on the PSD

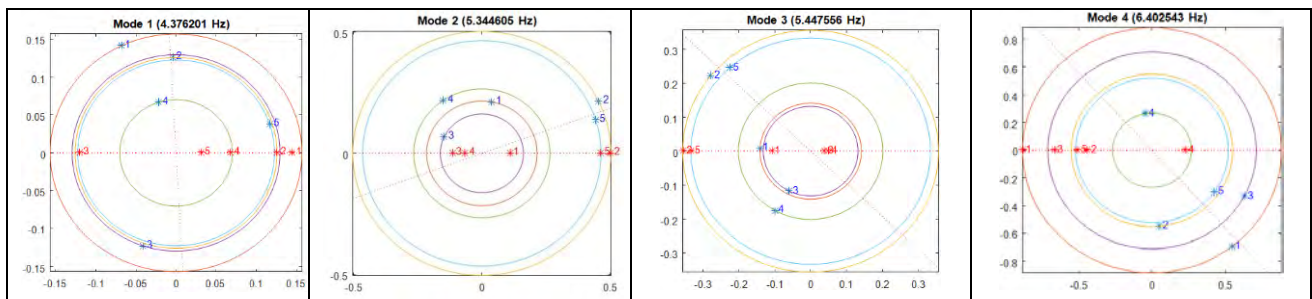


Figure5.3.51. Diagrams of the complex modeshapes (blue color) and the corresponding real modeshapes (red color). Blue points in no straight line demonstrate that the bridge is non-classically damped.

5.3.2. Results from Software 2

Using the previously presented **Software 2** (chapter 4), the modal frequencies and modal damping ratios of the bridge were extracted, and the mode shape components of each configuration were combined to form and illustrate the complex modeshapes of each configuration. According to the results, the bridge seems to be non – classically damped, so it is more convenient, not to show the mode shapes on the bridge’s geometry.

Table5.3.2. Eigenfrequencies and damping ratios computed by Software 2, for spans 14,15 for various load cases on the bridge, compared to the results from the developed software.

Software 2									
Load cases, Sensor Configuration	Span	Mode 1 (Hz)	Damping ratio	Mode 2 (Hz)	Damping ratio	Mode 3 (Hz)	Damping ratio	Mode 4 (Hz)	Damping ratio
No trucks, time 10:10	15	4.293	0.0029	4.444	0.0085	4.940	0.0234	6.733	0.0102
2 trucks, time 11:10	15			4.545	0.0292	5.193	0.029	6.749	0.0116
3 trucks, time 12:10	15	4.290	0.0186	4.579	0.0184	5.297	0.0185	6.772	0.0052
4 trucks,time 13:10	15	4.248	0.0178	4.574	0.0331	5.232	0.0475	6.71	0.0125
No trucks, time 13:30	15	4.098	0.0118	4.455	0.0214	4.940	0.0232	6.500	0.0154
No trucks, time 13:50	14			4.393	0.0194	4.893	0.0176	6.455	0.0174
2 trucks, time 14:10	14	4.267	0.0299	4.496	0.0169	5.092	0.0384	6.522	0.0122
3 trucks, time 14:50	14	4.298	0.0115	4.554	0.0150	5.121	0.0237	6.647	0.0168
4 trucks, time 15:10	14	4.296	0.075	4.578	0.0527	5.193	0.0317	6.645	0.0151
No trucks, time 15:50	14			4.393	0.0160	4.869	0.0347	6.389	0.0198

Developed software									
Load cases, Sensor Configuration	Span	Mode 1 (Hz)	Damping ratio	Mode 2 (Hz)	Damping ratio	Mode 3 (Hz)	Damping ratio	Mode 4 (Hz)	Damping ratio
No trucks, time 10:10	15	4.28	0.00096	4.41	0.0124	4.98	0.0025	6.72	0.0023
2 trucks, time 11:10	15			4.38 4.49 4.67	0.00052 0.0049 0.0014	5.178	0.0010	6.725	0.0015
3 trucks, time 12:10	15			4.56	0.00036	5.176 5.296	0.0015 0.0025	6.57 7.035	0.00099 0.0022
4 trucks,time 13:10	15			4.59	0.0179	4.77	0.0039	6.57 6.71	0.0021 0.0076
No trucks, time 13:30	15	4.099	0.0051	4.32	0.0026	4.88	0.0063	6.52	0.0080
No trucks, time 13:50	14	4.284	0.00083	4.573	0.00032	4.862	0.00023	6.537	0.0002
2 trucks, time 14:10	14			4.495	0.0065	5.075	0.0106	6.517	0.00055
3 trucks, time 14:50	14			4.338 4.569	0.00069 0.001	5.074	0.00021	6.631	0.0011
4 trucks, time 15:10	14	4.29	0.000219	4.51 4.62	0.0007 0.0014	5.18	0.000164	6.634	0.00073
No trucks, time 15:50	14			4.37	0.0083	5.34 5.44	0.0083 0.0026	6.402	0.0117

5.3.3. Conclusions

First of all, we should note the conclusions about the operation of the two spans. The eigenfrequencies, which have been calculated for the vertical, bending modes for the unloaded span 15, fluctuate around 4.27 Hz, 4.44 Hz, 4.94 Hz and 6.73 Hz. The eigenfrequencies, which have been calculated for the vertical, bending modes for the unloaded span 14, have, slightly, smaller values: 4.40 Hz, 4.89 Hz and 6.48 Hz. The first three modal frequencies differ from each other 0.5% and the last modes differ 3%. These small differences are attributed to the expected variations on the mechanical - geometrical conditions in each span. By comparing the modal frequencies of a specific span (14 or 15) for the case of no load on the span and the cases of loaded span (2, 3 and 4 vehicles), it is made clear that some eigenfrequencies (Mode 2 and 3) increase in the case of the loading. The first mode seems to be unaffected by the change of loading. These results show that these two spans (14, 15) have similar behavior, according to their modal properties for various load cases. Consequently, possible differences in the structural conditions of both spans are not recorded in the values of the eigenfrequencies. The damping ratios are, relatively, small at around 1-2% for both spans. No significant rise of the damping ratios is observed for span 14 compared to span 15. Possible structural fractures would have resulted into an increase of the damping ratios. Since, this effect is not recorded for span 14, it is deduced that both spans behave in a similar way, as far as their dynamic properties are concerned, for the different load cases.

Comparing the results that are acquired by the developed software and Software 2, it is clearly seen that they have a good enough match for their calculated modal frequencies but not so much for the damping ratios. According to the analyses made by both software, we see that the excited modes are 4 vertical modes. On the figures that show the diagrams of the complex modeshapes, it is clearly seen that the damping type of the bridge is intensely non-classical. This is because of the fact that the points, which correspond to the complex shapes are not put in a straight line but they are rather scattered. A satisfying reason for this behavior could be the local energy loss because of friction. Sources of friction on this bridge could be heavy block structures that exist along the bridge and separated the driving lanes. Consequently, the presented eigenfrequencies do not have the expected behavior and their use for the structure's condition evaluation doesn't offer useful results.

To sum up, the variation of the dynamic properties (modal frequencies and damping ratios) in both spans, for the different load cases, is very similar. The current modal analysis does not prove that there's a change in the structural condition of span 14, since no significant change is depicted in the produced modal properties compared to span 15. But as already mentioned, the acquired results can't offer a safe conclusion, since the friction in the interface between the added blocks and the bridge alters the expected structural behavior.

6. Conclusions

The main theme of this thesis was to develop a software for the automated display of stabilization diagrams, after modal analysis has taken place. The theory, on which this automated procedure was based, was the DD-SSI algorithm combined with some clustering techniques. The acquired results by the developed software have been presented in chapter 5 along with the results, for the same applications, of two other softwares. By applying this created software, several conclusions can be made.

First of all, the developed software is significantly sensitive to the input information it takes. Slightly different inputs can lead to a different result. Some conclusions about the inserted by the user, parameters, are the following:

- **Minimum and maximum model order:** It is very difficult to anticipate, which range of model orders is going to give the best results. From the experience gained by the use of the software, the lowest order should be at least the number of the expected to be identified modes and the maximum order should be high enough, to ensure that the weakly excited modes are also identified.
- **Parameters i, j of the Hankel matrix:** Although the boundaries of the parameters have already been presented, some conclusions about their selection can be deduced. Firstly, a high value of the parameter i does not promise a better result. The value of i should not be very high because more spurious modes are produced. An effective selection for parameter i, was the value of the upper bound of the model order or bigger than that. The parameter j should be as big as it can be, because it clears the noise of the measurements.
- **Selection of sensors:** When measurements in a certain direction need to be examined, then it is optimal to choose measurements from the sensors that measure in that direction. Also, when some modes are very close to each other, as a numerical value and they concern a different direction, it is more useful to isolate the sensors of a certain direction, so that all the modes in his direction are identified.
- **Clustering thresholds:** When the measured data is not very clear, then it is useful to change the proposed threshold values and make them looser. In order to make the decision of which thresholds should be enlarged, the user has to consider the feedback he gets from the results. For instance, when a specific amount of modes is expected, at a certain range of frequencies and the filtering or the clustering “kills” these modes, then the user should loosen the thresholds, which affect the modes. In detail, during the clustering procedure there are four thresholds one for the frequencies, one for the MAC, one for the damping ratios and one for MPC. There, someone could ignore the threshold about the damping ratios and the MPC, because sometimes they can throw away clusters which consist of real modes. Finally, the elimination percentage for the merged clusters can be adjusted if it excludes most of the clusters.

Generally, the input parameters for the developed software have to be tested through trial until the desired results are gained. Consequently, there are some features of the software that have to be improved.

The current software can be improved by proposing the whole automation of the procedure. This means that the user defined parameters would be automatically defined by following some rules as well as the values of the used thresholds and the model order range. Another issue of the software is that it doesn't produce the global modeshape automatically but the already computed local mode shapes are saved and another software is needed to be used, in order to get the assembled modeshapes.

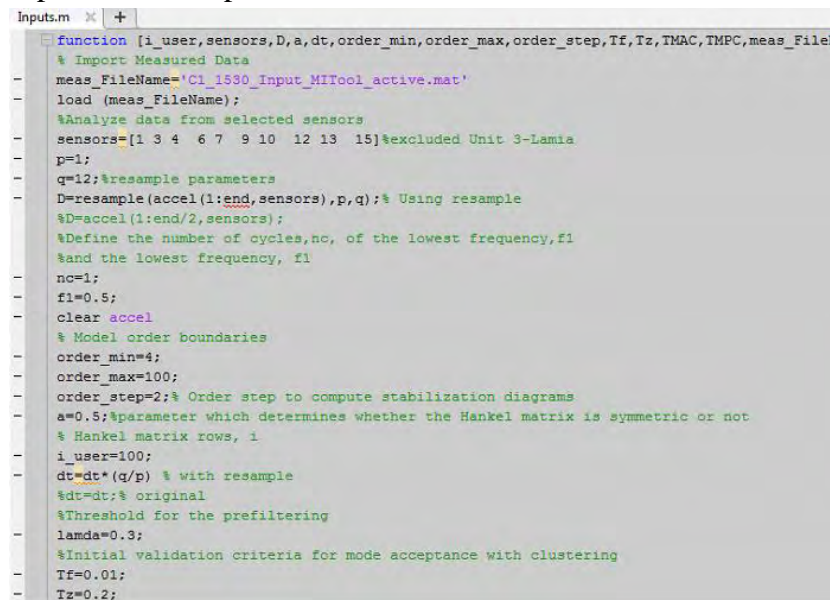
In conclusion, this thesis presents a useful tool and its applications for an automated modal analysis of a structure, with a little need for the user's intervention. Although the automated procedures conquer the software, there is still place for the entire automation of it.

APPENDIX A: Developed software for the automated modal identification

In this Appendix a brief presentation of the developed software will be made and a description of how it is used (input parameters etc.). To begin with, the software has been encoded in MATLAB 2016 and uses orders and functions, which are available for this MATLAB edition.

The user of this software just has to define some input parameters and then run the main program. This software consists of some *.m* MATLAB files , which are:

- *Automated_DD-SSI_main.m* : it contains the code for the computation of the modes in different model orders, using the DD –SSI algorithm and then the clustering methodology. It is the main file that has to be ran in order to get the results.
- *Inputs.m*: it is a file that has to be opened in order for the user to define the input parameters. A picture of it is shown below:



```
function [i_user,sensors,D,a,dt,order_min,order_max,order_step,Tf,Tz,TMAC,TMPC,meas_File]
% Import Measured Data
meas_FileName='C1_1530_Input_MITool_active.mat'
load (meas_FileName);
%Analyze data from selected sensors
sensors=[1 3 4 6 7 9 10 12 13 15]%excluded Unit 3-Lamia
p=1;
q=12;%resample parameters
D=resample(accel(1:end,sensors),p,q);% Using resample
%D=accel(1:end/2,sensors);
%Define the number of cycles,nc, of the lowest frequency,f1
%and the lowest frequency, f1
nc=1;
f1=0.5;
clear accel
% Model order boundaries
order_min=4;
order_max=100;
order_step=2;% Order step to compute stabilization diagrams
a=0.5;%parameter which determines whether the Hankel matrix is symmetric or not
% Hankel matrix rows, 1
i_user=100;
dt=dt*(q/p) % with resample
%dt=dt;% original
%Threshold for the prefiltering
lamda=0.3;
%Initial validation criteria for mode acceptance with clustering
Tf=0.01;
Tz=0.2;
```

Figure A.1. Image of the Inputs.m file

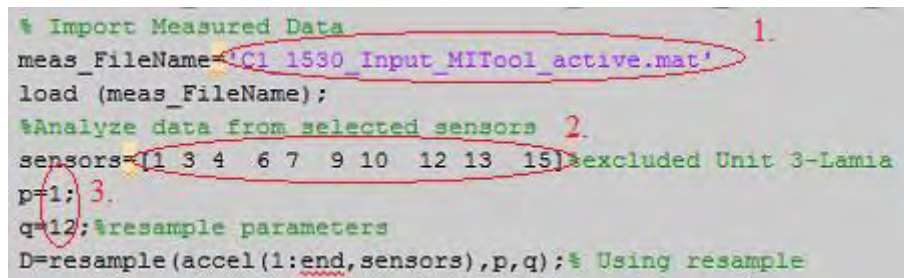
- *pre_filter.m*: it includes the encoded Hard Validation criteria , through which the modes go and a first filtering is achieved. This file doesn't need to be ran or modified by the user. The parameter “lamda” can be adjusted through the Inputs.m file.
- *randomize.m*: this file includes the code for the needed randomization of the modes before the clustering procedure begins. This file also doesn't need to be modified.

Since the most important *.m* files that the program uses have been presented, let's talk about the input parameters that the user has to insert, so that the software can be used.

In the Inputs.m file, the user has to give information about 9 parameters. First of all, he has to insert the file with the measurements (accelerations). Once the .mat file with the experimental measurements is loaded, the user has to define from which sensors information will be used. After the sensor numbers have been defined (according to the desired direction) ,then the parameters for “resample” have to be decided. Let’s note here, that it is possible to use all of the sensors as well. As far as the resampling parameters are concerned, the value, which is given to q represents how many times the sampling frequency will be divided and as a result, how many times the sampling time will be multiplied. The definition of the resampling order in MATLAB is the following, “resample” = resampling uniform or non-uniform data to a new fixed rate. For example:

$$Y = \text{resample}(X,P,Q)$$

resamples the values, X, of a uniformly sampled signal at P/Q times the original sample rate using a polyphaser anti-aliasing filter. If X is a matrix, then resample treats each column as an independent channel. Resampling is used, so that the memory problem can be faced because it reduces the produced frequencies to lower ones. The frequency limit is, actually, given by the user and the parameter q. In addition, resample can be useful, in order to identify lower eigenfrequencies, which are lost ,when we have the production of high frequencies as well. The above mentioned input information is depicted in the picture below:



```

% Import Measured Data
meas_FileName='C:\1530\Input_MITool_active.mat';
load (meas_FileName);
%Analyze data from selected sensors
sensors=[1 3 4 6 7 9 10 12 13 15]; %excluded Unit 3-Lamia
p=1;
q=12; %resample parameters
D=resample(accel(1:end,sensors),p,q); % Using resample

```

The image shows a MATLAB script with three red circles and numbers indicating key steps: 1. The file name 'C:\1530\Input_MITool_active.mat' is circled. 2. The sensors array [1 3 4 6 7 9 10 12 13 15] is circled. 3. The resampling parameters p=1 and q=12 are circled.

Figure A.2. Inputs 1. Load file with measurements, 2. Sensors 3. Parameters for “resample”

After the input data has been loaded and resampled then the user-defined parameters for the DD – SSI algorithm have to be inserted(fig.A.3). These are, as already mentioned in chapter 2, the lower (*order_min*) and upper limit (*order_max*) of the model orders ,in which the modes will be calculated and the Hankel matrix parameter *i_user*. There is also the *order_step*, which is the step from one model order to another (usually every two orders) and a parameter *a*, which determines whether or not the Hankel matrix will be symmetric.

```

% Model order boundaries
order_min=4; 4.
order_max=100;
order_step=2;% Order step to compute stabilization diagrams
a=0.5;%parameter which determines whether the Hankel matrix is symmetric or not
% Hankel matrix rows, 1
i_user=100; 6.
dt=dt*(q/p) % with resample

```

Figure A.3. Inputs: 4. Model order parameters, 5. Hankel matrix symmetry parameter, 6. Hankel matrix rows, i.

Finally, the thresholds for the hard validation criteria have to be determined as well as for the clustering procedures. Parameter “lamda” refers to the pre-filtering.m and is related to the hard validation criteria. Parameters Tf, Tz, TMAC, TMPC refer to thresholds for frequency, damping ratios, MAC and MPC, respectively. Last but not least, there is the parameter “eliminate”, which determines the percentage of modes under which the merged clusters are eliminated. All of them should be assigned with values that are recommended from literature and have been presented in the current thesis (chapter 3) and then adjusted according to the acquired results. The needed adjustments are made with the critical ability of the user.

```

%Threshold for the prefiltering
lamda=0.3; 7.
%Initial validation criteria for mode acceptance with clustering
Tf=0.01;
Tz=0.2; 8.
TMAC=0.02;
TMPC=0.1;
%percentage for the merged clusters elimination
eliminate=0.50; 9.

```

Figure A.4. Inserted thresholds: 7. Hard validation parameter, 8. Thresholds for clustering, 9. Merged clusters elimination percentage.

When the demanded inputs are given, the user has to save the *Inputs.m* file and then run the *Automated_DD-SSI_main.m*. After that he has to wait until the results (stabilization diagrams etc.) are produced. So, all the user intervention finishes after the user defined parameters have been inserted. The results produced by the developed software have already been presented thoroughly for each application in chapter 5. Just to name them they are: the time histories, the singular values, the DD-SSI produced modes, the prefiltered modes, the clustered modes, the merged clusters, the merged clusters on the PSD graph, the complex modeshapes and for some cases the real modeshapes.

APPENDIX B: Output of Software 2

In this Appendix, an example of the results acquired for Bridge 2, by Software 2, is presented. These numerical results of the frequencies and the damping ratios are used and depicted in Table 5.2.2. An example of the results gained for configuration 1 of Bridge 2 is following.

Configuration 1 (Time 13:30; 20 minutes long) – free of trucks

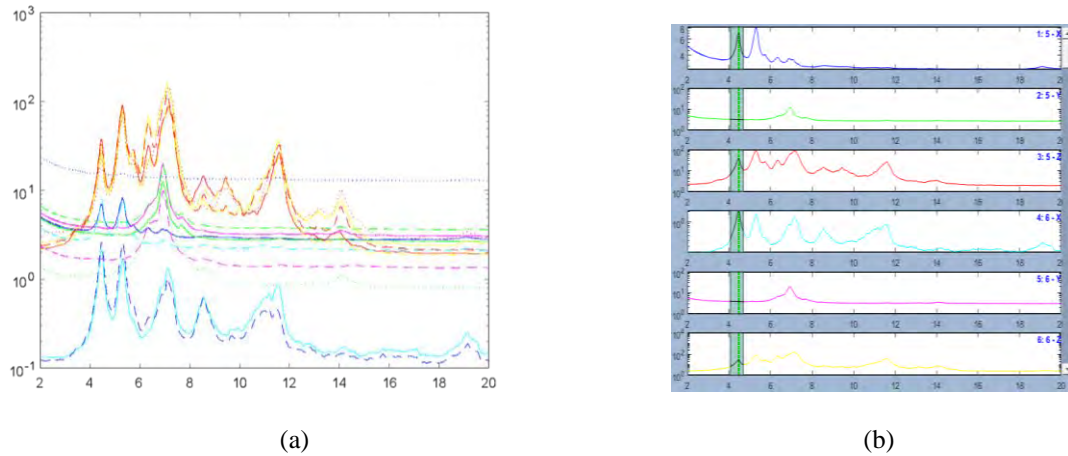


Figure B.1. (a) Power Spectral Densities for Configuration 1. (b) Fit in frequency domain around the first mode. PERFECT FIT IN ALL CHANNELS

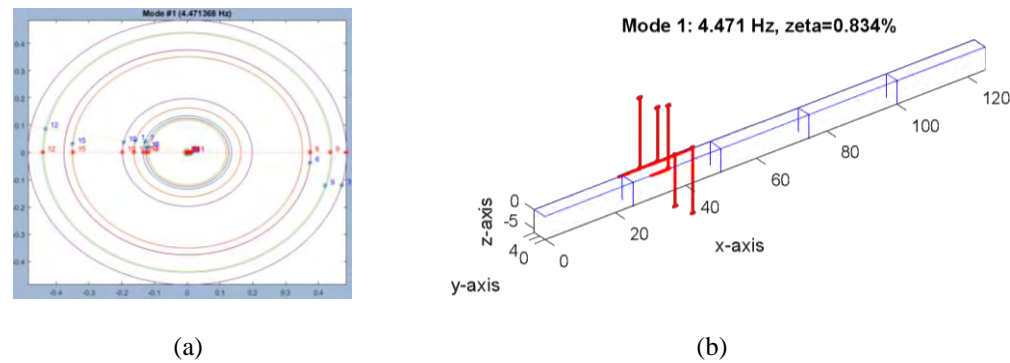


Figure B.2. (a) Damping type for mode 1, configuration 1. The mode is close to classically damped. (b) Mode shape for mode 1 for the Sensor Configuration 1.

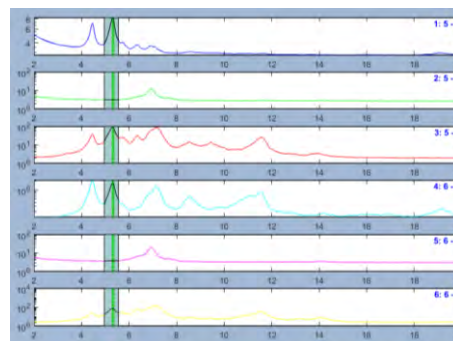


Figure B.3. Fit in frequency domain around the second mode. PERFECT FIT IN ALL CHANNELS

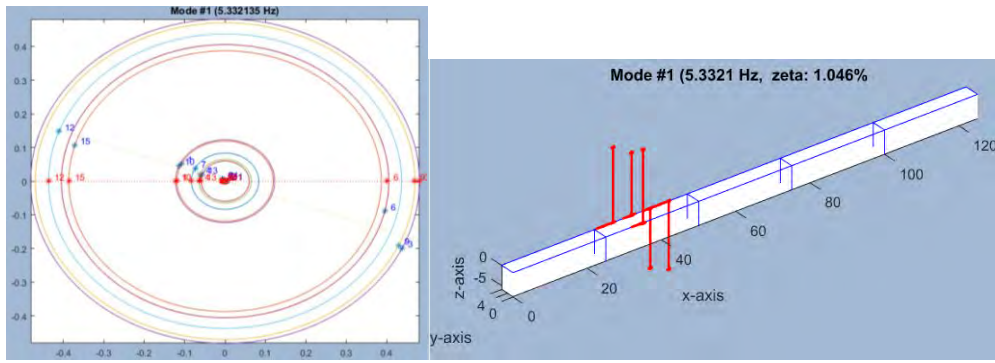


Figure B.4.(a) Damping type for mode 2, configuration 1. The mode is closely to classically damped.
(b) Modeshape for mode 2, sensor configuration 1.

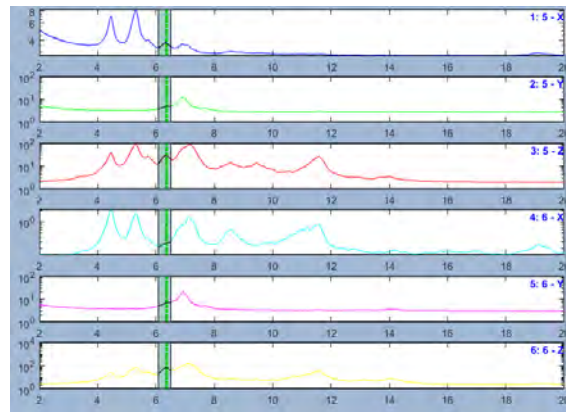


Figure B.5.Fit in frequency domain around the third mode. PERFECT FIT IN ALL CHANNELS

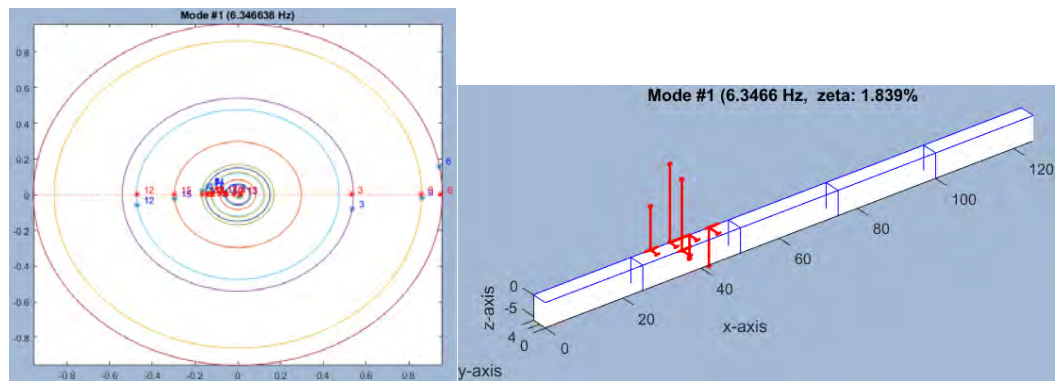


Figure B.6. (a) Damping type for mode 3, configuration 1. The mode is closely to classically damped.
(b) Modeshape for mode 3 for the Sensor Configuration 1.

7. Literature

- [1] P. Van Overschee, B. De Moor, “Subspace Identification for Linear Systems”, Kluwer Academic Publishers (1996)
- [2] Moaveni Babak, “System and damage identification of civil structures”, UC San Diego, UC San Diego Electronic Theses and Dissertations (2003).
- [3] C. Priori, M. De Angelis, R. Betti, “On the selection of user-defined parameters in data-driven stochastic subspace identification” (2017).
- [4] ViroteBoonyapinyo, Tharach Janesupasaeree, “Data-driven stochastic subspace identification of flutter derivatives of bridge decks”(2010)
- [5] Bart L.R. De Moor, “On the Number of Rows and Columns in Subspace Identification Methods” (2003)
- [6] Edwin Reynders, Jeroen Houbrechts, Guido De Roeck, “Fully automated (operational) modal analysis” (2012)
- [7] Pappa R, Elliott K, Schenk A. “A consistent-mode indicator for the eigensystem realization algorithm.” (1992)
- [8] Miao Sun, Mehrisadat Makki Alamdari, Hamed Kalhori, “Automated Operational Modal Analysis of a Cable-Stayed Bridge” (2017)
- [9] Costas Argyris, “Bayesian uncertainty quantification and optimal experimental design in data-driven simulations of engineering system” (2017)
- [10] Chunli Wu, Hanbing Liu , Xuxi Qin , Jing Wang, “Stabilization diagrams to distinguish physical modes and spurious modes for structural parameter identification”(2017)
- [11] Rhara de Almeida Cardoso, Alexandre Cury and Flávio Barbosa, “A clustering-based strategy for automated structural modal identification” (2017)
- [12] R. Brincker, L. Zhang, P. Andersen, “Modal Identification of output-only systems using frequency domain decomposition”, *Smart Mater. Struct.* 10 (2001)
- [13] J. Juang, R. Pappa, “An eigensystem realization algorithm for modal parameter identification and model reduction”, *J. Guid. Control and Dynam.* 8 (5)(1985)620-627
- [14] Au, S.K. “Assembling mode shapes by least squares”. *Mechanical Systems and Signal Processing*, vol. 25(1): 163–17 (2011).
- [15] Evangelos Ntotsios, “Structural Identification of Complex Structures based on Vibration Measurements” (2009)

